5-14-2018

Investigating Trace Metal Sequestration of Reducing Environments in Modern and Ancient Settings

Adam Charles Turner
Louisiana State University and Agricultural and Mechanical College

INVESTIGATING CHEMICAL SEQUESTRATION OF TRACE METALS IN REDUCING ENVIRONMENTS OF MODERN AND ANCIENT ENVIRONMENTS

A Dissertation

Submitted to the Graduate Faculty of the
Louisiana State University and
Agricultural and Mechanical College
in partial fulfillment of the
requirements for the degree of
Doctor of Philosophy

in

The Department of Geology and Geophysics

by
Adam Charles Turner
B.S. University of Arizona, 2007
B.S. Arizona State University, 2013
August 2018

ACKNOWLEDGEMENT

I would like to thank first and foremost my major advisor, Dr. Achim Herrmann, who has provided me with the opportunities to work here at Louisiana State University and at Arizona State University, and who has spent countless hours helping me to succeed. I would like to thank the committee members for their time and guidance to me through the doctorate process. I would also like to thank Dr. Thomas Algeo, for his help in reviewing and guiding my work in the Late Pennsylvanian Midcontinent Sea. Dr. Yongbo Peng provided integral lab support and analysis for stable isotope work. Wanda LeBlanc provided much needed lab support. Dr. Kanchan Maiti helped facilitate my fieldwork in the Gulf of Mexico and was a pleasure to work with. Financial support which made this work possible was supplied by the National Science Foundation Sedimentary Geology and Paleobiology program (grant EAR-1313514) and the donors of the Petroleum Research Fund, administered by the American Chemical Society (ACS PRF 55392-DNI2).

I would also like to thank my family and friends. Without their moral support, I would not have survived the strenuous process of creating this dissertation.

TABLE OF CONTENTS

ABSTRACT

The incorporation of trace metals into a variety of reducing sediments are important proxies for the oxic state of the water mass in which the sediments form. While much work has been done interpreting these proxies, questions remain on the exact processes and products in which trace metal proxies form. This work employs bulk geochemical techniques to investigate circulation in the Late Pennsylvanian North American Midcontinent Sea (NAMS), and then uses sequential extractions to further understand the chemical phases in which trace metals are incorporated. Sequential extractions are then used to further investigate how trace metals are sequestered in modern environments, in environments both similar to the NAMS (Gulf of Mexico) and dissimilar (The Bahamas).

The NAMS experienced glacioeustatic rises and falls, during which repetitive sedimentary sequences termed cyclothems accumulated on a stable platform, depositing organic-rich core shales under a stratified water column with anoxic deep waters. The present study investigates circulation patterns of the NAMS by examining trace-element enrichments, organic carbon content, and carbon-nitrogen stable isotopes sampled at high resolution within a single cyclothemic black shale, the Heebner Shale, at six sites on the northern Midcontinent Shelf and two sites in the Illinois Basin. The Heebner Shale is the core shale member of the Upper Pennsylvanian (lowermost Gzhelian) Oread Limestone Formation in Kansas and Iowa, and it is correlative with the Teutopolis Shale of the Mattoon Formation in Illinois. Major elements and clay-mineral assemblages show influences from three distinct terrestrial sources, and their spatial patterns imply large-scale clockwise (anticyclonic) rotation of the NAMS watermass driven by either the Coriolis Effect or the hydrodynamics of riverine discharge into the NAMS.

In The Bahamas, syndepositional diagenesis and its effects on trace metal sequestration were investigated using stable isotopes and sequential extractions on four cores. While syndepositional diagenesis provides a pathway for authigenic enrichment of trace metals, the enrichment is sequestered in the exchangeable phase. The carbonate phase reflects concentrations similar to primary precipitates. Similar experiments were carried out in the Gulf of Mexico (GOM) “dead zone”, in which authigenic enrichment in the exchangeable phase recorded historic hypoxic levels.

CHAPTER 1 INTRODUCTION

1.1 Objective and Goals

Trace metals incorporated into a variety of sediments and time periods can provide clues as to the redox state of local and global environments at the time of deposition. Despite the intense interest in trace metal concentrations in sediment, uncertainties exist about how trace metals are actually sequestered into the sediment. This study uses sequential extractions on a variety of siliciclastic and carbonate sediments, with different redox conditions and time periods, in order to systematically study how trace metals are incorporated into sediment, and how that information can be applied as pale-redox indicators.

Sequential extractions have long been recognized by soil scientists as a method to chemically differentiate how metals are bound to the sediment. Presently, I employ a modified Tessier sequential extraction technique in order to investigate the different phases in which trace metals (primarily U and Mo) are hosted. Stable isotope and XRF measurements provide complimentary data to better understand environments of deposition and early diagenesis.

This work examines two modern environments, one which is dominated by siliciclastic input (Northern Gulf of Mexico) and one which is largely free of siliciclastic input (Exuma Islands, The Bahamas). The Northern Gulf of Mexico provides a well-studied hypoxic zone, dominated by flux from the Mississippi River. The seasonally oxic bottom waters provide an excellent natural laboratory to investigate trace metal uptake in mildly reducing environments, with a corresponding historic record of bottom water hypoxia of the last ~30 years. In The Bahamas, an oxic water column overlays pore waters that often become euxinic (reducing, free H_2S) in the first few cm of sediment. Four different locations were analyzed in The Bahamas in order to track trace metal uptake across sediments with a variety of organic content, terrestrial influence, and syndepositional diagenesis.

The Late Pennsylvanian North American Midcontinent Sea (NAMS) was investigated based on its strongly reducing, euxinic water column during shale deposition during black shale deposition and less reducing, dysoxic water column under grey shale deposition. This siliciclastic dominated system

provides the opportunity to examine trace metal uptake over the evolution of water column conditions, on a time scale much greater (thousands of years) than can be analyzed in modern sediments.

An integration of data about sequestration and uptake from these varied environments will help elucidate the mechanisms of trace metal uptake.

1.2 Organization

This dissertation is split into three major chapters in the format of peer-reviewed journals, with an additional chapter (chapter 5) discussing sequential extractions specifically in the NAMS. Chapter 2 will be submitted to Paleogeography, Paleoclimatology, Paleoecology upon completion of review among the coauthors. Chapter 3 and 4 are planned to be submitted to ACS Earth and Space Chemistry.

Chapter 2 focuses on the study of bulk sediment geochemistry of the NAMS, specifically the circulation patterns that it can help inform. By performing a high resolution (both spatially and temporally) study of a single cyclothem, patterns of trace metal enrichment and stable isotopes can be used to investigate the depositional system. Chapter 5 takes the information gained in chapters 3 and 4 about trace metal speciation using sequential extractions, and applies it to two of the study sections from chapter 2. Chapters 3 and 4 focus on the chemical speciation of trace metals in modern sediments, by looking at four study sections from The Bahamas (chapter 3) and one section from the Northern Gulf of Mexico (chapter 4).

CHAPTER 2 CIRCULATION PATTERNS IN THE LATE PENNSYLVANIAN NORTH AMERICAN MIDCONTINENT SEA INFERRED FROM SPATIAL GRADIENTS IN SEDIMENT CHEMISTRY AND MINERALOGY

2.1 Introduction

During Late Pennsylvanian glacioeustatic highstands of the Late Paleozoic Ice Age (LPIA), an immense sea known as the North American Midcontinent Sea (NAMS) spread across $>1 \times 10^6$ km^2 of the interior of the Laurentian Craton (Algeo and Heckel, 2008; Heckel, 1977). Watermass circulation patterns within the NAMS have been a subject of debate (Algeo et al., 2008a; Coveney et al., 1991; Cruse and Lyons, 2004; Hatch and Leventhal, 1997; Heckel, 1977; Witzke, 1987; Zangerl, 1963). Witzke (1987) proposed a "quasiestuarine" circulation model, refined by Algeo et al. (2008a) into the "superestuarine" circulation model in order to account for vertical stratification and deepwater anoxia within a broad epeiric (= epicontinental) sea lacking a marginal sill (i.e., having a deep-water connection to the open ocean, henceforth termed "open-ended"). In this model, the NAMS had a brackish, oceanward-flowing surface layer due to heavy riverine discharge into its eastern (proximal) end, and an anoxic, saline deepwater layer owing to lateral advection of preconditioned, oxygen-poor mid-depth (thermoclinal) waters from the tropical eastern Panthalassic Ocean through a deep-water corridor at its western (distal) end (Fig. 2.1). The advected deep waters remained isolated from the atmosphere by the brackish surface layer, resulting in widespread anoxia (euxinia) in the deep watermass. Development of large-scale estuarine-type circulation within the NAMS was promoted by its limited bathymetric relief, nearly complete lateral enclosure by landmasses, and strong riverine discharge into its proximal end. The superestuarine circulation model provides a new framework for investigating stratified, open-ended epeiric seas of the past, for which there exists no precise modern analog (Algeo et al., 2008a).

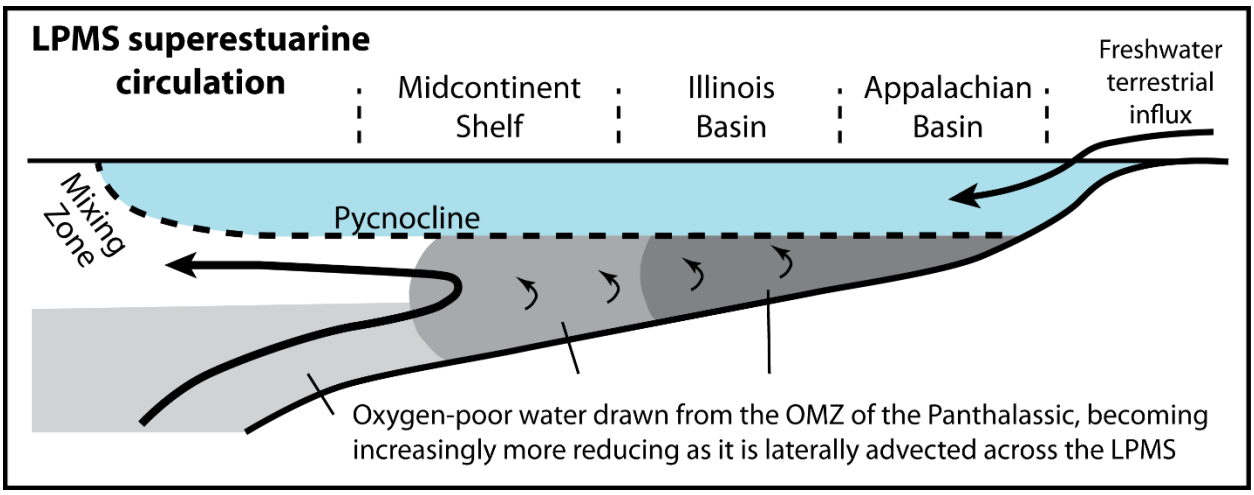

Figure 2.1 A schematic representation of superestuarine circulation in the NAMS. Oxygen-poor water is laterally advected from an oxygen minimum zone (OMZ) in the western tropical Panthalassic Ocean into the NAMS. As it migrates, this watermass becomes increasingly reducing due to respiratory oxygen demand (due to organic matter oxidation) and insufficient oxygen resupply (due to strong vertical stratification). Riverine runoff from surrounding landmasses generated a reduced-salinity surface layer within the geographically confined NAMS. Modified from Algeo et al. (2008a).

In addition to large-scale estuarine circulation, epeiric seas can exhibit internal gyral circulation. All modern epeiric seas show gyral circulation, although the direction of circulation in given hemisphere is not fixed. In the Northern Hemisphere, the Black Sea, the Hudson Bay, and the Baltic Sea all show cyclonic (counter-clockwise, or CCW) rotation (Emery and Csanady, 1973; Prinsenberg, 1986), whereas the "old" Aral Sea exhibited anticyclonic circulation (clockwise, or CW) rotation (Zavialov, 2010). Seasonally reversing circulation is also possible, as in the Southern Hemisphere Gulf of Carpentaria (Church and Fobes, 1981). Gyral circulation in modern seas and large lakes has been attributed to the deflection of river inflows due to the Coriolis Effect, geostrophic circulation due to seasonal variations in temperature and wind patterns, wind drag, storm effects, and bathymetric influences (Beletsky et al., 1999; Bennett, 1975; Emery and Csanady, 1973). Vertical stratification in large water bodies can enhance gyral circulation (Schwab et al., 1995). For the NAMS, earlier studies have inferred both a CCW gyral circulation pattern based on lateral gradients in redox conditions and clay-mineral assemblages (Algeo and Heckel, 2008; Algeo et al., 2008a) and a CW gyral circulation pattern based on paleoredox and facies patterns (Yang et al., 2003).

The present study aims to further evaluate gyral circulation patterns within the NAMS based on spatial patterns of sediment geochemical and mineralogical composition. The present study has distinct advantages over earlier studies addressing this issue in making use of (1) a two-dimensional geographic array of sample sites that provides improved spatial coverage across the NAMS, as opposed to the one-dimensional (linear) array of sites used by Algeo and Heckel (2008) and the limited geographic area of the study by Yang et al. (2003); and (2) a larger number of geochemical and mineralogical proxies. We analyzed the uppermost Pennsylvanian (Virgilian) Heebner cyclothemic core shale (or its equivalent) at seven sites across the NAMS, generating geochemical and mineralogical data at cm-scale stratigraphic resolution. Our dataset thus represents probably the more comprehensive analysis of a single Pennsylvanian cyclothemic core shale to date. The fine resolution and broad spatial extent of this study allow for analysis of the temporal evolution of circulation patterns during Heebner Shale deposition, an understanding of which has regional climatic and oceanographic implications.

2.1.1 Geological setting and background

The NAMS was a largely land-locked epeiric sea, being enclosed by the Ouachita Mountains to the southwest, the Alleghenian Mountains to the south, and the Laurentian Craton to the northeast and north (Fig. 2.2; note: all directions are Late Pennsylvanian orientations, i.e., prior to the later ~50° CCW rotation of North America). The NAMS maintained communication with the Eastern Tropical Panthalassic Ocean (ETPO), through a long (~1000 km) sinuous deepwater corridor (Algeo et al., 2008b; Heckel, 1977). Located between the paleo-equator and ~20°N, with the southern orogenic arc within the paleo-intertropical convergence zone (ITCZ), the NAMS experienced high precipitation levels providing large freshwater inputs, especially on its southern and eastern margins, setting up a reduced-salinity surface layer (Algeo and Heckel, 2008).

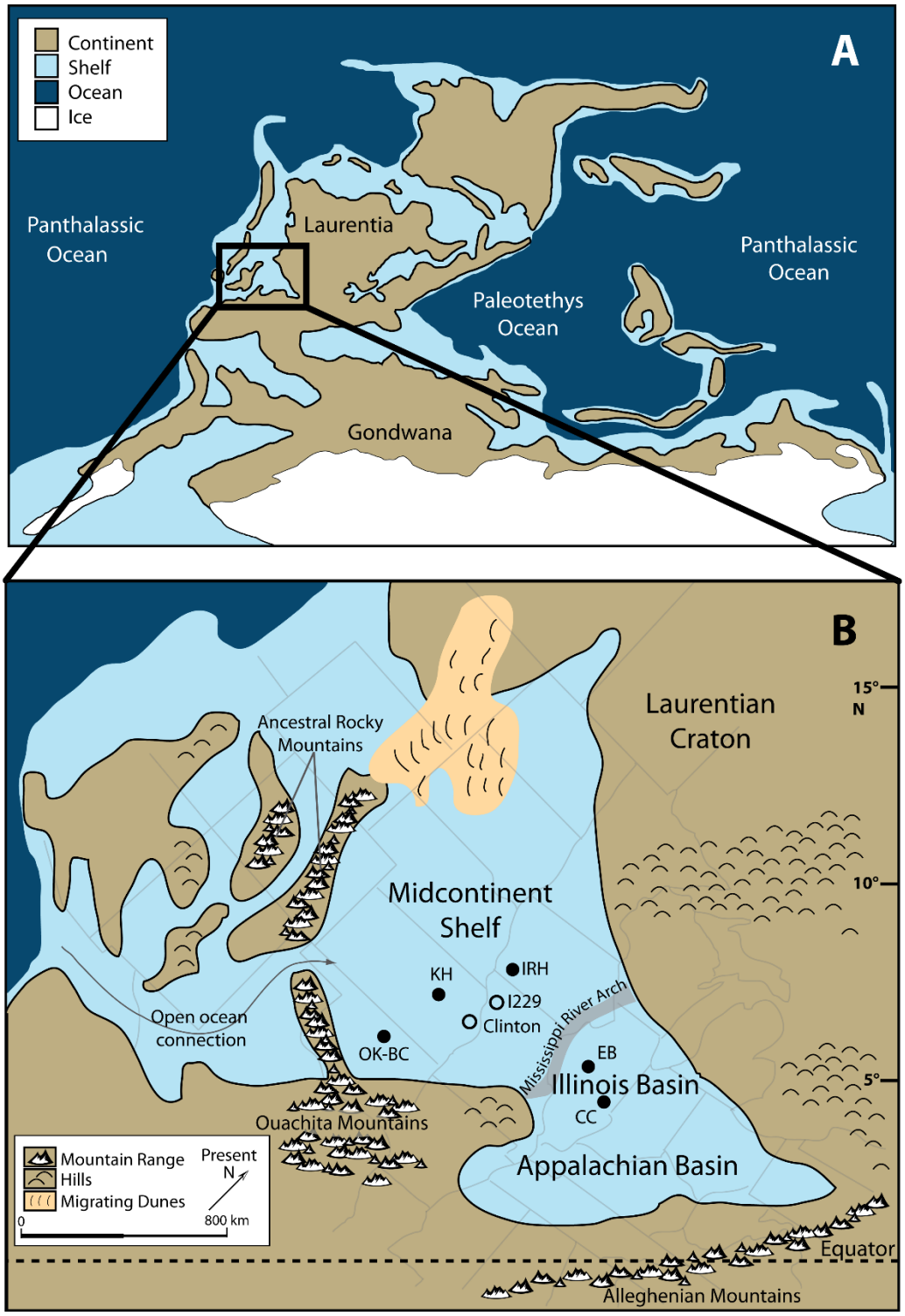

Figure 2.2 Paleogeographic map of study area. Open circles are outcrops and closed circles are drillcores used in this study. Present state outlines provide scale and orientation. Sources: (A) modified from Ron Blakey (https://deeptimemaps.com/); (B) modified from Algeo et al. (2008a).

The stratigraphic architecture of the NAMS is dominated by repetitive lithologic successions, termed cyclothems, that reflect fluctuating water depths (Heckel, 1977, 1994). Cyclothems have widely been interpreted as the result of successive rapid (~10^5 yr) glacioeustatic transgressions and regressions across the shallow continental interior (Algeo and Heckel, 2008; Heckel, 1977; Yang, 2007). The scale of sea-level fluctuations driven by waxing and waning of contemporaneous Gondwanan icesheets has been a matter of debate, with estimated amplitudes ranging from ~20 m to > 150 m (Heckel, 1977; Joachimski et al., 2006; Montañez and Poulsen, 2013; Rosenau et al., 2014; Soreghan and Giles, 1999). Water depths on the outer margin of the Midcontinent Shelf were probably no more than ~100 m during highstands (Algeo et al., 2008a).

In the Midcontinent region, cyclothems consist of four members: a thin basal transgressive limestone, a "core" shale, a thick regressive limestone, and an "outside" shale that represents shallow-water siliciclastic deposition and/or subaerial paleosol development (Heckel, 1977; Wanless and Shephard, 1936). The core shale (named for its central position in cyclothemic successions) consists of a fissile black shale submember underlying a bioturbated gray shale submember (Algeo et al., 2004; Heckel, 1977; Hoffman et al., 1998). The black shales are finely laminated with abundant phosphate nodules and, other than pelagic or nektic organisms, a general lack of biota. Cyclothems are stratigraphically correlative across long distances in the NAMS (>1000 km) (Boardman and Heckel, 1989; Heckel, 1977, 1994), even to the degree that lithologically distinctive cm-thick layers can be correlated over 100s of km (Algeo and Heckel, 2008). These characteristics have led to interpretations of sediment-starved, sustained anoxic and potentially euxinic conditions during core shale deposition.

Previous work on the Heebner Shale provides a robust stratigraphic and paleoenvironmental framework for the present study. It is the second of three minor cyclothems of the Upper Pennsylvanian Oread Cyclothem (Wanless and Shepard, 1936), overlying the transgressive Leavenworth Limestone and underlying the regressive Plattsmouth Limestone (Evans, 1967; Heckel, 1994; Yang et al., 2003). It contains the first appearance of the conodont *Idiognathodus simulator*, which has been proposed to mark the base of the Gzhelian Stage of the Late Pennsylvanian (Ellison, 1941; Villa et al., 2009). The Heebner

Shale exhibits lateral continuity across the Midcontinent region, extending from Iowa to Oklahoma (Evans, 1967), and it has a stratigraphic equivalent east of the Mississippi River Arch, the Teutopolis Shale, that extends across the Illinois Basin (Heckel, 1994). It was deposited during an interval of climatic drying and enhanced seasonality in the latest Pennsylvanian (e.g., Cecil et al., 2003; Tabor and Montañez, 2002) that was associated with expanded Southern Hemisphere glaciation (Montañez and Poulesen, 2013).

2.2 Methods and materials

2.2.1. Sample collection and preparation

This work analyzes seven sections (five drillcores and two outcrops) of the lower Gzhelian (= North American Virgilian stage) Heebner Shale Member of the Oread Limestone on the northern Midcontinent Shelf and the correlative Teutopolis Shale of the Mattoon Formation in the Illinois Basin (Rosenau, 2013). These sections provide a two-dimensional geographic framework extending north-south from Oklahoma to Iowa and east-west from Kansas to Illinois. Cores were sampled at state geological survey core repositories whereas outcrops were sampled on site (Table 2.1). Samples from each section were collected at regular, closely-spaced intervals (0.5 to 2 cm for drillcores and ~5 cm for outcrops). Each sample was cleaned of surface debris and powdered using a tungsten ball mill.

Drillcore	Location	Curated By	Thickness of Heebner Shale, no. analyses
CC (City of Charleston #1)	330’ FSL, 1100’ FEL, Sec. 9, T12N, R9E; 39.492°N, 88.199°W; Coles Co., IL	Illinois Geological Survey	1.45 m, n = 90
EB (ISGS #1 Englebart)	40’ FSL, 340’ FEL, Sec. 9, T8N, R8E; 39.146°N, 88.318°W; elev. 575’; Jasper Co., IL	Illinois Geological Survey	1.91 m, n = 137
IRH (Iowa Riverton)	SW-SE-SE-SE, Sec. 20, T67N, R41W; 40.600°N, 95.575°W; Fremont Co., IA	Iowa Geological Survey	0.88 m, n = 88
KH (KGS Heinen #1)	NW-NW-SW, Sec. 25, T4S, R13E; 39.674°N, 95.919°W; Nemaha Co., KS	Kansas Geological Survey	0.81 m, n = 96
OK-BC	35.310°N, 99.687°W; Beckham Co., OK	Oklahoma Geological Survey	3.25 m, n = 185

Table 2.1 Location information for the five study cores.

2.2.2. Major- and trace-element analysis

Major- and trace-element concentrations were determined on whole-rock samples through X-ray fluorescence (XRF) analysis using a wavelength-dispersive Rigaku 3040 XRF spectrometer at the University of Cincinnati. Results were calibrated using both USGS and internal standards (analyzed by XRAL Incorporated). Analytical precision based on replicate analyses was better than ±2 % of reported values for major elements and better than ±5 % for trace elements (TEs), and detection limits for trace elements ranged from 2 to 5 ppm. Trace-element EFs were calculated as $X_{EF} = [(TE_{sample}/Al_{sample}) / (TE_{PAAS}/Al_{PAAS})]$, where PAAS is Post-Archean Average Shale (Taylor and McLennan, 1985).

Total organic carbon (TOC), total inorganic carbon (TIC), and total sulfur (TS) concentrations were determined using an Eltra 2000 C-S analyzer, also at the University of Cincinnati. Data quality was monitored via multiple analyses of USGS SDO-1 standard (C = 9.65 %, S = 5.35 %) and an internal lab standard DBS-1 (C = 3.50 %, S = 1.97 %), yielding an analytical precision (2σ) of ±2.5 % of reported values for C and ±5 % for S. An aliquot of each sample was digested in 2N HCl at 50 °C for 12 h to dissolve carbonate minerals, and the residue was filtered and analyzed to determine TOC, with TIC obtained by difference from total carbon (TC).

2.2.3. Nitrogen isotope analysis

Nitrogen isotope analyses ($\delta^{15}N$) were performed at the Stable Isotope Laboratory of Boise State University and the Oxy-Anion Stable Isotope Consortium (OASIC) at Louisiana State University. Boise State analyses were carried out using a 2010 ThermoFisher Delta V Plus continuous flow isotope ratio mass spectrometer coupled with GasBench II. Louisiana State analyses were carried out using a Thermo Scientific MAT253 IRMS with dual-inlet, coupled with a Gas Bench and Thermal Conversion Elemental Analyzer (TCEA). Samples were weighed out into combustible tin containers as ~5-15 mg aliquots to yield ~100 μg of N. Results are reported as per mille (‰) variation from standard N_2 in air in delta notation, where $\delta^{15}N_{air} = (({}^{15}N/{}^{14}N)_{sample}/({}^{15}N/{}^{14}N)_{standard} - 1) \times 1000$. Nitrogen isotopic compositions were calibrated using an acetanilide standard with a $\delta^{15}N_{air}$ value of 1.61 ‰. Analytical precision was better than 0.1 ‰.

2.2.4. Organic carbon isotope analysis

Organic carbon isotopic analyses ($\delta^{13}C_{org}$) were performed on a Thermo Scientific MAT253 IRMS with dual-inlet, coupled with a Gas Bench and Thermal Conversion Elemental Analyzer (TCEA) at the Oxy-Anion Stable Isotope Consortium (OASIC) at Louisiana State University. An aliquot of each sample was decalcified through three-fold treatment with 1 M hydrochloric acid. Samples were then rinsed, dried, and weighed into combustible tin containers. Approximately 2-20 mg of bulk decalcified sample was used to yield ~400 μg of carbon. Mass calibrations were performed to allow adjustment of carbon content based on TOC%. Results are reported as per mille (‰) variation from the international VPDB standard in delta notation, where $\delta^{13}C_{VPDB} = (({}^{13}C/{}^{12}C)_{sample}/({}^{13}C/{}^{12}C)_{standard} - 1) \times 1000$. Carbon isotopic compositions were calibrated using an acetanilide standard with $\delta^{13}C_{VPDB}$ value of -27.6 ‰. Analytical precision was better than 0.1 ‰.

2.3 Results

2.3.1. Internal correlation of the Heebner Shale across the NAMS

The Heebner Shale consists of fissile to blocky black shale overlain by bioturbated gray shale containing some fossils. The black shale submember ranges from 325 cm (OK-BC) to 81 cm (KH) in

thickness, with most sections about 90 - 150 cm thick (Table 2.1). Previous studies have subdivided core shales into three or four units based on their geochemical properties, especially TOC, TEs, and $\delta^{15}N$ (Hoffman et al., 1998; Algeo et al., 2004, 2008a; Herrmann et al., 2012, 2015). The present study follows a similar strategy but recognizes a total of five internal units: Lower Black Shale 1 (LBS-1), Lower Black Shale 2 (LBS-2), Upper Black Shale-1 (UBS-1), Upper Black Shale-2 (UBS-2) and Gray Shale (GS) (Fig. 2.3). These subdivisions are based on consistent and readily recognizable criteria. The base of LBS-1 is the base of the black shale submember of a core shale. $\delta^{15}N$ profiles exhibit a single positive excursion in each Upper Pennsylvanian Midcontinent black shale (Algeo et al., 2008b) that is widely correlatable across the NAMS (Herrmann et al., 2015); it is the basis for recognizing the LBS-1/LBS-2 contact. In two of the present study sections (the CC drillcore and I-229 outcrop), there is no recognizable LBS-1 unit because the positive $\delta^{15}N$ excursion is found at the base of the black shale submember. The LBS-2/UBS-1 contact (originally just the LBS/UBS contact) is marked by peak concentrations of TOC and most trace metals, and is interpreted to represent the maximum flooding surface (MFS) of a cyclothem (Algeo et al., 2004). From a peak of 10-30 % at the MFS, TOC falls progressively (although cyclically) through the UBS to <2.5 % to mark the transition to the GS interval. The UBS-1 and UBS-2 units are distinguished based on an abrupt decline in trace-metal enrichment factors: Mo_{EF} values are elevated in the LBS-1, LBS-2 and UBS-1 but decline abruptly to near-background values (~1.0) at the UBS-1/UBS-2 transition. The gray shale submember of a core shale (GS unit) is marked by a decline to TOC <2.5 %, distinctly lighter color, pronounced bioturbation, and little to no trace-metal enrichment (Algeo et al., 2004).

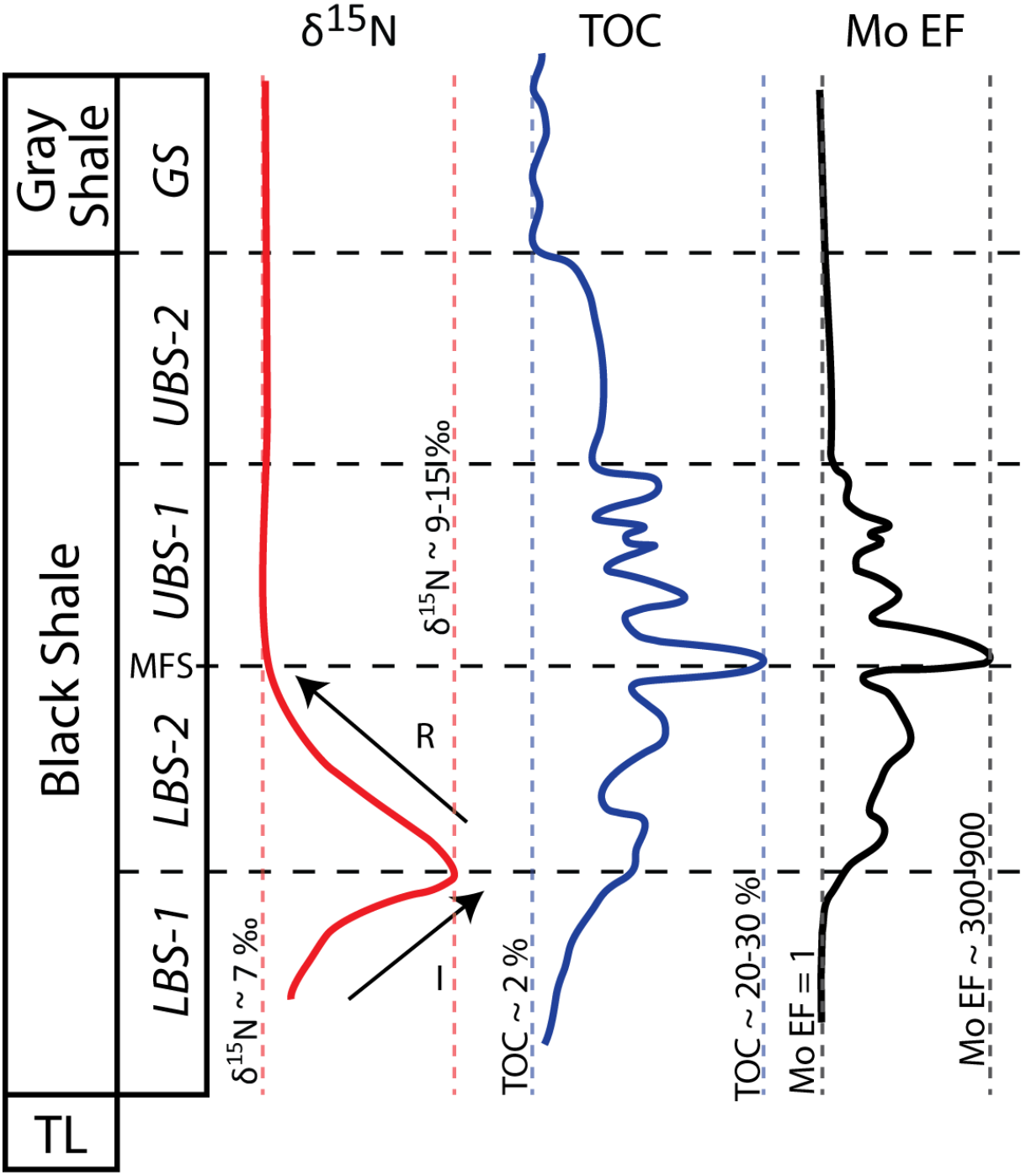

Figure 2.3 Generalized geochemical signatures used to identify depositional units of the Heebner Shale. TL = transgressive limestone, LBS = lower black shale, UBS = upper black shale, GS = gray shale, and MFS is the maximum flooding surface (per Algeo et al., 2004). TOC = total organic carbon, Mo_{EF} = molybdenum enrichment factor, and I and R show the intensification and relaxation stages of $\delta^{15}N$ excursions, respectively. Note that LBS-2 is equivalent to "MBS" of Herrmann et al. (2015). See text for discussion.

2.3.2. Total organic carbon

TOC is enriched (>2.5 %) in the Heebner Shale, varying both spatially (between sections) and temporally (within individual sections) across the NAMS (Fig. 2.4). The OK-BC section (located on the northern margin of the Anadarko Basin) exhibits lower average TOC values (~5-20 %) than the other study locations due to siliciclastic dilution from the Ozark and Wichita-Amarillo uplifts to the south (Algeo and Herrmann, 2017; Schultz and Coveney, 1992; Yang et al., 2003). The IRH section exhibits the highest TOC contents (peaks of ~25-30 %), Midcontinent Shelf sections other than IRH and OK-BC have TOC peaks of ~20 %, and Illinois Basin sections have peak TOC values of ~25 %. In each study section, TOC increases upsection from <2.5 % at the base of LBS-1 to ~18-26 % at the MFS (= LBS-2/UBS-1 contact). TOC then decreases upsection through UBS-1, before stabilizing at ~5 % in UBS-2, and then dropping again to <2.5 % in the GS. Core CC has an anomalous TOC peak within UBS-2 (~20 %) that does not exhibit concurrent TE enrichment and that has not been observed at any other sample site.

The black shale submembers of all study sites exhibit high-frequency TOC cyclicity (at length scales of 2-10 cm) between minima of ~5-20 % and maxima of ~15-30 %, a pattern that was also observed in older cyclothemic core shales (Algeo et al., 2004, 2008b). The number of internal TOC peaks is nearly the same (~8 to 10) in all study sections, and their characteristics (e.g., the number and shape of peaks, clustering of peaks, and relationship to other stratigraphic markers such as the positive $\delta^{15}N$ marker) allow correlation of most individual TOC maxima across the entire study area with little to no uncertainty. Thus, this procedure provides a highly detailed, regional, internal correlation framework for the Heebner Shale of unparalleled (~1- to 5-cm resolution) stratigraphic resolution (Fig. 2.4). Similar high-resolution correlation frameworks were previously developed for the Stark and Hushpuckney shales, slightly older Upper Pennsylvanian cyclothemic core shales of the NAMS (Algeo and Heckel, 2008; Herrmann et al., 2015).

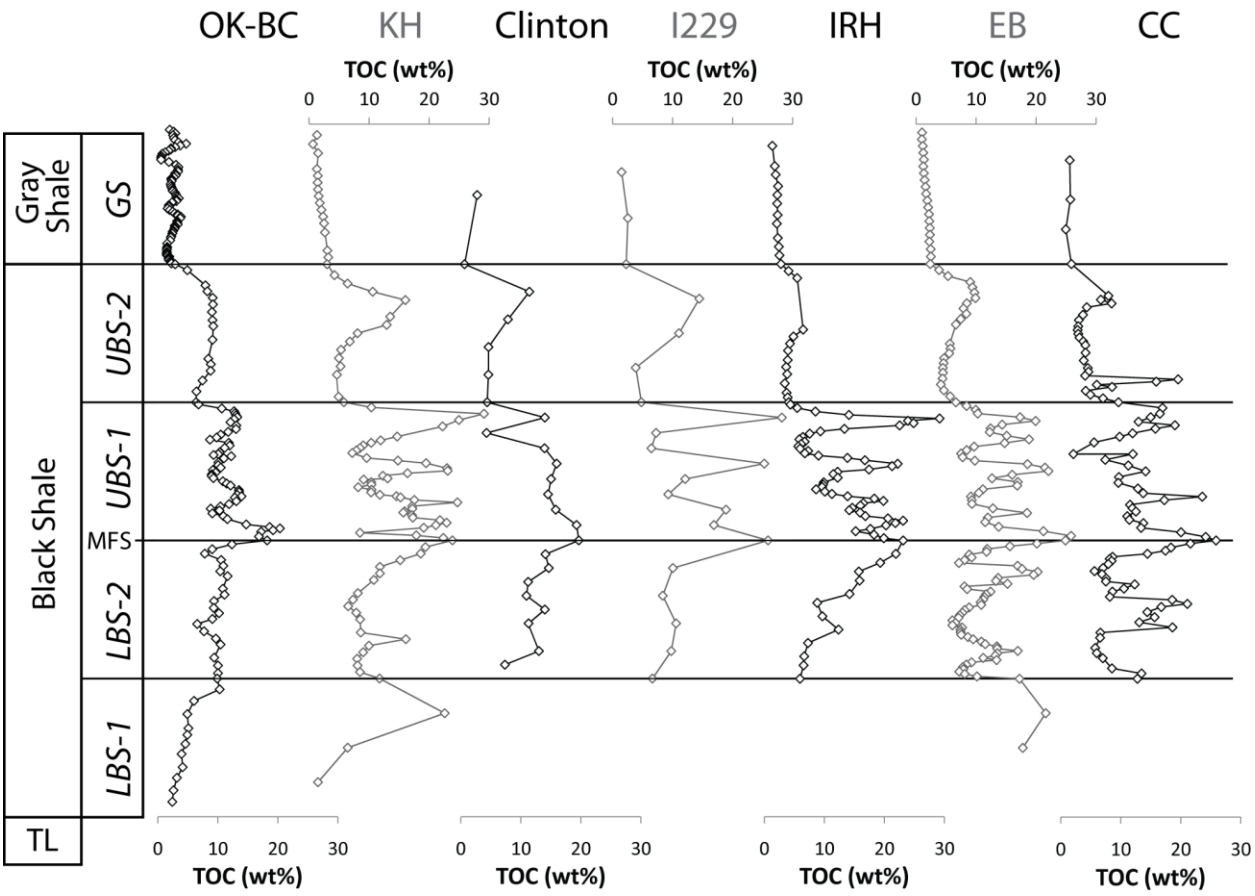

Figure 2.4. Depth-adjusted total organic carbon (TOC) profiles for all study locales. See Figure 2.3 caption for other abbreviations

TOC-vs-C/N plots can be used for determining sources of organic matter, i.e., marine versus terrestrial. The OK-BC, EB, and CC sections exhibit higher C/N ratios (~20 - 35) than other Midcontinent Shelf sections (~10 - 25) (Fig. 2.5). The LBS-1 and LBS-2 units generally yield the highest C/N ratios (~25 in the midcontinent and ~ 30 in the Illinois Basin), followed by a decline at the MFS (= LBS-2/UBS-1 contact) (~20). The UBS-2 and GS units have the lowest C/N ratios (~15 - 20).

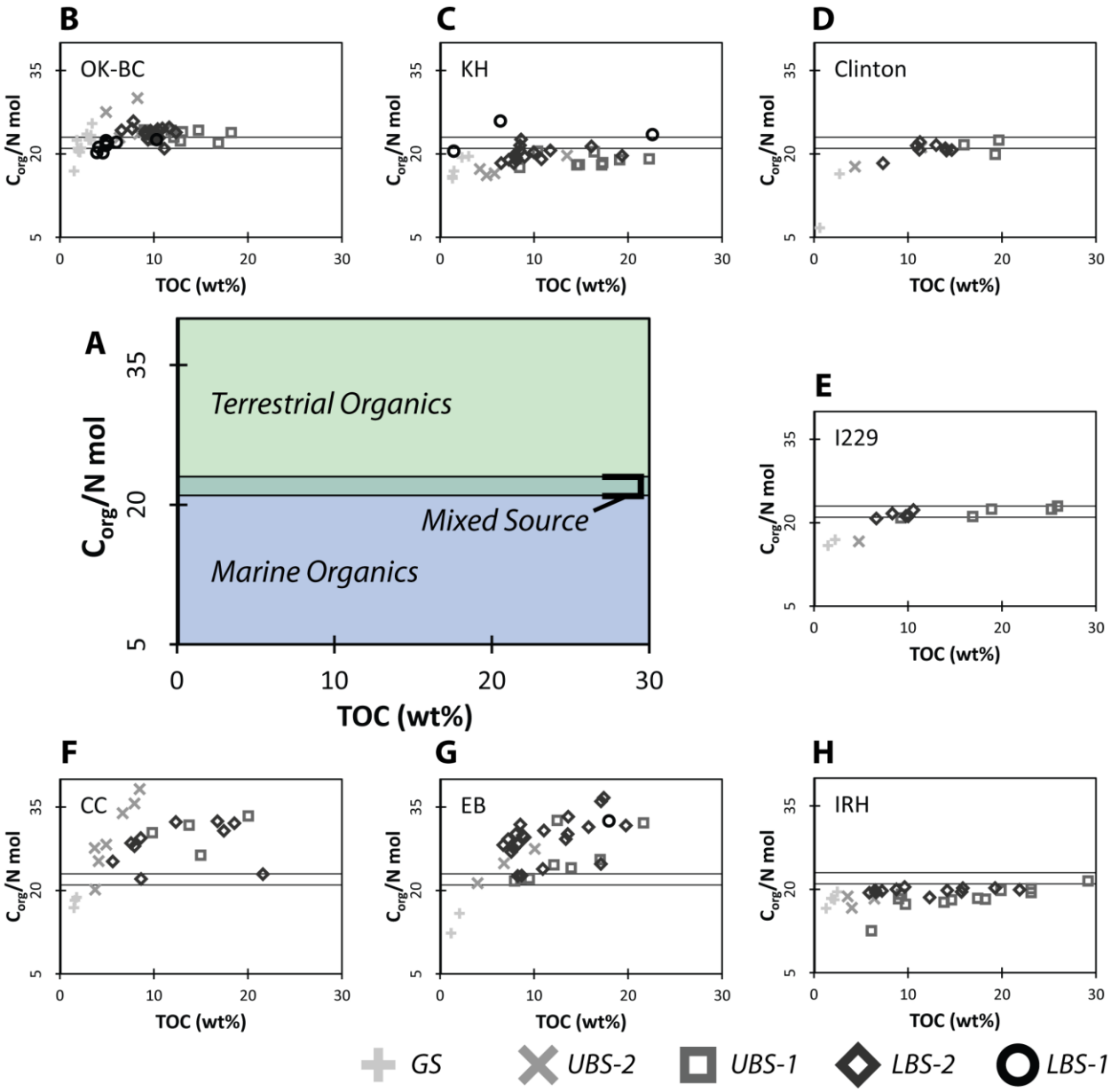

Figure 2.5 Crossplots of C_{org}/N molar to TOC%, plotted by depositional unit (symbols). Interpretation of C_{org}/N ratios is based on Algeo et al. (2008b), who identified C_{org}/N ratios of ~19-23 and ~21-25 for marine- and terrestrial organic matter, respectively, in slightly older NAMS shales. Here, we adopt ratios of 21-23 as reflective of mixed OM sources, with lower and higher values indicative of dominantly marine versus terrestrial OM sources, respectively. In the present study, Illinois Basin samples contain a much larger proportion of terrestrial OM than other study locales. The LBS-1, LBS-2, UBS-1 and UBS-2 units commonly exhibit mixed OM sources, and GS contains mainly marine OM.

2.3.3. Major elements

Siliciclastic sediment sources can have unique clay-mineral compositions that allow identification of different detrital fractions and, potentially, their transport paths in marine environments (Wehausen and Brumsack, 1998). Differences in source mineralogy and weathering intensity can produce unique ratios of K/Al to Mg/Al, reflecting varying proportions of K-rich clays (e.g., illite) and Mg-rich clays (e.g., smectite or chlorite). For the Heebner Shale, samples from the six study sections for which major-element data are available cluster into three unique zones (Fig. 2.6). The OK-BC and IRH sections have similarly high enrichments of K/Al (0.25-0.45) and Mg/Al (0.3-0.9), representing type Z1. Samples from OK-BC have a tighter range of Mg/Al than IRH (0.3-0.6 versus 0.3-0.9). The EB section exhibits by similar K/Al values (0.3-0.4) but lower Mg/Al ratios (0.2-0.3). The KH, I229, and CC sections are characterized by lower ratios for both K/Al (0.10-0.25) and Mg/Al (0.2-0.3).

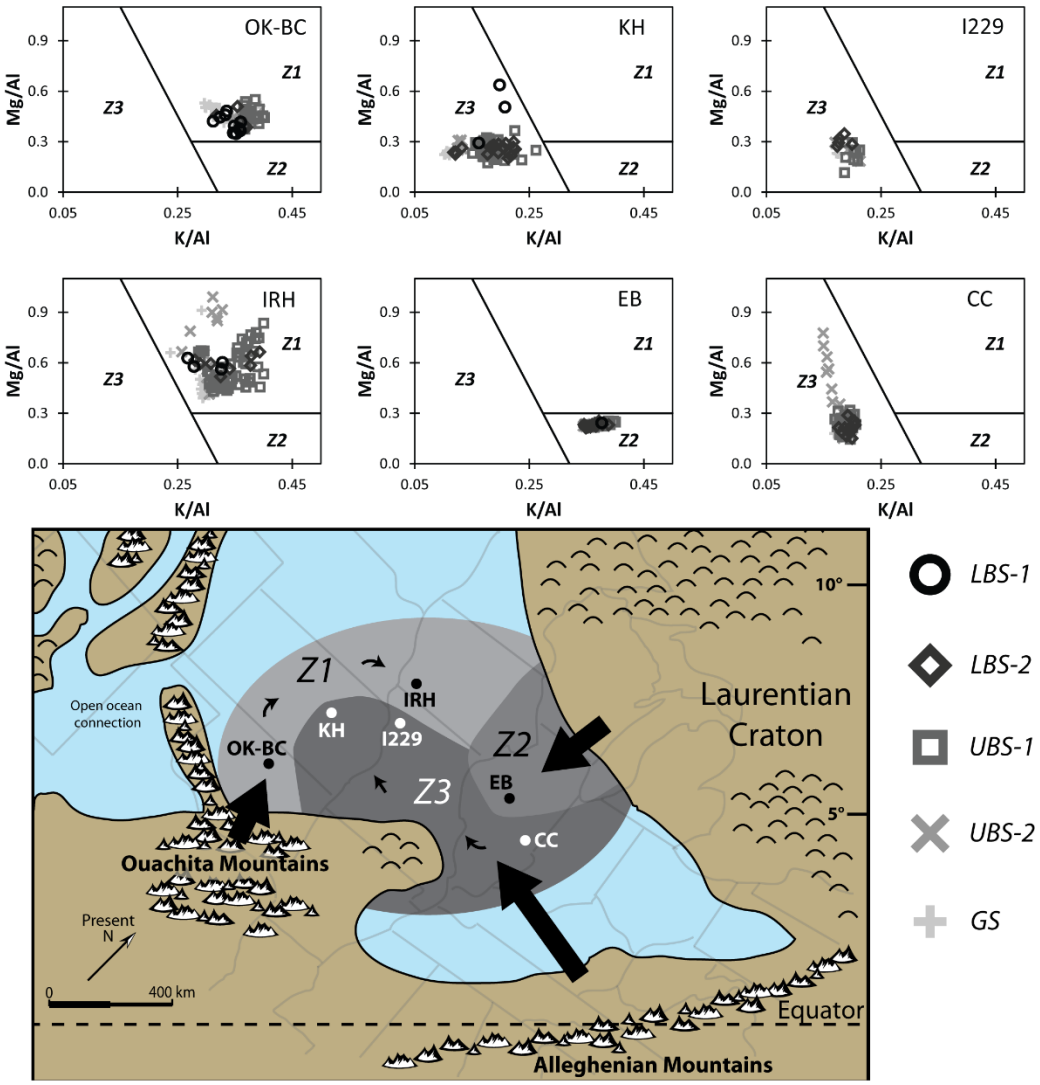

Figure 2.6 Crossplots of whole-rock Mg/Al against K/Al for sample locales, plotted by depositional unit (symbols). Samples cluster in three distinct fields (Z1, Z2, Z3) interpreted as evidence of three different terrestrial siliciclastic source fluxes (map, large arrows), with subsequent redistribution in the marine environment (map, small arrows).

2.3.4. Stable carbon and nitrogen isotopes

$\delta^{13}C$ values exhibit a negative excursion observed in sample sites across the NAMS. In the Heebner core shale, background $\delta^{13}C$ values of the LBS-1 and GS range between ~ –25 and –27 ‰. Maximum excursions in the LBS-2 range from ~ –28 to –30 ‰, with an excursion magnitude of ~2.5 to 4 ‰ (Fig. 2.7). In LBS-1, $\delta^{13}C$ values decrease upcore (from ~ –26 ‰ in Midcontinent Shelf samples and ~ –28 ‰ in Illinois Basin samples) to peak negative values in LBS-2. In LBS-2, Midcontinent Shelf samples are relatively stable at ~ –30 ‰ and Illinois Basin samples are relatively steady at ~ –28 ‰. $\delta^{13}C$

values increase steadily through UBS-1, UBS-2, and GS, returning to background values of ~ –27 ‰ in Midcontinent Shelf samples and ~ –25 ‰ in Illinois Basin samples.

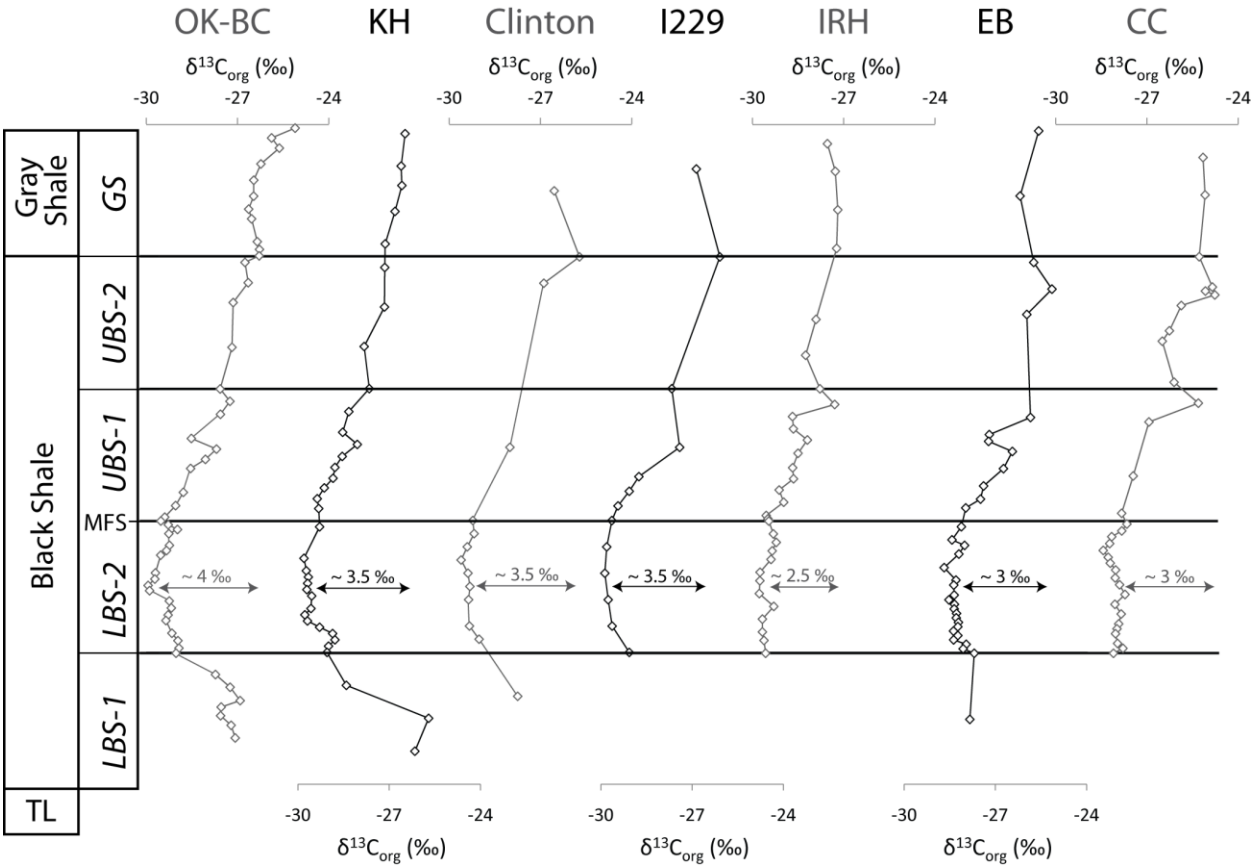

Figure 2.7 Depth-adjusted carbon isotope profiles for all study locales. Negative excursions of ~2.5 to 4 ‰ are observed within the LBS-2 unit at all locales.

Nitrogen isotopes in cyclothems of the NAMS are relatively constant in UBS-1, UBS-2 and GS, with a background $\delta^{15}N$ value of ~ +5 to +7 ‰ and exhibit a pronounced positive excursion (~2.5 to 7.5 ‰), peaking at the LBS-1-LBS-2 boundary. Heebner $\delta^{15}N$ excursion values exhibit a gradient with heaviest nearest OK-BC and in the Illinois Basin, and lightest at IRH (Fig. 2.8). In the LBS-1, values increase from background (~ 7 ‰ in the Midcontinent Shelf samples and ~ 5 ‰ in the Illinois Basin samples) to the maximum excursion at the LBS-1/LBS-2 boundary. During deposition of LBS-2, $\delta^{15}N$ values return (or "relax") to background values (~ 7 ‰ for Midcontinent Shelf samples and ~ 5 ‰ in Illinois Basin samples), with little intra-core variation through the UBS-1, UBS-2, and GS.

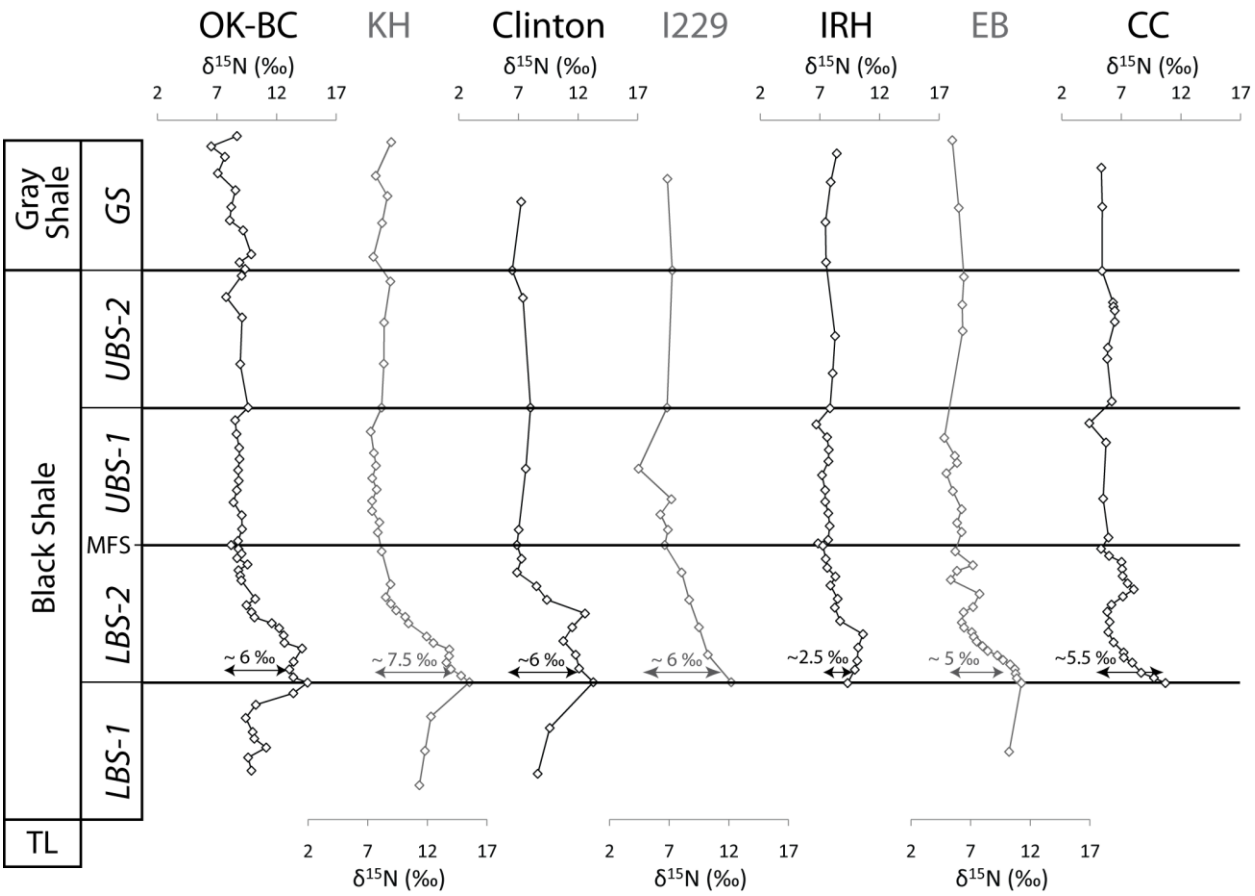

Figure 2.8 Depth-adjusted nitrogen isotope profiles for all study locales. By definition, excursions peak at the LBS-1/LBS-2 contact before returning to background levels below the MFS. The Illinois Basin locales (EB and CC) exhibit an additional minor excursion within upper LBS-2 or lower UBS-1.

2.3.5. Molybdenum concentrations and enrichment factors

Molybdenum is present in oxic seawater as Mo(VI), mostly in the form of soluble molybdate, whereas it is reduced to Mo(IV), mostly in the form of particle-reactive thiomolybdates, in the presence of hydrogen sulfide levels sufficient to activate a "switch point" (>~11 μM H_2S_{aq}) (Erickson and Helz, 2000; Helz et al., 1996). Thiomolybdates are scavenged from the water column by forming bonds with metal-rich particles, organic particles, and iron sulfides (Tribovillard et al., 2006). Mo concentrations are therefore generally high (>25 ppm) in sediments deposited under euxinic environments (Scott and Lyons, 2012; Tribovillard et al., 2006). Depth-adjusted plots of Mo enrichment factors (EF) (Fig. 2.9) show strong variability across the NAMS, with the most enriched sections being furthest to the northeast (at IRH), with gradients toward lower values eastward into the Illinois Basin and southwestward into the

Anadarko Basin. Within each section, Mo_{EF} increases upsection through LBS-1 and LBS-2 to a peak (commonly ~300-900) at the MFS (= LBS-2/UBS-1 contact). Mo_{EF} remains high in UBS-1 but declines abruptly to lower values (~10-100) in UBS-2, with a second drop in the GS (~1-10).

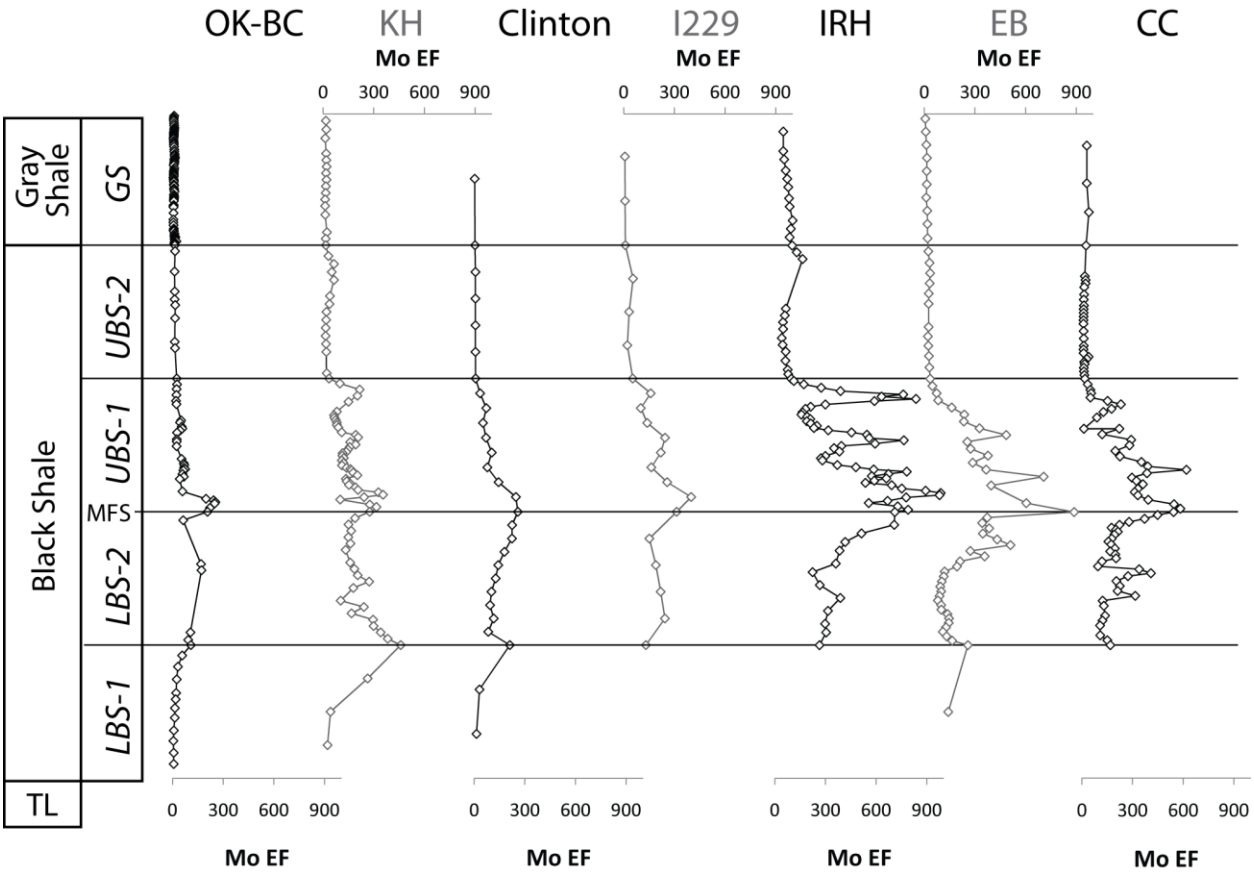

Figure 2.9 Depth-adjusted molybdenum enrichment factor profiles for all study locales.

Crossplots of TEs versus TOC can be used to evaluate redox conditions and trace-metal depletion in euxinic marine systems, e.g., due to falling aqueous trace-metal concentrations linked to authigenic removal to the sediment in (semi-)restricted marine systems (Algeo and Maynard, 2004; Algeo and Lyons, 2006; Algeo and Rowe, 2012). In the Heebner Shale, Mo and TOC show covariation in UBS-1 and LBS-2, indicating euxinic environments (Fig. 2.10) (cf. Algeo and Lyons, 2006). Mo-TOC crossplots (Fig. 2.10) for euxinic facies (LBS-2 and UBS-1) exhibit a wide range of slopes (~5-30), plotting in the "moderately" or "strongly" restricted fields.

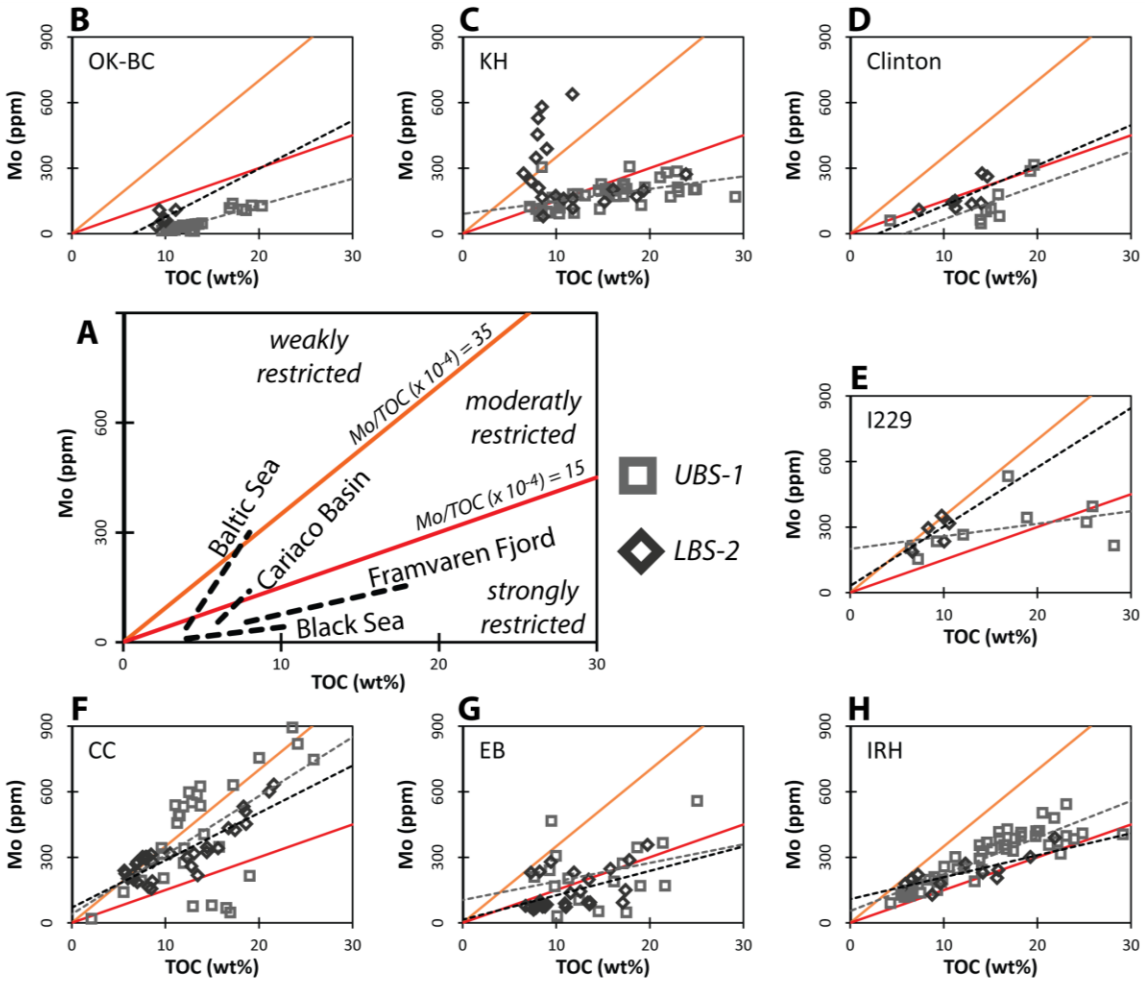

Figure 2.10 Mo versus TOC for all study locales, plotted by depositional unit (symbols). Dashed lines represent sample trends from modern basins and solid lines separate fields of weak, moderate, and strong watermass restriction (from Algeo and Lyons, 2006; Jilbert and Slomp, 2013).

Mo_{EF} versus U_{EF} crossplots are used to investigate patterns of authigenic trace-element enrichment in sediments and their relationship to water-column processes such as Fe-Mn redox cycling (Algeo and Tribovillard, 2009). In the Heebner Shale, Mo_{EF} and U_{EF} generally increase from LBS-1 to LBS-2 and UBS-1 and then decrease to UBS-2 (Fig. 2.11). EFs are sufficiently high in LBS-1 to UBS-1 to indicate generally euxinic conditions, but more modest EFs in UBS-2 and GS are consistent with mainly suboxic or strongly fluctuating redox conditions. The samples for each section do not follow any single pattern as determined from modern marine studies (Algeo and Tribovillard, 2009) but, instead, fall broadly across the open-marine, restricted-marine, and particulate shuttle trends (Fig. 2.11). The same pattern was previously noted for older Pennsylvanian cyclothemic core shales (Algeo and Tribovillard,

2009) and was interpreted to reflect a complex redox history, characterized especially by high-frequency redox fluctuations.

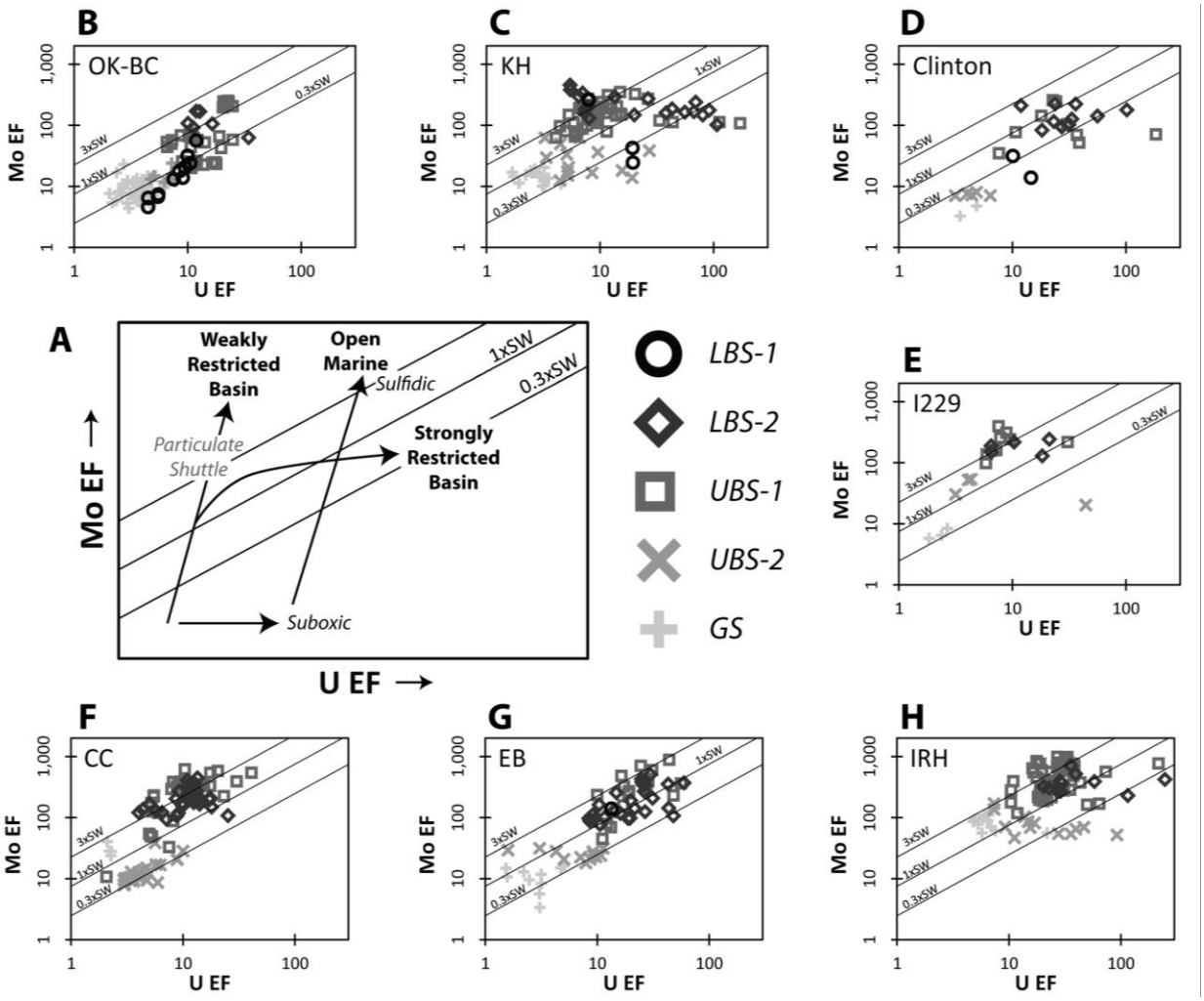

Figure 2.11 Molybdenum versus U enrichment factors for all study locales, plotted by depositional unit (symbols). Panel A shows the interpretative legend for redox conditions. Diagonal lines show 0.3×, 1×, and 3× modern seawater Mo/U ratios for reference (after Algeo and Tribovillard, 2009).

2.4. Discussion

2.4.1. General watermass conditions in NAMS during Heebner Shale deposition

2.4.1.1. Degree of deep watermass restriction

In euxinic, reducing environments, Mo/TOC ratios are used to track removal of Mo to the sediment and can help investigate the degree of subpycnoclinal restriction of a euxinic environment (Algeo and Lyons, 2006; Algeo, 2012; Herrmann et al., 2012; Neumeister, 2016). While direct evidence

of a pycnocline in the NAMS is challenging, fresh water fluxes in modern restricted seas such as the Black Sea or the Baltic Sea support watermass density gradients, setting up a pycnocline. The open ocean generally has a density differential of <1 psu, however the Black Sea and Baltic Sea have deep-to-shallow density differentials of ~5 and 4 psu respectively (Algeo et al., 2008a). Algeo et al. (2008a) estimated a differential of ~11±4 psu in the NAMS, sufficient to sustain a strong pynocline.

High Mo/TOC ratios (~45) are indicative of low restriction while lower ratios (~4.5) are the resulted of restricted deep waters with longer bottom water renewal times. For the Heebner Shale, euxinic conditions in LBS-2 and UBS-1 can be established by elevated Mo_{EF} (~20-900; Fig. 2.9) and covariation between Mo concentrations and TOC (Fig. 2.10), consistent with previous work examining iron speciation and other geochemical analyses illustrating that analogous shales experienced euxinic or ferruginous anoxic conditions (e.g. Algeo and Heckel, 2008; Cruse and Lyons, 2004; Hatch and Leventhal, 1997; Herrmann et al., 2012). Examining only the LBS-2 and UBS-1 where euxinic conditions have been established, Mo-TOC ratios are indicative of moderately restricted to strongly restricted basins (Fig. 2.10) (Algeo and Lyons, 2006).

Mo concentration-TOC crossplots of the euxinic intervals of the NAMS can be calibrated to modern environments in order to semi-quantify restriction (Fig. 2.10). The modern Framvaren Fjord and Cariaco Basin have Mo/TOC ratios of ~10 and 40 respectively (Algeo and Lyons, 2006; Jilbert and Slomp, 2013). In the Heebner core shale, best fit lines of LBS-2 samples have Mo/TOC ratios of 11-27 with an average of 19. UBS-1 samples have Mo/TOC ratios of 6-29, with an average of 13. These low ratios suggest a restricted environment in the LBS-2 and UBS-1 of the NAMS, more similar to Framvaren Fjord than the Cariaco Basin.

Restricted, euxinic basins lead to reservoir effects for molybdenum, and result in a relative depletion in Mo_{EF} with respect to U_{EF} (Algeo and Maynard, 2008; Algeo and Tribovillard, 2009). This is observed in the LBS-2 and UBS-1 in Mo_{EF}-U_{EF} crossplots by the flat Mo_{EF} trend during these intervals (Fig. 2.11). Mo is removed more quickly than the open ocean can provide resupply, resulting in the relative depletion in sediment with respect to U. Under constant oxic conditions, in open marine

environments, sediment would not preferentially incorporate U or Mo, thus it would incorporate sea water U:Mo ratios. The abundances of Mo and U may differ in the past than what they are today, though samples directly incorporating sea water values would trend parallel to the modern sea water ratio (Fig. 2.11). Euxinic conditions lead to preferential incorporation of Mo over U into the sediment (Algeo and Tribovillard, 2009; Scholz et al., 2013). In strongly restricted basins, relative Mo enrichments will be followed by relative Mo depletion due to reservoir effects, with non-parallel trendlines (more shallow) with respect to the seawater reference lines (Fig. 2.11A). The geochemical proxies, taken together, provide robust evidence for water masses with long renewal times during the euxinic intervals of the LBS-2 and UBS-1. Though there is limited evidence for intrabasinal bathymetric restriction (Algeo et al., 2008a; Algeo and Herrmann, 2018; Algeo et al., 2008b), small bathymetric perturbations (Algeo and Herrmann, 2018) or the sheer size of the NAMS (> 1000 km across) could provide restrictive conditions for bottom water in which Mo could be incorporated into the sediment, decreasing the aqueous concentration of Mo in the deep watermass (Herrmann et al., 2012).

Recent work on the Hushpuckney Shale (an analogous NAMS shale) has attributed trends in Midcontinent Shelf Mo and U enrichments to nutrient trapping associated with the Mississippi River Arch bathymetric high, termed the estuarine wedge effect (Algeo and Herrmann, 2018). The Hushpuckney exhibits elevated Mo_{EF} and U_{EF}, and decreased TOC at sample sites on the Midcontinent Shelf with respect to the Illinois Basin. While nutrient trapping explains Hushpuckney TE enrichments, Heebner Shale samples exhibit different patterns, with similar Mo_{EF} and U_{EF}, and TOC between the Midcontinent Shelf and the Illinois Basin. This could be due to erosion of the Mississippi River Arch after deposition of the Hushpuckney shale or deeper water environments during Heebner deposition allowing the euxinic salt water wedge to extend unimpeded across the Mississippi River Arch. Reduced marine organics (as evidenced by C_{org}/N mol ratios, discussed further in section 4.2.2; Fig. 2.5) and elevated Mo_{EF} and U_{EF} are observed in the Illinois Basin sample locales (EB and CC), suggesting that the estuarine wedge effect may have been a dominant process in trace metal uptake in these TE-enriched (Mo_{EF} up to 900; Fig. 2.9) study sites (Algeo and Herrmann, 2018). This provides further evidence of

basin scale circulation of oxygen poor bottom waters across the Midcontinent Shelf into the Illinois Basin.

2.4.1.2. Water-column denitrification in the NAMS

$\delta^{15}N$ values indicate that seawater circulated through the NAMS, recorded as a positive $\delta^{15}N$ excursion at the LBS-1/LBS-2 boundary. The excursion is smallest (~ +2 ‰) at IRH, where less restricted access to seawater renewal was recorded by TE abundance in the LBS-2 and UBS-1, and larger (~ +5 ‰) into the Illinois Basin and towards OK-BC (Fig. 2.8). The positive excursion is the result of upwelling in the eastern tropical Panthalassic Ocean supplying nutrients and fueling denitrification (Algeo et al., 2008a). Denitrified water was then drawn into the NAMS and the positive isotopic signature from the seawater is incorporated into the sediment in a time-correlative excursion (Algeo et al., 2008a; Herrmann et al., 2015). In reducing conditions, such as the subpycnoclinal waters, further denitrification would take place as it circulates away from the open ocean connection towards areas with longer ocean water renewal times. Thus the location with the weakest $\delta^{15}N$ excursion (IRH, Fig. 2.8) would have the most direct connections to the open ocean and areas with larger excursions representing water masses in which further denitrification has taken place (Illinois Basin and Paleo Southwestern Midcontinent Shelf).

Terrestrial $\delta^{15}N$ are thought to be ~ 0-4.7 ‰ (Rimmer, 2006; Whiticar, 1996), suggesting that the increased $\delta^{15}N$ values towards paleo-shore lines are due to further denitrification rather than terrestrial organic input. Illinois cores have decreased $\delta^{15}N$ backgrounds and additional, smaller positive $\delta^{15}N$ excursions in the upper LBS-2 and the UBS-1. Decreased $\delta^{15}N$ backgrounds are likely due to the isotopically light input of terrigenous materials. C/N ratios confirm that there are large proportions of terrestrial organics in the Illinois basin with respect to the Midcontinent Shelf. The regional extent and smooth nature of the large (~5 ‰) excursion at the LBS-1- LBS-2 boundary implies a large scale trend, in this case circulation of denitrified water, as opposed to the smaller, not well correlatable excursions (~1 ‰) of the Illinois Basin UBS-1 and LBS-2 which are more consistent with a local process. The smaller, additional excursions correspond with TOC minimums (Fig. 2.4) suggesting that they correspond with

periods of reduced terrestrial input. Thus the smaller changes in $\delta^{15}N$ represent shifts from primarily terrestrial organics (~ 0 to +4.7 ‰) to more marine organics seen in other sample locations (~ +7 ‰).

2.4.2. Gyral circulation patterns in NAMS during Heebner Shale deposition

2.4.2.1. Background: controls on gyral circulation in modern epeiric marine systems

Gyral circulation is controlled mainly by wind-induced drag and the Coriolis Effect, which is due to the Earth's rotation (Emery and Csanady, 1973). It operates more strongly in the surface layer of large watermasses, down to the base of the wind-mixed surface layer (~100-200 m), than in the deep ocean, where currents are far slower than in the surface layer. Wind-induced drag forces decrease with depth, with deep ocean current being driven through gradients in temperature and salinity. In stratified water bodies, the kinetic energy associated with gyral circulation may be confined to the layer above the pycnocline, intensifying gyral circulation (Schwab et al., 1995). In this context, large shallow epeiric seas, especially those with vertically stratified water columns (such as the NAMS), should be subject to comparatively strong gyral circulation patterns.

In the open ocean, wind drag imparts a net force (termed "Ekman transport") on surface waters that is ~45° to the right (left) of the wind direction in the Northern (Southern) Hemisphere. Low-latitude Trade Winds in conjunction with mid-latitude Westerlies drive large subtropical gyres in the Atlantic, Indian, and Pacific oceans, with CW rotation in the Northern Hemisphere and CCW rotation in the Southern Hemisphere owing to the Coriolis Effect. However, the direction of gyral rotation can deviate from this general pattern in smaller ocean basins and semi-enclosed water bodies if other forces override the Coriolis Effect. There are two main types of overriding forces: (1) frictional forces exerted by local wind or water circulation patterns, and (2) jet-type effects related to water flow into a basin. The CCW-rotating subpolar gyres in the North Atlantic and North Pacific oceans are examples of frictional drag from the much larger, CW-rotating subtropical gyres, acting like a two-gear system. Wind curl, or the asymmetric distribution of surface wind stress, can be produced due to geographic asymmetries of basins, resulting in CCW circulation in the Northern Hemisphere, as seen in the modern Baltic Sea and Black Sea (Emery and Csanady, 1973; Prinsenberg, 1986). Bathymetric highs may isolate individual basins of

larger seas and allow for both cyclonic and anticyclonic gyres in close proximity, such as in the Baltic Sea (Lehmann et al., 2002).

2.4.2.2. Organic carbon sources and NAMS circulation

Ratios of organic carbon to nitrogen can potentially differentiate between terrestrial and marine organic matter sources (Fig. 2.5). Terrestrial organics generally have a much higher primary C/N ratio (> 20) than marine organics (4-10) (Meyers, 1994), although degradation in the burial environment can result in higher C/N ratios of sedimentary organic matter of marine origin (Lamb et al., 2006). Algeo et al. (2008b) estimated sedimentary TOC/N ratios of ~19-23 for marine organic matter and ~21-25 for terrigenous organic matter in older Pennsylvanian core shales (i.e., the Muncie Creek, Stark, and Hushpuckney shales; Fig. 2.5) based on correlations to organic maceral abundances. They inferred that the higher-than-typical TOC/N ratios for marine organic matter in these shales were due either to preferential bacterial destruction of labile N-bearing compounds (i.e., a diagenetic cause) or to low nutrient N:P ratios relative to the Redfield ratio (C:N:P = 106:16:1) (i.e., a primary environmental cause). Previous studies have found up to 50-70 % terrestrial organics in the black shale (specifically the LBS) using Rock-Eval and vitrinite reflectance (Algeo and Heckel, 2008; Ece, 1985, 1987, 1989; Wenger and Baker, 1986).

In the present study units, we encountered a wider range of sedimentary TOC/N ratios than previously reported for older Pennsylvanian core shales (10 – 30). Adopting a TOC/N ratio of 21-23 as an approximate threshold between marine and terrestrial organic sources (per Algeo et al., 2008b), our present study sections define three groups: (1) the four Midcontinent Shelf sections (KH, Clinton, I229, and IRH) exhibit TOC/N mostly <21-23, implying dominantly marine organic sources, (2) the two Illinois Basin sections (EB and CC) exhibit TOC/N mostly >21-23, implying dominantly terrestrial organic sources, and (3) the northern Anadarko Basin section (OK-BC) exhibits TOC/N values that mostly straddle the 21-23 threshold, suggesting organic matter derived in subequal amounts from marine and terrestrial sources. There is some stratigraphic variation (i.e., by unit) in the proportion of marine and terrestrial organics within each section (the most consistent feature being relatively more marine organics

in the GS unit), but the geographic pattern is more pronounced. The geographic pattern conforms quite well with paleoenvironments within the NAMS: (1) the Midcontinent Shelf was located relatively far (at least several 100 km) from land areas, limiting terrestrial inputs (Heckel, 1977; Algeo et al., 2008a), (2) the Illinois Basin was shallower and closer to land areas, leading to extensive peripheral coal-swamp development (Heckel, 1977), and (3) the Anadarko Basin was the site of both upwelling along the southern margin of the Midcontinent Shelf, stimulating marine productivity, and large-scale terrigenous siliciclastic inputs from the rising Ouachita-Wichita uplifts, co-delivering terrestrial organic material (Heckel, 1977, Yang et al., 2003).

Organic $\delta^{13}C$ values can provide further insights regarding organic matter sources and diagenetic effects. Marine organic matter is typically sourced from seawater bicarbonate, which has a $\delta^{13}C$ of ca. 0 ‰, whereas terrestrial organic matter is sourced from atmospheric CO_2, which had a pre-industrial $\delta^{13}C$ of ca. –7 ‰, though in the Late Paleozoic, marine organics had similar $\delta^{13}C$ values to terrestrial organics, owing to increased availability of atmospheric CO_2 (Popp et al., 1989, Meyers, 1994). Relative to their respective sources, the $\delta^{13}C$ compositions of marine and terrestrial organic matter are shifted by –20 to –25 ‰ as a result of photosynthetic fractionation (ε_p) (Hayes et al., 1999). Non-photosynthetic organisms can provide secondary inputs of organic carbon to the sediment, augmenting the $\delta^{13}C$ of preserved TOC. This is the case in the Black sea, where sulfide-oxidizing bacteria flourish along the oxycline, fixing DIC which is isotopically lighter than DIC of the photic zone (Hayes et al., 1999). In the geographically restricted NAMS, there is a ~2.5 - 4 ‰ negative excursion during the LBS-2 (Fig. 2.7). A relatively strong input flux into the NAMS during the LBS-1 and LBS-2 provides terrigenous organics to distal settings (evidenced by TOC/N ratios), stimulating production of sulfide and creating water column conditions favorable to sulfide-oxidizing bacteria (similar to the Black Sea). This input of isotopically light organic material drives the negative $\delta^{13}C$ excursion in the LBS-2, consistent with generally higher C/N ratios for the LBS-2, UBS-1 and UBS-2 across the NAMS (Fig. 2.5). The minimum $\delta^{13}C$ value is ~ -30‰ in all Midcontinent Shelf sections, but -28 to -29‰ in the two Illinois Basin sections (Fig. 2.7), suggesting slight differences in microbial communities between these two areas, with a greater proportion

of anaerobic chemoautotrophs on the Midcontinent Shelf (Ruby et al., 1987). While the $\delta^{13}C$ excursion provides an opportunity to trace the input of terrigenous organics, it can help illuminate spatial variations as well. The excursion will be most pronounced (largest excursion and quick return to background) near the source of terrestrial organics. During Heebner deposition, IRH has the smallest excursion and retains the most negative $\delta^{13}C$ background, indicating less influence from terrestrial runoff, though prolonged input of chemoautotrophic organisms to the sediment.

The magnitude and extent of $\delta^{13}C$ excursions along with C/N ratios provide evidence of significant terrestrial inputs during Heebner Shale deposition. In the Heebner Shale, organic carbon speciation shows elevated terrestrial contributions in three sample locations, OK-BC, EB, and CC (Fig. 2.5). Elevated terrestrial organic contributions indicate that these sample locations were near a source of terrestrial carbon. OK-BC is on the paleo-west extreme of the NAMS samples, while EB and CC are on the paleo-southeast, requiring at least two unique sources for terrestrial organics. This is consistent with expected paleogeography, in which a young mountain belt, the Ouachita Orogen, is near OK-BC, and a continental mass to the east is capable of supplying the Illinois Basin samples. The spatial resolution of this study allow for the demonstration of terrestrial influence well into the Midcontinent Shelf, far (~1000 km) from the inputs of the Appalachian Basin, consistent with previous salinity studies (Roark et al., 2017). The terrestrial organics in the Northern Midcontinent Shelf provide evidence for basin scale circulation, capable of transporting the terrestrial organics away from the source. C/N ratios of this study show terrestrial organics originate near the Illinois Basin and OK-BC, while $\delta^{13}C$ values show a migration of these organics to the north from OK-BC and west from the Illinois Basin.

2.4.2.3. Clay-mineral distributions and NAMS circulation

Sediment provenance is investigated through clay mineral speciation proxies, in the form of K and Mg enrichments (Wehausen and Brumsack, 1998). Previous studies have shown temporal trends in clay content of analogous NAMS shales (Algeo et al., 2004), though change in K-Mg ratios of the Heebner are independent of depositional unit, indicating that weathering products and input locations change very little over the course of core shale deposition.

Samples from the NAMS self-segregate into three zones with unique K and Mg ratios (Fig. 2.6). Zone 1 (Z1) has elevated Mg/Al (~0.4-0.8) and K/Al (~0.3-0.4), zone 2 (Z2) contains elevated K/Al (~0.35-0.4) and diminished Mg/Al (~0.2), and zone 3 (Z3) contains low Mg/Al (~0.1-0.3) and K/Al (~0.1-0.2). Each zone likely represents a unique sediment provenance. Samples which aggregate into each zone thus share similar source of sediment. KH, I229, and CC plot in Z3, suggesting transport of a common sediment source over a great distance (at least 800 km). Core KH intersects a linear transect between OK-BC and IRH, which plot in Z1, suggesting a non-linear (gyral) sediment transport between OK-BC and IRH (Fig. 2.6). Though Core EB is spatially near (~300 km) core CC in the Illinois Basin, EB plots in Z2 and thus has a unique sediment source. Samples nearest to the sediment source will have the most elevated terrestrial organic runoff (OK-BC, EB, and CC, Fig. 2.5), such that the freshwater and sediment input nodes would be the Ouachita Mountains, the Laurentian Craton, and the Alleghenian Mountains, consistent with expected paleogeography inputs based on mountain ranges (thick black arrows, Fig. 2.6). The three inputs along with the shape of the sediment provenance zones and migration of terrestrial organics would suggest a basin-scale clockwise rotation of the NAMS water.

2.4.2.4. Nitrogen-isotope evidence for gyral NAMS circulation

Terrestrial $\delta^{15}N$ are thought to be ~0-4.7 ‰ (Rimmer, 2006; Whiticar, 1996), suggesting that the increased $\delta^{15}N$ values towards paleo-shore lines are due to further denitrification rather than terrestrial organic input. Illinois cores have decreased $\delta^{15}N$ backgrounds and additional, smaller positive $\delta^{15}N$ excursions in the upper LBS-2 and the UBS-1. Decreased $\delta^{15}N$ backgrounds are likely due to the isotopically light input of terrigenous materials. C/N ratios confirm that there are large proportions of terrestrial organics in the Illinois basin with respect to the Midcontinent Shelf. The regional extent and smooth nature of the large (~5 ‰) excursion at the LBS-1- LBS-2 boundary implies a large-scale trend, in this case circulation of denitrified water, as opposed to the smaller, not well correlatable excursions (~1 ‰) of the Illinois Basin UBS-1 and LBS-2 which are more consistent with a local process. The smaller, additional excursions correspond with TOC minimums (Fig. 2.4) suggesting that they correspond with

periods of reduced terrestrial input. Thus the smaller changes in $\delta^{15}N$ represent shifts from primarily terrestrial organics (~0 to 4.7 ‰) to more marine organics seen in other sample locations (~7 ‰).

While $\delta^{15}N$ values indicate that the LBS-1 experienced seawater inundation into the NAMS, not all sample sites record this interval (I229 and CC). The missing interval suggests either (1) local bathymetric highs keeping sample locations above the chemocline or (2) local circulation patterns preventing the deposition of organic rich, black shale during this interval. Changes in paleo-bathymetry are difficult to discern, however there is no evidence for substantial high points across the Midcontinent Shelf of the NAMS (Algeo and Heckel, 2008; Algeo et al., 2008a; Heckel, 1977), though there is evidence for bathymetric highs separating basins (Algeo and Herrmann, 2017). As a result of some combination of the two possibilities, initiation of black shale deposition may not have occurred as a time correlative event across the NAMS.

The $\delta^{15}N$ positive excursion observed across the NAMS provides evidence for a denitrified water mass, circulating throughout the sea and becoming more denitrified as it migrates. Thus, the $\delta^{15}N$ peak tracks the sub-oxic bottom water from the north (where the excursion is smallest) to the east and south west, where (where the excursion intensifies). The excursion is most pronounced in the southwest, providing further evidence of a clockwise, basin scale gyre.

2.4.3. Integrated depositional model

Trace metal and stable isotope patterns demonstrate large scale mixing patterns which evolve temporally in the NAMS. The superestuarine circulation model is consistent with this circulation, with an oxygen poor, reducing bottom water entrained below a brackish water layer supplied by continental runoff, though the high spatial resolution of this study allows for a more three dimensional approach than previous wedge diagrams (Fig. 2.1) (Algeo et al., 2008a; Herrmann et al., 2015). To depict circulation patterns on a spatial and temporal basis, Figure 2.12 illustrates the subpycnoclinal bottom water on left and oxygenated brackish water layer on right. Proxies discussed above demonstrate at least three sources of terrestrial runoff to the system (Fig. 2.12, right) while previous studies (e.g., Algeo et al., 20008a) and

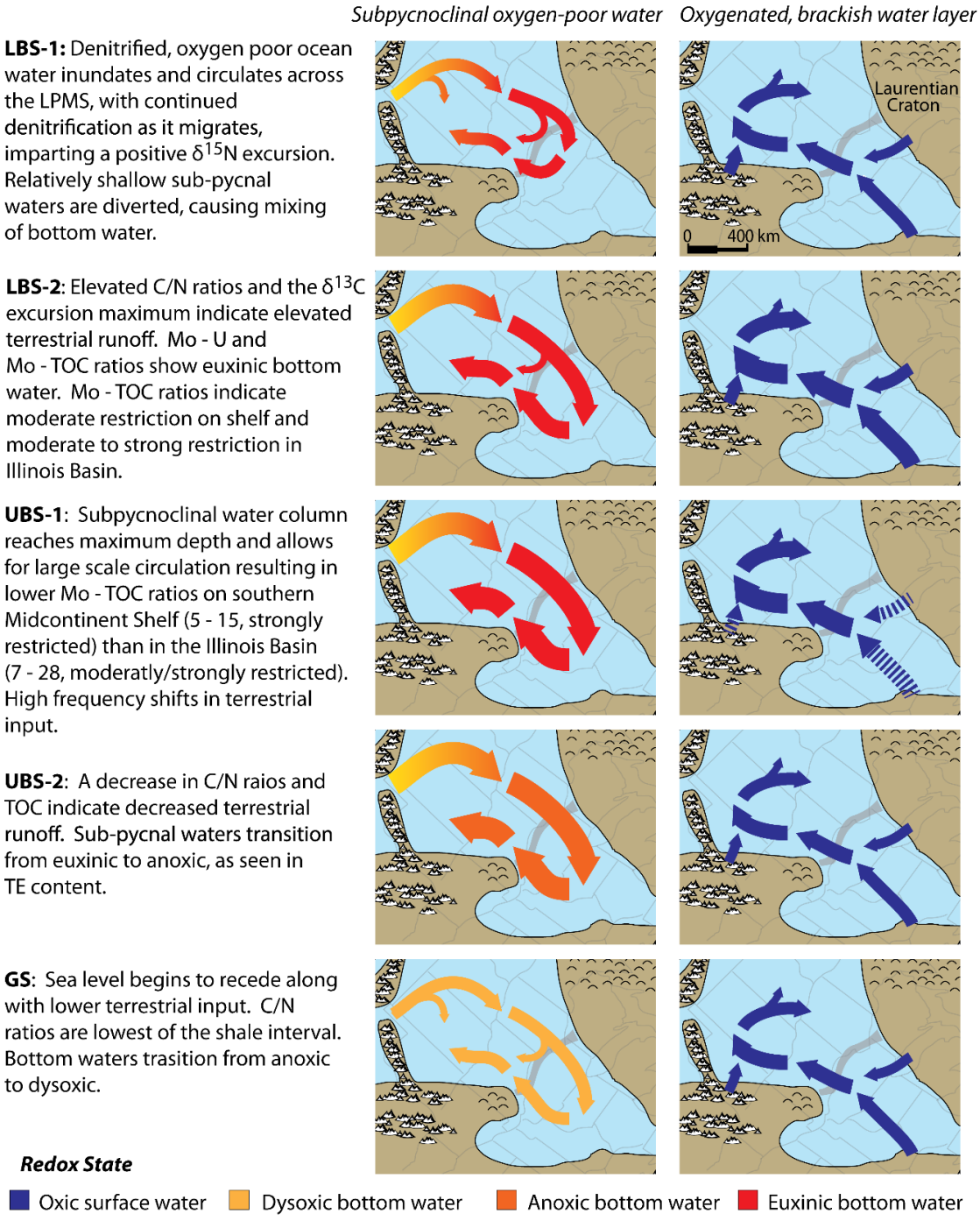

Figure 2.12 An integrated model of deposition for the Heebner Shale. The weight of the arrows is proportional to water column thickness. Strong runoff coupled with rising sea level floods the NAMS during the LBS-1. Water is circulated, and further denitrified as it innundates the Midcontinent Shelf. Euxinic conditions and freshwater runoff persisted through the LBS-2 and UBS-1. During deposition of UBS-2, freshwater input decreased and reducing conditions of bottom waters began to break down. By the GS, sea level was decreasing and bottom water became dysoxic.

aqueous Mo reductions in this study indicate a single source of oxygen-poor ocean water (Fig. 2.12, left). Proxies from this study support a basin scale clockwise rotation, indicating that the NAMS seems to have been large enough to be driven by Coriolis Effects similar to a large ocean basin and that tidal forces must have been small enough not to trigger counterclockwise flow due to inflow of waters during the tidal cycle.

Stable isotopes and C/N ratios show an influx of both open marine water and freshwater during LBS-1. At that time, sea level was relatively low (maximum flooding does not occur until UBS-1), which allowed limited bathymetric relief to deflect some of the bottom waters (Fig. 2.12). This provides anoxic (non-euxinic) waters to the western Midcontinent Shelf (OK-BS, KH), as recorded by trace metal covariation. Intensifying $\delta^{15}N$ values indicate that as sea level climbed during the LBS-1, there was large scale circulation of denitrified waters.

$\delta^{15}N$ values reached a peak at the boundary between the LBS-1 and the LBS-2. Sea levels continued to rise during the LBS-2, though some bottom water is diverted still at the Mississippi River Arch, resulting in Mo/TOC ratios that are slightly higher on the Midcontinent Shelf (~18 to 27) than in the Illinois Basin (~10 to 17). Proxies show restricted environments with long bottom water renewal times (hundreds of years) in the LBS-2. Trace metal covariation show widespread euxinic conditions. The $\delta^{13}C$ negative excursion reaches a minimum during this period, implying maximum terrestrial discharge into the NAMS (Fig. 2.12). The $\delta^{13}C$ negative excursion has the lowest amplitude at sample site IRH, suggesting the brackish water layer takes longest to reach this area, supporting a clockwise path of rotation.

Widespread euxinic conditions persist across the NAMS into the UBS-1. High frequency shifts in TOC enrichment have been attributed to Milankovitch cycles or other paleoclimate perturbations, and illustrate large scale shifts in nutrient supply and flux of terrestrial organics to the NAMS (Algeo and Heckel, 2008). Sea levels are at their maximum extent, allowing for the large scale circulation of bottom water with no evidence of deflection from bathymetric features, as seen by lowest Mo/TOC values near the western Midcontinent Shelf (~5 to 15) and moderately higher values in the Illinois Basin (~7 to 28).

UBS-2 is marked by a decrease in Mo_{EF}, and a shift from euxinic subpycnoclinal environments to anoxic. Terrestrial runoff is reduced as seen in a decrease of C/N ratios and a positive trend in $\delta^{13}C$ values. Finally, as sea level recedes in the GS, Mo-TOC and Mo-U covariations mark the transition of subpycnoclinal conditions from anoxic to dysoxic (Fig. 2.12). C/N ratios are lowest in the GS, suggesting least terrestrial runoff of the core shale intervals.

2.5. Summaries

This study presents new high-resolution geochemical data from the Late Pennsylvanian Heebner Shale that support the superestuarine circulation model for the North American Midcontinent Sea (NAMS), and that provide evidence for second-order circulation features, in particular, gyral circulation patterns. Seven study sections (five cores and two outcrops) were used to generate a two-dimensional paleogeographic framework in order to resolve spatial trends. Cm-scale sampling of the core shale allowed for high-resolution temporal correlation of geochemical proxies and a study of the evolution of redox conditions throughout the interval of core shale deposition. During deposition of the Heebner Shale, the NAMS experienced widespread reducing, semi-restricted conditions. The existence of basin-scale anticyclonic (clockwise) circulation implies that the NAMS was sufficiently large for the Coriolis Effect to have been the dominant influence on internal gyral circulation. Tidal forces were too weak to have influenced gyral circulation, although effects linked to discharge of large rivers into the NAMS potentially may have been important also.

Anticyclonic (clockwise) gyral circulation in the NAMS is indicated by spatial patterns of organic matter types, carbon and nitrogen isotopes, and major-element ratios (which reflect the composition of clay-mineral assemblages). These proxies suggest that there were three discrete paleogeographic sources for inputs of terrestrial material into the NAMS: (1) the Laurentian Craton (NE), (2) the Alleghenian-Ozark region (S-SE), and (3) the Ouachita Mountains (SW). Inputs of terrestrial organics and sediment are sourced from the uplifting Ouachita Mountains, the equatorial Alleghenian Mountains, and the Laurentian Craton A relative drawdown of Mo concentrations with respect to U provide evidence of reservoir effects, where Mo is sequestered into the sediment at a rate greater than it is resupplied by the

open ocean. Nitrogen isotopes show a migration of sub-oxic, bottom water from the northernmost sample site to the Illinois Basin and to the southwest. The nitrogen isotopic excursion at the LBS-1 – LBS-2 interface increases in magnitude as waters migrate away from the open ocean source, indicative of further denitrification. The preceding evidence points towards basin-scale gyral circulation of a stratified water mass in the NAMS following a clockwise motion.

2.6 References

Algeo, T.J., Heckel, P.H., 2008. The Late Pennsylvanian Midcontinent Sea of North America: A review. Palaeogeography, Palaeoclimatology, Palaeoecology 268, 205-221.

Algeo, T.J., Herrmann, A.D., 2018. An ancient estuarine-circulation nutrient trap: The Late Pennsylvanian Midcontinent Sea of North America. Geology 46(2), 143-146.

Algeo, T.J., Lyons, T.W., 2006. Mo-total organic carbon covariation in modern anoxic marine environments: Implications for analysis of paleoredox and paleohydrographic conditions. Paleoceanography 21.

Algeo, T.J., Maynard, J.B., 2004. Trace-element behavior and redox facies in core shales of Upper Pennsylvanian Kansas-type cyclothems. Chemical Geology 206, 289-318.

Algeo, T.J., Maynard, J.B., 2008. Trace-metal covariation as a guide to water-mass conditions in ancient anoxic marine environments. Geosphere 4(5), 872-887.

Algeo, T.J., Rowe, H., 2012. Paleoceanographic applications of trace-metal concentration data. Chemical Geology 324, 6-18.

Algeo, T.J., Tribovillard, N., 2009. Environmental analysis of paleoceanographic systems based on molybdenum–uranium covariation. Chemical Geology 268, 211-225.

Algeo, T.J., Schwark, L., Hower, J.C., 2004. High-resolution geochemistry and sequence stratigraphy of the Hushpuckney Shale (Swope Formation, eastern Kansas): implications for climato-environmental dynamics of the Late Pennsylvanian Midcontinent Seaway. Chemical Geology 206, 259-288.

Algeo, T.J., Heckel, P.H., Maynard, J.B., Blakey, R., Rowe, H., 2008a. Modern and ancient epeiric seas and the super-estuarine circulation model of marine anoxia. In: Pratt, B., Holmden, C. (Eds.), Dynamics of Epeiric Seas: Sedimentological, Paleontological and Geochemical Perspectives. Geological Association Canada Special Publication 48, pp. 7-38.

Algeo, T.J., Rowe, H., Hower, J.C., Schwark, L., Herrmann, A., Heckel, P., 2008b. Changes in ocean denitrification during Late Carboniferous glacial–interglacial cycles. Nature Geoscience 1, 709-714.

Beletsky, D., Saylor, J.H., Schwab, D.J., 1999. Mean circulation in the Great Lakes. Journal of Great Lakes Research 25, 78-93.

Bennett, J.R., 1975. Another explanation of the observed cyclonic circulation of large lakes. Limnology and Oceanography 20, 108-110.

Boardman, D.R., Heckel, P.H., 1989. Glacial-eustatic sea-level curve for early Late Pennsylvanian sequence in north-central Texas and biostratigraphic correlation with curve for midcontinent North America. Geology 17(9), 802-805.

Cecil, C.B., Dulong, F.T., Edgar, N.T., Stamm, R.G., Wardlaw, B.R., West, R.R., 2003. Climate control on the stratigraphy of a Middle Pennsylvanian cyclothem in North America. In: Cecil, C.B., Edgar, N.T. (Eds.), Climate controls on stratigraphy. SEPM-Soc. Sedim. Geol. Spec. Publ 77, pp. 29-50.

Church, J., Fobes, A., 1981. Non-linear model of the tides in the Gulf of Carpentaria. Marine and Freshwater Research 32, 685-697.

Coveney, R.M., Jr., Glascock, M.D., 1989. A review of the origins of metal-rich Pennsylvanian black shales, central USA, with an inferred role for basinal brines. Applied Geochemistry 4(4), 347-367.

Coveney, R.M., Jr., Watney, W.L., Maples, C.G., 1991. Contrasting depositional models for Pennsylvanian black shale discerned from molybdenum abundances. Geology 19, 147-150.

Cruse, A.M., Lyons, T.W., 2004. Trace metal records of regional paleoenvironmental variability in Pennsylvanian (Upper Carboniferous) black shales. Chemical Geology 206, 319-345.

Ece, O.I., 1985. Depositional environment, stratigraphy, petrology, paleogeography and organic thermal maturation of the Desmoinesian cyclothemic Excello Black Shale in Oklahoma, Kansas and Missouri. Unpubl. Ph.D. dissertation, Univ. of Tulsa, Tulsa, Oklahoma, 291 pp.

Ece, O.I., 1987. Petrology of the Desmoinesian Excello black shale of the Midcontinent region of the United States. Clays and Clay Minerals 35, 262-270.

Ece, O.I., 1989. Organic Maturation and Paleoceanographic/Paleogeographic Implications of the Desmoinesian Cyclothemic Excello Black Shale of the Midcontinent, USA. The Shale Shaker Digest XII, Volumes XXXVI-XXXIX (1985-1989), 273-287.

Ellison, S., 1941. Revision of the Pennsylvanian conodonts. Journal of Paleontology 15(2), 107-143.

Emery, K.O., Csanady, G., 1973. Surface circulation of lakes and nearly land-locked seas. Proceedings of the National Academy of Sciences (U.S.A.) 70, 93-97.

Erickson, B.E., Helz, G.R., 2000. Molybdenum (VI) speciation in sulfidic waters: stability and lability of thiomolybdates. Geochimica et Cosmochimica Acta 64, 1149-1158.

Evans, J.K., 1967. Depositional environment of a Pennsylvanian black shale (Heebner) in Kansas and adjacent states. Unpubl. Ph.D. dissertation, Rice University, Houston, Texas.

Hatch, J., Leventhal, J., 1997. Early diagenetic partial oxidation of organic matter and sulfides in the Middle Pennsylvanian (Desmoinesian) Excello Shale Member of the Fort Scott Limestone and equivalents, northern Midcontinent region, USA. Chemical Geology 134, 215-235.

Hayes, J. M., Freeman, K. H., PoPP, B. N., & Hoham, C. H. (1990). Compound-specific isotopic analyses: a novel tool for reconstruction of ancient biogeochemical processes. Organic Geochemistry, 16(4-6), 1115-1128.

Heckel, P.H., 1977. Origin of phosphatic black shale facies in Pennsylvanian cyclothems of mid-continent North America. American Association of Petroleum Geologists Bulletin 61, 1045-1068.

Heckel, P.H., 1980. Paleogeography of eustatic model for deposition of Midcontinent Upper Pennsylvanian cyclothems. In: Fouch, T.D., Magathan, E.R. (Eds.), Paleozoic Paleogeography of the West-Central United States: Rocky Mountain Symposium 1, 1980, Rocky Mountains Section (SEPM), pp. 197-215.

Heckel, P.H., 1994. Evaluation of evidence for glacio-eustatic control over marine Pennsylvanian cyclothems in North America and consideration of possible tectonic effects. In: Dennison, J.M., Ettensohn, F.R. (Eds.), Tectonic and Eustatic Controls on Sedimentary Cycles. SEPM, Concepts in Sedimentology and Paleontology 4, pp. 65-87.

Helz, G., Miller, C., Charnock, J., Mosselmans, J., Pattrick, R., Garner, C., Vaughan, D., 1996. Mechanism of molybdenum removal from the sea and its concentration in black shales: EXAFS evidence. Geochimica et Cosmochimica Acta 60, 3631-3642.

Herrmann, A.D., Barrick, J.E., Algeo, T.J., 2015. The relationship of conodont biofacies to spatially variable water mass properties in the Late Pennsylvanian Midcontinent Sea. Paleoceanography 30, 269-283.

Herrmann, A.D., Kendall, B., Algeo, T.J., Gordon, G.W., Wasylenki, L.E., Anbar, A.D., 2012. Anomalous molybdenum isotope trends in Upper Pennsylvanian euxinic facies: Significance for use of δ^{98}Mo as a global marine redox proxy. Chemical Geology 324-325, 87-98.

Hoffman, D.L., Algeo, T.J., Maynard, J.B., Joachimski, M.M., Hower, J.C., Jaminski, J., 1998, Regional and stratigraphic variation in bottom-water anoxia in offshore core shales of Upper Pennsylvanian cyclothems from the Eastern Mid-continent Shelf (Kansas), USA. In: Schieber, J., Zimmerle, W., Sethi, P.S. (Eds.), Shales and Mudstones, v. 1: Schweizerbart, Stuttgart, pp. 243-269.

Jilbert, T., Slomp, C.P., 2013. Iron and manganese shuttles control the formation of authigenic phosphorus minerals in the euxinic basins of the Baltic Sea. Geochimica et Cosmochimica Acta 107, 155-169.

Joachimski, M.M., von Bitter, P.H., Buggisch, W., 2006. Constraints on Pennsylvanian glacioeustatic sea-level changes using oxygen isotopes of conodont apatite. Geology 34, 277-280.

Lamb, A. L., Wilson, G. P., & Leng, M. J. (2006). A review of coastal palaeoclimate and relative sea-level reconstructions using δ13C and C/N ratios in organic material. Earth-Science Reviews, 75(1-4), 29-57.

Lehmann, A., Krauss, W. and Hinrichsen, H.-H. (2002), Effects of remote and local atmospheric forcing on circulation and upwelling in the Baltic Sea. Tellus A, 54: 299–316.

Meyers, P.A., 1994. Preservation of elemental and isotopic source identification of sedimentary organic matter. Chemical Geology 114, 289-302.

Montañez, I.P., Poulsen, C.J., 2013. The Late Paleozoic Ice Age: An evolving paradigm. Annual Review of Earth and Planetary Sciences 41, 629-656.

Neumeister, S.A., Algeo, T.J., Bechtel, A., Gawlick, H.J., Gratzer, R., Sachsenhofer, R.F., 2016. Redox conditions and depositional environment of the Lower Jurassic Bächental bituminous marls (Tyrol, Austria). Austrian Journal of Earth Sciences 109.

Prinsenberg, S.J., 1986. The circulation pattern and current structure of Hudson Bay, Elsevier oceanography series. In: Martini, I.P. (Ed.), Canadian Inland Seas: Oceanography Series 44, Elsevier, Amsterdam, pp. 187-204.

Popp, B. N., Takigiku, R., Hayes, J. M., Louda, J. W., & Baker, E. W. (1989). The post-Paleozoic chronology and mechanism of 13 C depletion in primary marine organic matter. American Journal of Science, 289(4), 436-454.

Rimmer, S.M., Rowe, H.D., Taulbee, D.N., Hower, J.C., 2006. Influence of maceral content on $\delta^{13}C$ and $\delta^{15}N$ in a Middle Pennsylvanian coal. Chemical Geology 225, 77-90.

Ruby, E. G., Jannasch, H. W., & Deuser, W. G. (1987). Fractionation of stable carbon isotopes during chemoautotrophic growth of sulfur-oxidizing bacteria. Applied and Environmental Microbiology, 53(8), 1940-1943.

Roark, A., Flake, R., Grossman, E.L., Olszewski, T., Lebold, J., Thomas, D., Marcantonio, F., Miller, B., Raymond, A., Yancey, T., 2017. Brachiopod geochemical records from across the Carboniferous seas of North America: Evidence for salinity gradients, stratification, and circulation patterns. Palaeogeography, Palaeoclimatology, Palaeoecology 485, 136-153.

Rosenau, N.A., 2013. Paleoclimate Reconstruction of Pennsylvanian Paleoequatorial Environments: Coupling Terrestrial and Marine Proxies. Unpubl. Ph.D. dissertation, Southern Methodist University, Dallas, Texas.

Rosenau, N.A., Tabor, N.J., Herrmann, A.D., 2014. Assessing the paleoenvironmental significance of Middle-Late Pennsylvanian conodont apatite $d^{18}O$ values in the Illinois Basin. Palaios 29, 250-265.

Scholz, F., McManus, J., Sommer, S., 2013. The manganese and iron shuttle in a modern euxinic basin and implications for molybdenum cycling at euxinic ocean margins. Chemical Geology 355, 56-68.

Schultz, R.B., Coveney, R.M., Jr., 1992. Time-dependent changes for Midcontinent Pennsylvania black shales, USA. Chemical Geology 99, 83-100.

Schwab, D.J., O'Connor, W.P., Mellor, G.L., 1995. On the net cyclonic circulation in large stratified lakes. Journal of Physical Oceanography 25, 1516-1520.

Scott, C., Lyons, T.W., 2012. Contrasting molybdenum cycling and isotopic properties in euxinic versus non-euxinic sediments and sedimentary rocks: Refining the paleoproxies. Chemical Geology 324, 19-27.

Soreghan, G.S., Giles, K.A., 1999. Amplitudes of late Pennsylvanian glacioeustasy. Geology 27(3), 255-258.

Tabor, N.J., Montañez, I.P., 2002. Shifts in late Palaeozoic atmospheric circulation over western equatorial Pangea: insights from pedogenic mineral $d^{18}O$ compositions. Geology 30, 1127-1130.

Taylor, S.R., McLennan, S.M., 1985. The Continental Crust: Its Composition and Evolution. Blackwell, Oxford, 312 pp.

Tribovillard, N., Algeo, T.J., Lyons, T., Riboulleau, A., 2006. Trace metals as paleoredox and paleoproductivity proxies: An update. Chemical Geology 232, 12-32.

Villa, E., Alekseev, A.S., Barrick, J.E., Boardman, D.R., Djenchuraeva, A.V., Fohrer, B., Forke, H., Goreva, N.V., Heckel, P.H., Isakova, T.N., Kossovaya, O., 2009. Selection of the conodont Idiognathodus simulator (Ellison) as the event marker for the base of the global Gzhelian Stage (Upper Pennsylvanian, Carboniferous). Palaeoworld 18(2-3), 114-119.

Wanless, H.R., Shepard, F.P., 1936. Sea level and climatic changes related to late Paleozoic cycles. Geological Society of America Bulletin 47(8), 1177-1206.

Wehausen, R., Brumsack, H., 1998. The formation of Pliocene Mediterranean sapropels: constraints from high-resolution major and minor element studies, Proceedings of the Ocean Drilling Program, Scientific Results, v. 160, pp. 207-218.

Wenger, L.M., Baker, D.R., 1986. Variations in organic geochemistry of anoxic-oxic black shale-carbonate sequences in the Pennsylvanian of the Midcontinent, USA. Organic Geochemistry 10, 85-92.

Wenger, L.M., Baker, D.R., Chung, H.M., McCulloh, T.H., 1988. Environmental control of carbon isotope variations in Pennsylvania black-shale sequences, Midcontinent, USA. Organic Geochemistry 13, 765-771.

Whiticar, M.J., 1996. Stable isotope geochemistry of coals, humic kerogens and related natural gases. International Journal of Coal Geology 32, 191-215.

Witzke, B.J., 1987. Models for circulation patterns in epicontinental seas applied to Paleozoic facies of North America craton. Paleoceanography 2, 229-248.

Yang, W., 2007. Transgressive wave ravinement on an epicontinental shelf as recorded by an Upper Pennsylvanian soil-nodule conglomerate-sandstone unit, Kansas and Oklahoma, USA. Sedimentary Geology 197, 189-205.

Yang, W., Bruemmer, M., Turner-Williams, M., 2003. Stratigraphic Architecture and Processes Controlling Coeval Deltaic, Platform Carbonate, and Condensed Shelf Sedimentation, Upper Pennsylvanian, Leavenworth Limestone-Heebner Shale-Plattsmouth Limestone-Heumader Shale Minor Cyclothem, SE Kansas and NE Oklahoma.

Zangerl, R., Richardson, E.S., Woodland, B.G., 1963. The paleoecological history of two Pennsylvanian black shales. In: Chicago Natural History Museum, Fieldiana (Geology Memoirs) 4, 352 pp.

Zavialov, P.O., 2010. Physical oceanography of the large Aral Sea. In: Kostianoy, A.G., Kosarev, A.N. (Eds.), The Aral Sea Environment. Springer, Berlin, pp. 123-145.

CHAPTER 3 TRACE METAL UPTAKE, RARE-EARTH ELEMENTS, AND STABLE ISOTOPIC VARIATION IN MODERN BAHAMIAN CARBONATE DURING SYNDEPOSITIONAL DIAGENESIS

3.1. Introduction

Carbonate geochemistry has long been a useful tool for investigating global ocean conditions during deposition such as global oxygen and carbon cycles over vast periods of time (Hoffman et al., 1998; Luo et al., 2010; Sahoo et al., 2012; Veizer and Hoefs, 1976) and more recently for looking at novel isotopes (U and Mo) in carbonates as global redox proxies (Brennecka et al., 2011; Voegelin et al., 2009; Weyer et al., 2008). The goal is to measure the chemical composition of seawater, as recorded in the rock record without post-depositional alteration, though studies have shown, this is not always the case (Derry, 2010; Higgins et al., 2018; Knauth and Kennedy, 2009; Oehlert and Swart, 2014; Romaniello et al., 2013, 2016). One of the primary modes in which the original chemical signatures may be altered is in early or syndepositional diagenesis, or alterations to the geochemical signature of sediment as deposition is occurring. The effects of syndepositional diagenesis may have significant impacts for important geochemical properties, such as rare earth element (REE) distributions and novel redox proxies, such as molybdenum and uranium isotope systems, and has been not yet been fully explored (Li and Jones, 2014; Romaniello et al., 2013, 2016). Recent studies have shown authigenic accumulations of trace metals (such as U and Mo) in shallow Bahamian carbonates and associated shifts in isotopic compositions however the mode of uptake and diagenetic controls needs to be further investigated (Andersen et al., 2014; Romaniello et al., 2013, 2016). This research investigates the form that redox-sensitive trace metals are sequestered in, with the goal of determining whether these signatures can be preserved through geologic time.

While carbonates show promise in preserving trace metal marine chemistry, further work needs to be done to fully understand the effect of early diagenesis and how it can affect the preservation of geochemical signatures of redox-sensitive proxies. Using the samples of Romaniello et al. (2013, 2016), this study employs sequential extractions, along with stable isotope analysis to investigate how REE and trace metals are incorporated into sediments, both the chemical phase in which they are hosted and

driving factors of their uptake, across a variety of diagenetically altered environments. The goal is to examine different syndepositional diagenetic environments, with varying degrees of organic content and composition, terrestrial and meteoric input, and degree of restriction from the open sea, the purpose being to systematically investigate the effects on the geochemical signatures of modern carbonates. This will allow the development of a framework to better understand how to apply this knowledge to paleo-environments.

3.2. Materials and Methods

3.2.1 Site Location

The Bahamian carbonate platform is one of the largest and best studied carbonate platforms (e.g. (Baker and Kastner, 1981; Oehlert and Swart, 2014; Romaniello et al., 2013, 2016; Swart, 2015)). As such, it is an ideal natural laboratory location to study early diagenesis of shallow carbonates. The geographic isolation of the platform, far from any continental masses, provides a unique environment for study of primary and authigenic geochemical signatures, isolated from terrestrial siliciclastic influence from nearby continents, though wind blown dust provides siliciclastic material (Muhs et al., 2007). Samples from this study were collected along the Exuma Islands, centered around Little Darby (Fig. 3.1). Previous geochemical work on these samples have been carried out by Romaniello et al. (2013, 2016).

Romaniello et al. (2013) collected four cores from a variety of environments and depths, and used in this study (Fig. 3.1). Cores 1 (42 cm long) and 2 (24 cm long) were taken in the area around the Little Darby research station, core 3 (22 cm long) was taken near Lee Stocking, and core 4 (30 cm long) was taken from a salt water pond (salinity maintained by a tidal connection to the open ocean, 39 ppt; Romaniello et al., 2013). Core 1 was taken in an area dominated by calcareous green algae and turtle grass. The core location was chosen to avoid adjacent shrimp (*Callianassa* sp.) mounds and burrows. Core 2 was taken on a tidal flat adjacent to core 1, approximately 100 m to the southeast. The tidal flat was largly free of any vegatation (tutle grass or green algae). Core 3 was taken in an are similar to core 1, with dense turtle grass and calcareous green algae, but in a deeper water (4 m) envrionment. Core 4,

taken from a salt water pond which was tidally connected to the open ocean. For detailed core description, see Romaniello et al. (2013).

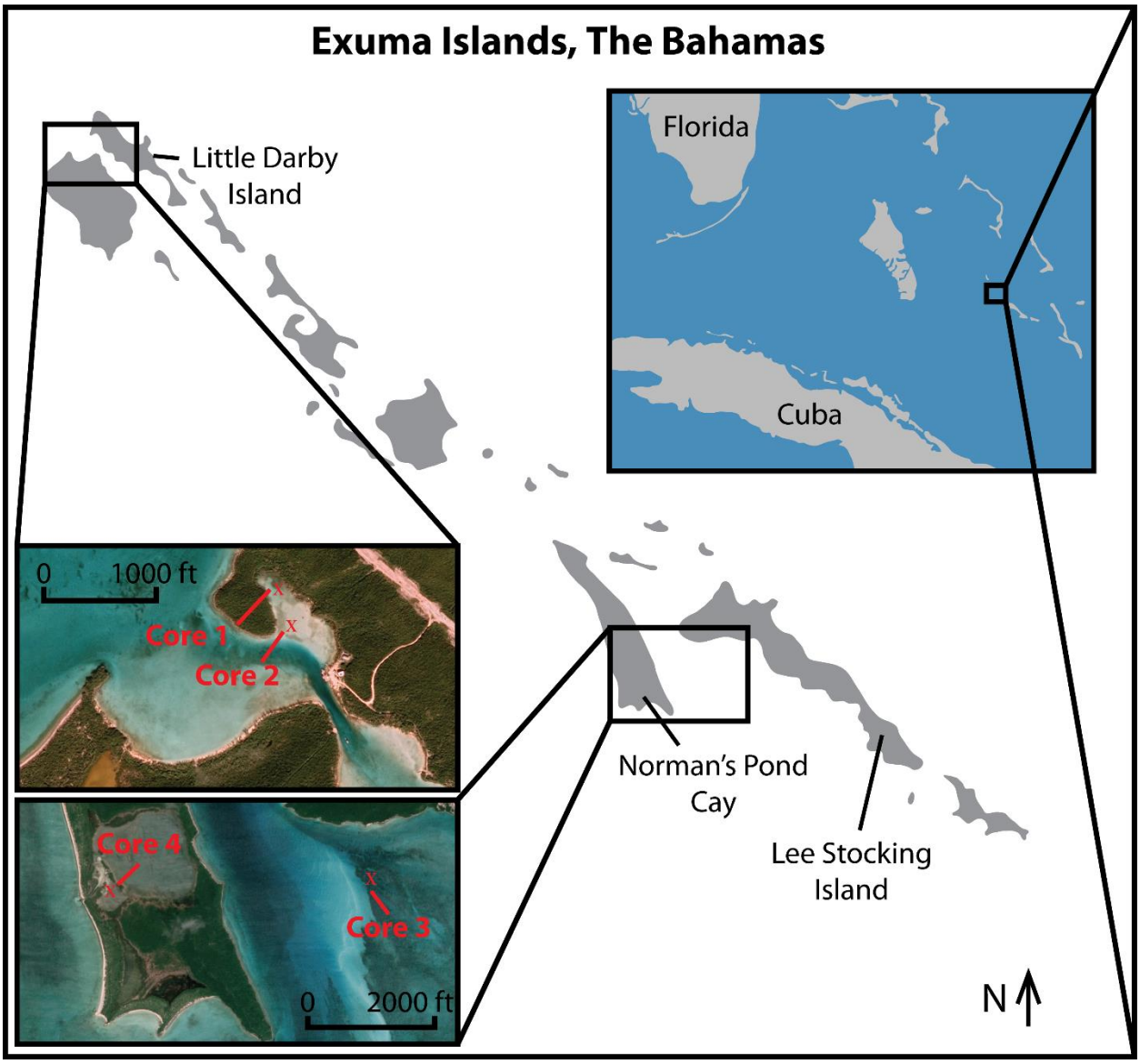

Figure 3.1 Sample locations of the four cores taken. Samples were collected on the Exuma Island Chain of the Greater Bahamas near and around Little Darby Island.

3.2.2 Inorganic Oxygen and Carbon isotope analysis

All stable isotope analyses were performed at the Oxy-Anion Stable Isotope Consortium (OASIC) at Louisiana State University. Isotopic measurements are reported in delta notation. ~200 μg of sample were dried at 75°C for 12 hours, then sealed and flushed with He for 2 minutes. Using a Thermo

Scientific Gas Bench II, samples were acidified with ~ 100 µL of concentrated phosphoric acid and kept at 75°C. Reaction took place over 3 hours, after which CO_2 from the samples were passed through a Nafion water trap to be analyzed on a Delta V Advantage mass spectrometer. NBS-19 and LSVEC were used as check standards. Precision is less than 0.04‰ f or $\delta^{13}C$ and 0.1‰ for $\delta^{18}O$.

3.2.3 Organic Nitrogen, Carbon, and Sulfur isotope and elemental analysis

Aliquots of samples were decalcified by acidifying three times with 1 N hydrochloric acid. Samples were then dried and weighed into combustible tin containers. Weights were determined by targeting ~400 µg of carbon and ~100 µg of N, approximately 2-20 mg of bulk decalcified sample. Organic carbon, nitrogen, and sulfur isotopes and elemental concentrations were analyzed using an Isoprim100 IRMS, coupled with a Micro Vario Cube elemental analyzer.

Nitrogen isotopic results are reported as per mille (‰) variation from standard N_2 in air in delta notation where $\delta^{15}N_{air} = (({}^{15}N/{}^{14}N)_{sample}/({}^{15}N/{}^{14}N)_{standard} - 1) \times 1000$. Nitrogen isotopic composition was calibrated using two glycine standards (high with $\delta^{15}N_{air} = +40.83$ ‰ and low with $\delta^{15}N_{air} = +1.35$ ‰). Analytical precision was < 0.1 ‰.

$\delta^{13}C_{org}$ is reported in ‰ VPDB variation. Mass calibrations were performed to allow adjustment of carbon content based on TOC%. TOC is calculated based on C concentration of organics and mass calculations based on weight of the original samples. Two glycine standards were used for isotopic value calibration (high with $\delta^{13}C_{VPDB} = -0.67$ ‰ and low with $\delta^{13}C_{VPDB} = -40.81$ ‰). Analytical precision was < 0.1 ‰.

Sulphur isotope compositions are reported in ‰ deviations from VCDT. Four in house standards are used for calibration, two silver sulfide and two barium sulfate (LSU-Ag2S-1: -4.3‰; LSU-Ag2S-2: +20.2‰; LSU-BaSO4-1: -4.5‰; LSU-BaSO4-2: +38.5‰). Analytical precision is < 0.2‰.

3.2.4 Sequential Extractions

Using a modified Tessier extraction (Šurija and Branica, 1995; Tessier et al., 1979), samples are chemically separated into partitions: Exchangeables, Carbonates, Oxyhydroxides, Organics, and Residual. Modifications from the Tessier method include modifying the exchangeable reagents to extract non-

crystalline uranium (Morin et al., 2016). Bicarbonate effectively leeches U from natural samples, held in solution as a U(VI)-carbonate complex (Phillips et al., 1995). Recent work has shown that sodium bicarbonate extraction is an effective wet chemistry technique to separate non-crystalline U(IV) (a form where U(VI) is reductively precipitated as U(IV), termed mononuclear U(IV)) from uraninite (Alessi et al., 2012). Other studies have shown the relative importance of non-crystalline U(IV) as a microbial reduction product in a variety of sediments (Alessi et al., 2014; Bhattacharyya et al., 2017; Morin et al., 2016; Sharp et al., 2011). Sodium bicarbonate dissociates in solution, supplying a bicarbonate ion and a Na anion. The use of bicarbonate over other ions such as carbonate provides a mild ionic strength while stable at pH values near neutral. This allows for the dissociation of loose ionic bonds while not affecting the pH and associated reactions. The charged bicarbonate ion likely has the greatest leeching effect on positively charged elements, such as U. The difference in ionic character of different elements adds complications when directly comparing concentrations of different elements of the exchangeable phase.

The chemical partitions are separated using progressively more aggressive chemical leaches (Table 3.1). After each chemical leaching, samples were centrifuged at 5000 rpm for 5 minutes, then the effluent was carefully pipetted off of the remaining solids. Twice, the solids were rinsed with 10 ml of deionized H_2O, centrifuged, and effluent removed before the next reagent was added. Total digests were performed using a combination of H_2O_2 and concentrated nitric acid at 80 ° C.

Sequential Extraction Reagents and Times			
Chemical Phase	**Reagent**	**Smp:Sol ratio**	**Physical Parameters**
Exchangeable	1 M Sodium Bicarbonate ($NaHCO_3$)	1:50	24 hours at room temperature
Carbonate	1 M Sodium Acetate (CH_3COONa) buffered to pH of 5 with Acetic Acid ($C_2H_4O_2$) followed by 1 M Nitric Acid (HNO_3)	1:50 (Sodium Acetate) 1:20 (Nitric)	24 hours at room temperature (Sodium Acetate) followed by 1 hour at room temperature (Nitric)
Oxide	1 M Hydroxylamine Hydrochloride in 25% Acetic Acid ($C_2H_4O_2$)	1:50	6 hours at 95° C
Organic	0.02 M Nitric Acid (HNO_3) in 30% Hydrogen Peroxide (H_2O_2)	1:50	>24 hours at 85° C
Residual	Concentrated Nitric Acid	1:10	>24 hours at 95° C

Table 1. The list of parameters, reagents, and chemical phases used during the sequential extraction. Extracts were performed using increasingly aggressive reagents, progressing down the table. Smp:Sol is abbreviated for sample to solution ratio.

Samples were analyzed using a Thermo iCAP-Qc quadrupole ICP-MS at Louisiana State University. In preparation for analysis, all samples were dried down and brought up in a 2% nitric acid solution. All acids and reagents used were trace metal grade and water was 18 Ω deionized. Individual chemical phases from the sequential extraction were run separately in order to reduce variations in matrix effects due to the variety of reagents used. The instrument was externally calibrated using a serial dilution of a solution containing QCP-QCS-3 multi element standard, REE standard, and single element standards of Ca, Mg, Rb, and Sr. Check standards and internal standards were used to ensure minimal instrument drift and sample suppression.

3.3. Results

3.3.1 Inorganic C and O isotopes

$\delta^{13}C_{carb}$ and $\delta^{18}O_{carb}$ show little variation in cores 1, 2, and 3 (Fig. 3.2). Average values, error defined by ± σ, number of samples are given in parenthesis. Core 1 $\delta^{13}C_{carb}$ ranges between ~ 3.5 to 4.1‰ (average 3.93‰ ± 0.22‰, n=8) and $\delta^{18}O_{carb}$ between ~ -0.4 to -0.8‰ (average -0.66‰ ± 0.18‰, n=8). Core 2 has $\delta^{13}C_{carb}$ values of ~4.2 – 4.8‰ (average 4.53‰ ± 0.13‰, n=5) and $\delta^{18}O_{carb}$ values ~0.2 – 0.0‰ (average -0.09‰ ± 0.16‰, n=5). Core 3 $\delta^{13}C_{carb}$ values range from ~3.4 - 3.8‰ (average 3.64‰ ±

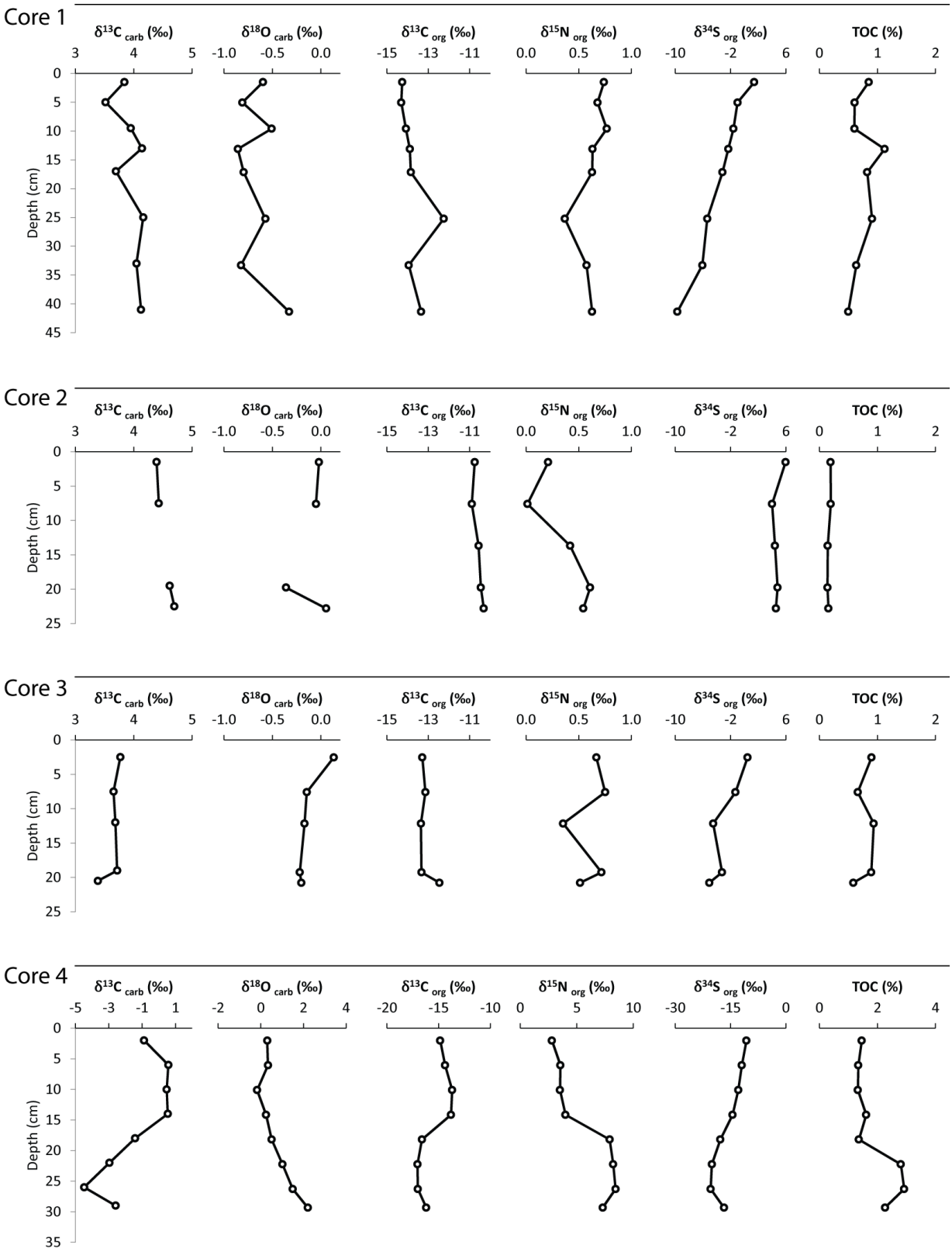

Figure 3.2 Stable isotope and TOC depth profiles of the four cores. Cores 1, 2, and 3 share an x-axis, while the scale shifts for Core 4.

0.13‰, n=5) and $\delta^{18}O_{carb}$ values of ~-0.2 – 0.1‰ (average -0.12‰ ± 0.13‰, n=5). Core 4 exhibits generally decreasing $\delta^{13}C_{carb}$ downcore from 1 - -5‰ (average -1.34‰ ± 1.76‰, n=8). Core 4 $\delta^{18}O_{carb}$ values generally increase downcore, from ~0 - 2‰ (average 0.74‰ ± 0.73‰, n=8).

3.3.2 Organic C, N and S isotopes and elemental concentrations

The organic fraction of the carbon isotopes in core 1, $\delta^{13}C_{org}$, range from ~-12.2 - -14.2‰ (average -13.74‰ ± 0.63‰, n=8; Fig. 3.2). Core 2 $\delta^{13}C_{org}$ is near constant at ~ -10.5‰ (average -10.6‰ ± 0.21‰, n=5). Core 3 $\delta^{13}C_{org}$ is nearly constant at ~-13‰ (average -13.11‰ ± 0.34‰, n=5). Core 4 generally trends lighter downcore, from ~-14 - -17‰ (average -15.45‰ ± 1.33‰, n=8). TOC of core 1 ranges from ~0.5 to 1.1%, with a general decreasing trend downcore (average 0.76% ± 0.19%, n=8). Core 2 TOC varies from ~ 0.2 – 0.6% (average 0.17% ± 0.02%, n=5). TOC in core 3 generally decreases downcore from ~0.9 – 0.6 (average 0.79% ± 0.14%, n=5). In core 4, TOC increases downcore from ~1.3 – 2.9% (average 1.89% ± 0.63%, n=8).

$\delta^{15}N_{org}$ values of the organics remain generally constant in core 1, at ~ 0.4 - 0.8‰ (average 0.63‰ ± 0.11‰, n=8; Fig. 3.2). Core 2 has $\delta^{15}N_{org}$ values of ~0.0 - 0.6‰ (average 0.36‰ ± 0.22‰, n=5). $\delta^{15}N_{org}$ values for core 4 generally increase downcore from ~2.8 – 8.4‰ (average 5.72‰ ± 2.29‰, n=8). N elemental concentration of the organic fraction is generally constant in core 1, at 0.09% (average 0.09% ± 0.03%, n=8). Core 2 has constant N concentrations at ~0.02% (average 0.02% ± 0.002%, n=5). Core 3 N varies from 0.06 – 0.10% (average 0.09% ± 0.02%, n=5). Core 4 N concentrations of the organic fraction increase downcore from ~0.1 – 0.4% (average 0.24% ± 0.11%, n=8).

Sulfur isotopes ($\delta^{34}S$) of the organic fraction of the samples in core 1 become depleted downcore, from +1.4 - -9.7‰ (Fig. 3.2). Core 2 $\delta^{34}S$ values remain generally constant at ~5‰ (average 4.74‰ ± 0.65‰, n=5). Core 3 $\delta^{34}S$ values decrease downcore from ~+0.5 - -5.0‰. $\delta^{34}S$ values in core 4 generally decrease downcore from ~-11 - -20‰. Elemental S concentrations are fairly constant in Core 1, 2, and 3 (average 0.04% ± 0.01%, 0.01% ± 0.001%, and 0.05% ± 0.02% respectively, n=8, 5, 5 respectively). Core 4 S concentrations increases downcore form ~0.1 – 0.3% (average 0.18% ± 0.09%, n=8).

3.3.3 Sequential extraction

3.3.3.1 Minor Elements (Sr, Rb, and Mg)

Sr remains generally constant downcore in cores 1, 2, and 3, with nearly all of the measured Sr present in the carbonate phase (> 99%) (Fig. 3.3). In the carbonate phase, Core 1 Sr ranges between ~0.535 and 0.774 wt%, core 2 between ~0.783 and 0.808 wt%, and core 3 between ~0.564 and 0.599 wt%. Core 4 decreases downcore from ~0.451 to ~0.259 wt%. Rb is scarce in cores 1, 2, and 3, with ~0.1 ppm each in the carbonate, oxide, and residual phases. Core 4 contains ~2 – 3 ppm Rb in the residual phase, and ~ 1 ppm in the oxide phase. Mg is dominantly in the carbonate phase (~85 – 97%, average 90.3%). Core 1 and 3 contain ~ 1% Mg each in the carbonate phase, while core 2 contains ~ 0.4%. Core 4 increases downcore in Mg concentration in the carbonate phase, from ~ 7 – 2%.

3.3.3.2 Trace Metals (U, Fe, Mo, and V)

Uranium appears in all phases, in all cores (Fig. 3.4), though it is most concentrated in the exchangeable and carbonate phases (Fig. 3.5). In total digests, the cores have ~ 5 – 11 ppm U, with core 2 having the least (~ 5 ppm) and core 4 with the most (~ 6 – 11 ppm). Core 1 and 3 have a total of ~ 5 – 6 ppm U. Core 1 and 3 show an increase in U concentration down core. Core 4 initially has an increase in U concentration downcore, then remains relatively stable in the second half of the core. Where there is an increase in U concentration in the total digest, it is reflected in an increase in U concentration in the exchangeable phase (Fig. 3.6). All other phases remain fairly constant with depth.

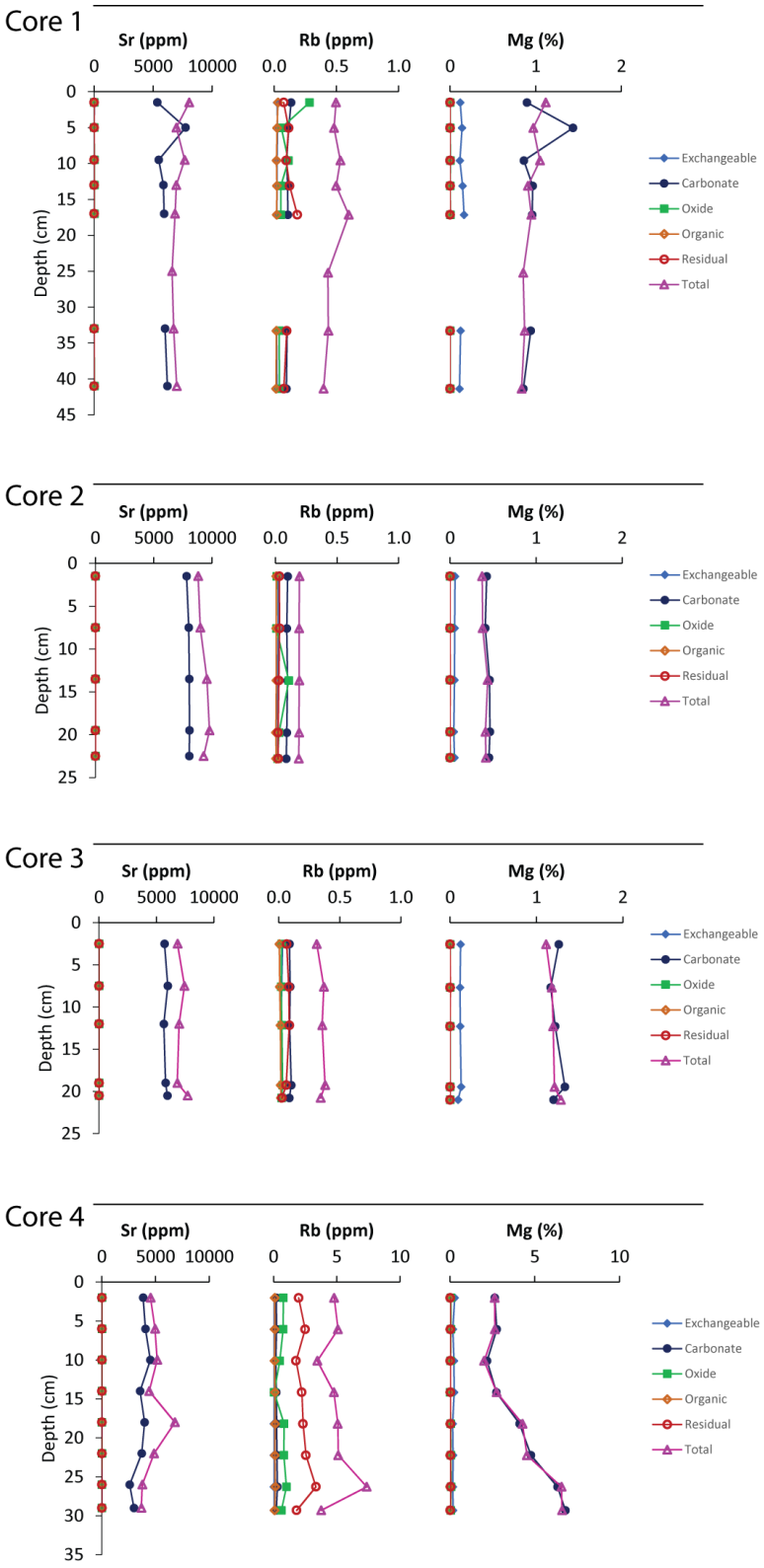

Figure 3.3 Depth profiles of minor elements Sr, Rb, and Mg of each sequential extraction phase, for each of the four cores.

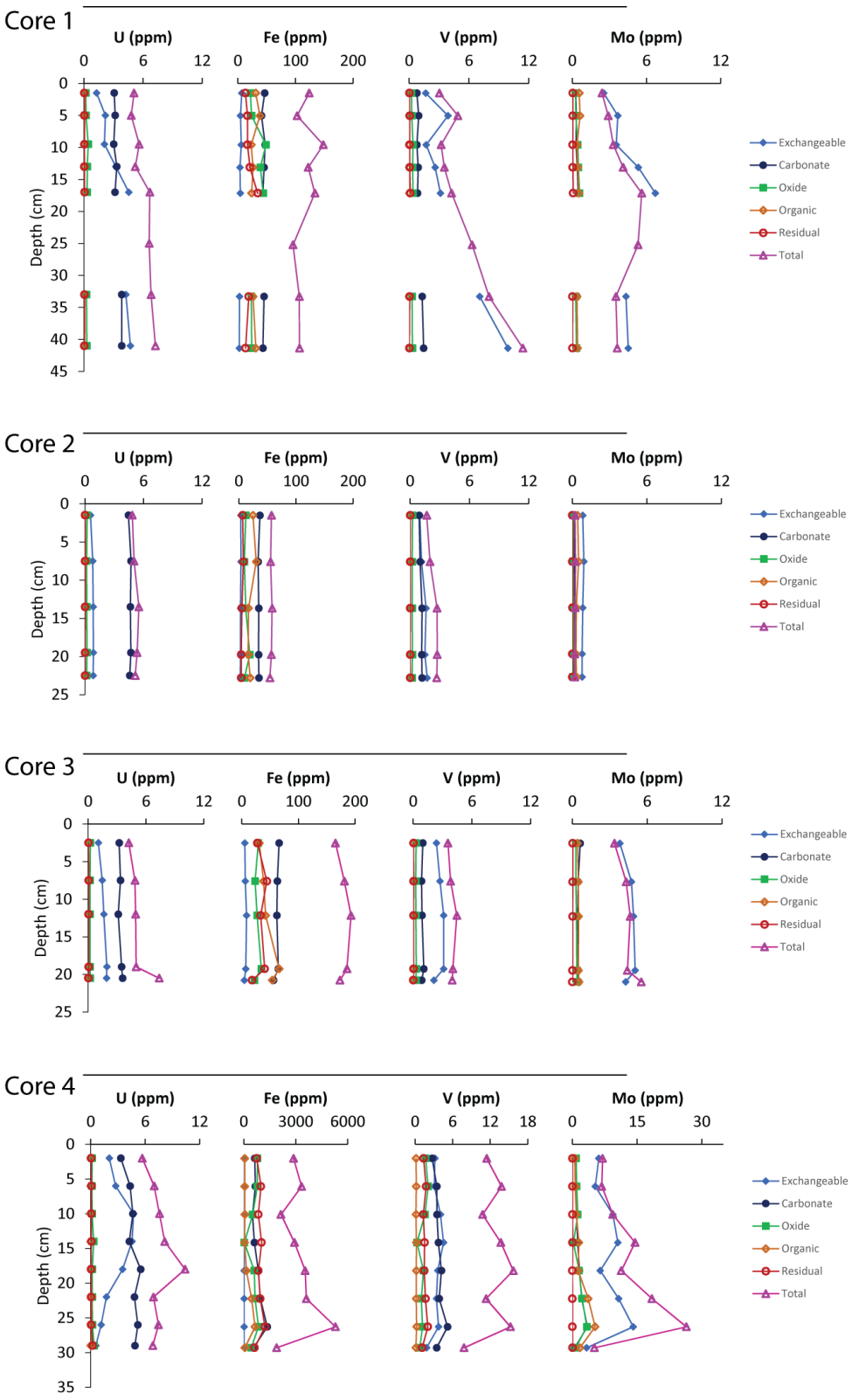

Figure 3.4 Depth profiles of redox-sensitive trace metals U, V, and Mo of each sequential extraction phase, for each of the four cores.

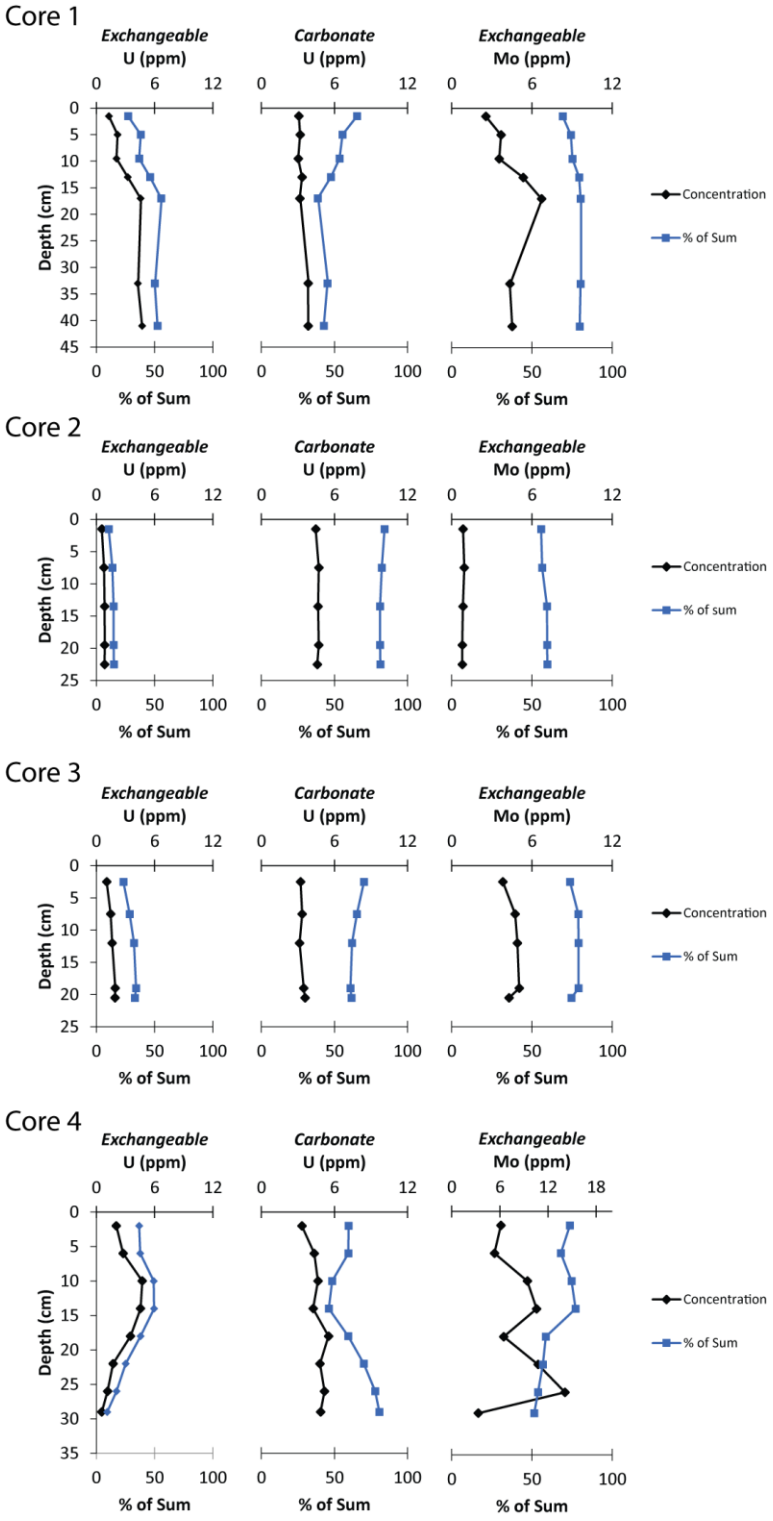

Figure 3.5 Mo and U in the primary host phases of the four cores. Exchangeable U shows an increase in both concentration and % of total U in cores 1, 2, and 3, and the top of core 4. Carbonate U concentration stays relatively stable, while the percentage of total U decreases as exchangeable U increases. The exchangeable phase hosts the majority of Mo (55 – 90%) in cores 1, 2, and 3, and the top of core 4. In the lower half of core 4, the % of total Mo in the exchangeable phase decreases.

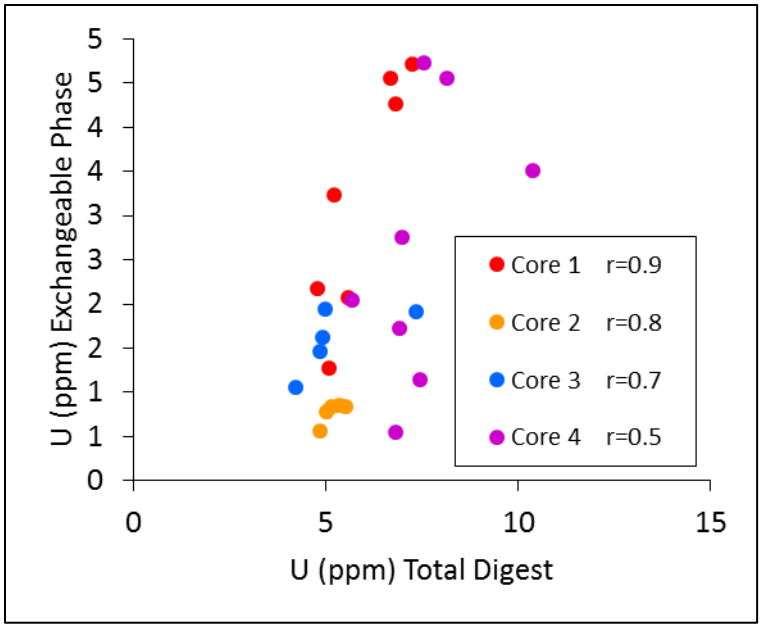

Figure 3.6 Cross plot of U from the exchangeable fraction and the total digest.

Fe is present in the cores in all phases (Fig. 3.4). In core 1, Fe is constant downcore, ~115 in the total digest, 6 ppm in exchangeable phase, 45 ppm in carbonate phase, 30 ppm in oxide phase, 35 ppm in organic phase, and 20 ppm in the residual phase. Core 2 has ~60 ppm in the total digest, 40 ppm in carbonate phase, 20 ppm in the organic phase, and < 10 ppm for exchangeable, oxide, and residual phases. Core 3 has ~190 ppm Fe in the total digest, 70 ppm in the carbonate phase, 50 ppm in organic phase, 40 ppm in residual phase, 30 ppm in oxide phase, and 5 ppm in exchangeable phase. Core 4 Fe concentration increases downcore in the total digest from ~2900 – 5800 ppm. Carbonate and residual phases increase downcore from ~650 – 1350 ppm. The oxide phase in core 4 varies from ~780 ppm near the top and bottom of the core, to near zero at the 14 cm sample. Organic Fe concentration increases in the bottom half of the core from near zero to ~620 ppm. Fe concentrations in the exchangeable phase of core 4 remain constant and near zero.

V is primarily in the exchangeable phase of cores 1, 2, and 3. In core 1, V increases downcore from ~2 – 12 ppm in the exchangeable phase, while remaining generally constant in the carbonate phase at ~1ppm and <1ppm in oxide, organic, and residual phases. V in core 2 increases slightly downcore in the exchangeable phase, from ~1 – 2 ppm, while staying constant at ~1 ppm in the exchangeable phase,

and < 1ppm in the oxide, organic, and residual phases. Core 3 V concentrations increase downcore in the exchangeable phase from ~ 3 – 4 ppm, while the carbonate phase remains constant at ~1ppm and oxide, organic, and residual phases have <1 ppm V. V concentrations in core 4 are generally constant with ~3 ppm in carbonate and exchangeable phases, ~1ppm in oxide and residual phases, and <1ppm in the organic phase.

Core 1 and 3 have Mo concentrations of ~ 2 – 6 ppm (Fig. 3.4). Core 4 has Mo concentrations of ~6 – 20 ppm, with the highest concentration in the bottom half of the core. Core 2 has very little Mo, < 1 ppm. The majority of Mo (50 – 90%) in cores 1, 2, and 3 is found in the exchangeable phase. In core 4, Mo occurs primarily in the exchangeable phase in the top half of the core, then distributes to carbonate, oxide, and organic phases in the bottom half (Fig. 3.4).

3.3.3.3 REE + Y (REY)

Sequential extraction phases other than carbonate contain concentrations of REYs that are near or below the limit of quantification for the ICP-MS. REEs are normalized to the standard Post-Archean Australian Shales (PAAS), notated by a shale normalized (SN) subscript (McLennan, 1989). Core 1, 2, and 3 exhibit heavy REE (HREE) enrichment, as evidenced by Nd_{SN}/Yb_{SN} ratios of 0.44 - 0.63, Y/Ho ratios of 50 – 60, and negative Ce anomalies ((Ce/Ce*); (Ce_{SN} / (0.5*La_{SN} + 0.5*Pr_{SN}))); seawater characteristics with no evidence of terrestrial contamination (De Baar et al., 1985; Tostevin et al., 2016). Cross plots of Ce/Ce* and Pr/Pr* (Pr / (0.5*Ce + 0.5*Nd)) indicate negative La anomalies (Bau and Dulski, 1996). The sum of shale normalized REEs and Y (ΣREY) ranges from 2.8 – 3.3 for core 1, 1.7 – 1.8 for core 2, and 3.5 – 3.8 for core 3. Core 4 exhibits neither Ce nor La anomalies. Core 4 has a moderate HREE enrichment (Nd_{SN}/Yb_{SN} ratios of 0.67 – 0.78) and Y/Ho ratios of 40 – 48. The ΣREY for core 4 ranges from 2.2 – 3.8.

3.4. Discussion

3.4.1 Potential for bioirrigation and other physical reworking

Physical reworking of the sediment, especially by burrowers such as *Callianassa* sp., may not reflect the physical characteristics of the original depositional environment (Tedesco and Wanless, 1991).

The reworking of sediment may effect the chemistry recorded in the sediment as well. Burrowers such as *Callianassa* sp. Have been shown to rework the top 10 – 15cm of carbonate sediment completely over the course of 6 – 21 years (Bentley Sr and Nittrouer, 2012). While physical events, such as storms may rework the top few cm of sediment, bioirrigation dominates the reworking of fine grained carbonate deposits, which may be applicable to the sand sized grains of this study site (Bentley and Nittrouer, 1997). In addition to the physical re-working of the sediment, burrows may provide oxidants to the sediment as well, not just to those that are burrowed through, but also radially away from the burrows through diffusion (Furukawa et al., 2000).

In the Bahamian sediments studied presently, O_2 porewater concentrations decrease to near zero in the first few mm of sediment (Romaniello et al., 2013). There are several pathways that geochemical signatures from this reducing environment may be incorporated into the sediment. Organic matter may be incorporated in the carbonate sturcture of recrystallizing carbonate (Ingalls et al., 2004), thus preserving the trace metals enriched in the organic material. In this case, trace metals would be released in the carbonate or organic phase of the sequential extraction. Additionally, reduced trace metals present as sulfides or mononuclear species may be incorporated into the carbonates directly as the recrystallize in the pore spaces, in which case the trace metals would be extracted in the carbonate phase. As a third possibility, trace metals may be loosely bound to carbonates, becoming more enriched with depth for the portion of carbonates that are not transported vertically during bioirrigation. In this last scenario, trace metals would most likely be extracted in the exchangeable phase.

3.4.2 Carbonate Stable Isotopes (C and O)

Carbonate sediment consists of inorganically precipitated carbonates and biogenically produced carbonates. Carbonates which are inorganically precipitated reflect equilibrium values of the solution from which they precipitate. Different mineralogies of carbonate (i.e. low Mg calcite (LMC), high Mg calcite (HMC), and aragonite) have distinctive equation which govern the equilibrium, and thus will be identifiable in the isotopic signatures (Fig. 3.7, shaded boxes) (Swart, 2015). Biogenic carbonates may reflect the equilibrium of their environment, or become more negative due to “vital effects” in which

lighter isotopes are preferentially incorporated. Calcareous green algae, which is commonly observed in and around the cores collected for this study, exhibits little of the "vital effect" pushing more negative isotopic values, though exhibits a wide range of $\delta^{13}C$ (0 - +6‰) and $\delta^{18}O$ (-4 - +2‰) values due to the calcification process (Lowenstam and Epstein, 1957; Swart, 2015). Different species of calcareous green algae can have varied isotopic compositions dependent on their calcification mechanisms. Species commonly found near the cores taken include *Halimeda* sp., which calcifies via intercellular calcification, and has typical $\delta^{13}C$ ranging between ~+1 - +1‰, and *Penicillus* sp., which calcifies via sheath calcification and has typical $\delta^{13}C$ ranging between ~-1 - +4‰ (and differentiates based on the plant biology, e.g. stalk, head, and rhizoid) (Böhm et al., 1978; Lee and Carpenter, 2001; Wilbur et al., 1969). Both species have $\delta^{18}O$ ranges of ~-4 - -1‰ (Lee and Carpenter, 2001).

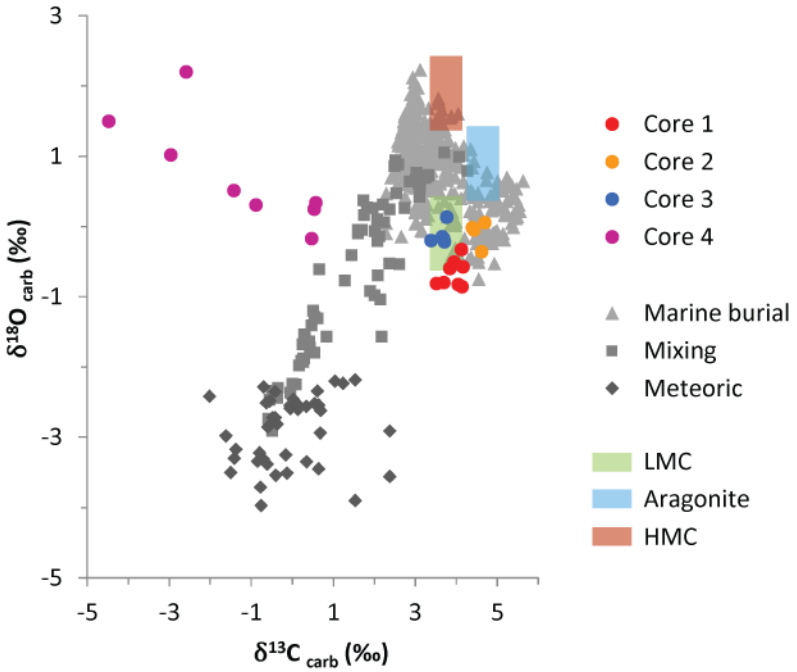

Figure 3.7 Cross plot of stable isotopes of the carbonate fraction compared with marine burial, marine and meteoric mixing, and meteorically influenced data from Oehlert and Swart (2014) taken from the "Clino" core from the Great Bahama Bank. Shaded regions represent approximate equilibrium of aragonite, LMC, and HMC deposited at the surface of the Great Bahama Bank (Swart, 2015).

Biogenic carbonates undergo extensive syndepositional dissolution and recrystallization, allowing for isotopic exchange between pore waters and secondary carbonate (Walter et al., 2007). Biogenic HMC and aragonite are dissolved and preferentially recrystallize forming the energetically favored LMC. Waters from which carbonates are precipitated have isotopic values which are effected primarily by meteoric water discharge, evaporation, $CaCO_3$ withdrawal, temperature, and pH (Patterson and Walter, 1994). Meteoric waters are typically depleted in $\delta^{18}O$ with respect to marine water (Knauth and Kennedy, 2009; Oehlert and Swart, 2014). Remineralization of organic matter present in pore waters and recrystallization of C into inorganic phases my lead to depleted $\delta^{13}C$ values (Oehlert and Swart, 2014). In deeper marine burial environments, covariations between $\delta^{13}C_{carb}$ and $\delta^{18}O_{carb}$ are indicative of meteoric diagenetic overprints replacing the marine signal or varying degrees of alteration due to a freshwater lens (Fig. 3.7, "mixed zone") (Swart and Oehlert, 2018).

Samples from cores 1, 2, and 3 have fairly constant $\delta^{13}C_{carb}$ and $\delta^{18}O_{carb}$ (Fig. 3.2) which plot near the equilibrium range for LMC, and are in the range of expected algal values. Primary precipitates are aragonitic, thus the isotopic values indicate a mixing of primary algal isotopic values and recrystallized LMC. Core 1 and 3 have slightly lighter $\delta^{13}C_{carb}$ values than core 2 (~3.5 versus ~4.5‰) which is likely due to inorganic precipitation of carbonate incorporating remineralized organic matter (as reflected in an increase in TOC) (Walter et al., 2007).

Core 4 exhibits depleted $\delta^{13}C_{carb}$ and enriched $\delta^{18}O_{carb}$ values, changing with depth (Fig. 3.2) and negatively correlated (Fig. 3.7, r = -0.8). Core 4, taken in a restricted salt water pond, contains is representative of two distinct environments, one in the upper 14 cm of the core and one in the lower 16 cm. The upper 14 cm has isotopic values which are likely driven by inorganic precipitation of carbonate. Elevated TOC (up to 3%) provide fuel for oxidation by organisms, and create a reducing environment (shown through trace metal proxies below). This is likely exacerbated by the input of terrestrial organics, which have isotopically light C with respect to marine organics (Meyers, 1994). The remineralized light C may then be recrystallized as inorganic carbonate, driving $\delta^{13}C_{carb}$ towards more negative values, and increasing with depth (Patterson and Walter, 1994). At the same time, in reducing environments, with

low pH, ^{18}O will be incorporated at rates higher than at high pH values (Swart, 2015). The combination of these two processes could lead to the down core variation of depleted $\delta^{13}C_{carb}$ and enriched $\delta^{18}O_{carb}$ values (Fig. 3.2) coupled with the negative covariation (Fig. 3.7, r = -0.8).

In the lower 16 cm of core 4, $\delta^{13}C_{carb}$ becomes more negative and $\delta^{18}O_{carb}$ becomes enriched. This corresponds a decrease in Sr and an increase in Mg (discussed below) and likely represents a unit of non-deposition and dolomitization. $\delta^{18}O_{carb}$ enrichments are associated with a transition from calcite to dolomite (Swart and Melim, 2000). The negative $\delta^{13}C_{carb}$ values are due to the type of organics being delivered during dolmitization (terrestrial), driving the $\delta^{13}C_{carb}$ of the pore water more negative.

3.4.3 Organic Stable Isotopes (C, O, and S)

In shallow water carbonates, the majority of the organic matter (OM) is derived from shallow water carbonate organisms (such as calcareous green algae or sea grass) or from terrestrial input (Oehlert and Swart, 2014). Marine organisms fix C from dissolved inorganic carbon (DIC) while terrestrial organic fix C from atmospheric CO_2 (Lajtha and Marshall, 1994). Terrestrial organics may be ~12 - 15‰ depleted in $\delta^{13}C_{org}$ with respect to those sourced from marine environments (Meyers, 1994; Swart, 2015). In the cores studied, a negative covariation between TOC and $\delta^{13}C_{org}$ suggest that the addition of terrestrial organics drives the changes in organic C isotopes (Fig. 3.8, A).

$\delta^{15}N_{org}$ of cores 1, 2, and 3, show little variations (Fig. 3.2) and poor correlation with TOC or $\delta^{13}C_{org}$, suggesting that little fractionation is taking place. Core 4 shows covariation between $\delta^{15}N_{org}$ and TOC, and a negative covariation between $\delta^{15}N_{org}$ and $\delta^{13}C_{org}$ (Fig. 3.8) indicating a relative increase of input of terrestrial organics in the lower core (C3 and C4 saltmarsh organics have $\delta^{15}N_{org}$ of ~6 - 14‰) (Cloern et al., 2002).

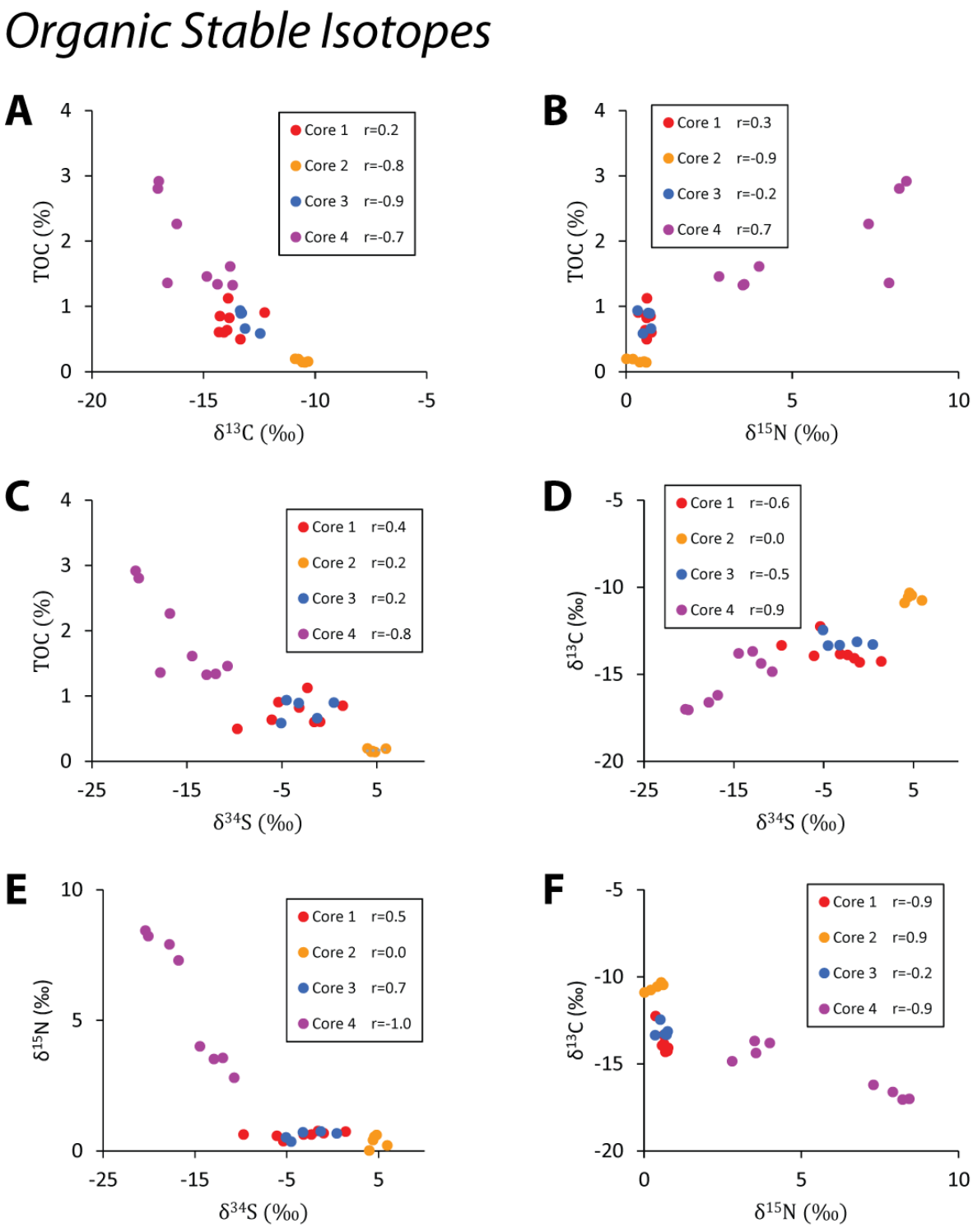

Figure 3.8 Cross plots of stable isotopes of de-calcified organic component, indicating various attributes of the diagenetic circumstances during deposition. (A) TOC versus $\delta^{13}C_{org}$. (B) TOC versus $\delta^{15}N_{org}$. (C) TOC versus $\delta^{34}S_{org}$. (D) $\delta^{13}C_{org}$ versus $\delta^{34}S_{org}$. (E) $\delta^{15}N_{org}$ versus $\delta^{34}S_{org}$. (F) $\delta^{13}C_{org}$ versus $\delta^{15}N_{org}$.

Sulphur isotopes experience fractionation in pore waters during bacterial sulphate reduction (BSR), in which pore water become isotopically heavy and preserved organics become isotopically light (Canfield et al., 1998; Swart, 2015). Sulphur oxidation and sediment disturbances keep levels of free H_2S relatively low. Cores 1 and 3 have depleted $\delta^{34}S_{org}$ values with respect to core 2, indicating that BSR occurred, preferentially releasing heavy S to the pore water and preserving light S, and in agreement with previously reported elevated H_2S (500 – 1500 µM) in pore waters (Romaniello et al., 2016). There is no covariation between TOC and $\delta^{34}S_{org}$, suggesting that this process affected a small percentage of TOC available for oxidation through decomposition by sulfate reduction (Walter and Burton, 1990) (Fig. 3.8). Core 2 has a positive, invariant $\delta^{34}S_{org}$ signature, due to decreased BSR (consistent with decreased H_2S reported by Romaniello et al., 2016). In core 4, $\delta^{34}S_{org}$ generally decreases with depth and negatively covaries with TOC (Fig. 3.8). Core 4 has the most negative $\delta^{34}S_{org}$ values, suggesting that BSR was an important process in the sediment pore waters. Organic decomposition by sulfate reduction creates reducing pore water environments with measurable levels of free H_2S, which can facilitate uptake of trace metals (discussed further below).

3.4.4 Minor Elements (Sr and Mg)

Sr and Mg substitute for Ca in $CaCO_3$, and can be used to explore the diagenetic history of sediment (Li and Jones, 2013, 2014; Stehli and Hower, 1961; Swart, 2015; Vahrenkamp and Swart, 1990). Aragonite and HMC typically contain elevated concentrations of Sr with respect to LMC and dolomite, thus can be used as indicators for dissolution and recrystallization. Mg is present in very low concentrations for aragonite, but indicates the presence of HMC or dolomite.. In cores 1, 2, and 3, concentrations of Sr (0.535 – 0.937 wt%) and Mg (0.4 – 1.4%) are similar to those found in The Bahamas (Swart and Melim, 2000). The majority of Sr in cores 1, 2, and 3 is found in the carbonate phase (Fig. 3.3), and not strongly correlated to Ca or $\delta^{18}O$ (Fig. 3.10). Sr in exchangeable, oxide, organic, and residual phases correlate well with Ca and poorly with the bulk $\delta^{18}O$ (an indicator of diagenesis), though are dilute compared to the carbonate phase (< 20 ppm) (Fig. 3.9, 3.11-13). Mg has a weak or negligible correlation with Sr and Ca in the carbonate and exchangeable phase, though stronger correlations in

oxide, organic, and residual phases in cores 1, 2, and 3 (Fig. 3.9-13). A strong covariation in the carbonate phase would be indicative of a HMC or dolomitization. Elevated Sr in core 2 of the carbonate phase (~0.6 wt%), with respect to cores 1 and 3 (~0.4 wt%) indicates that less of the original aragonite is being dissolved and recrystallized as LMC. This is consistent with the low levels of TOC and BSR in core 2. Bacterial degradation of organic matter and the coupled sulfide oxidation in pore waters provides the main acid source for carbonate dissolution (Walter et al., 1993).

In core 4 carbonate phase, Sr has a negative covariation with $\delta^{18}O$ and Mg, and a positive covariation with Ca, evidence of diagenesis (Fig. 3.10; r of -0.8, -0.8, and 0.9 respectively) (Li and Jones, 2014). Mg exhibits a negative covariation Ca (Fig. 3.10, r = -0.9). The majority of Sr and Mg occur in the carbonate phase, where two distinct trends exist. In the upper 14 cm of the core, there is high levels of Sr (~ 0.4 wt%) and low levels of Mg (~1 %), similar to that found in core 1 and 3. In the lower 16 cm of the core, Sr decreases (~0.25 wt%) and Mg increase (~6 %). This is indicative of dissolution and recrystallization of aragonite into dolomite (consistent with XRD carried out by Romaniello et al., 2013). As aragonite is dissolve, Sr is released to the pore waters, while Mg diffuses into the pore waters from terrestrial input and by dissolution of any HMC, incorporating into the dolomite (Swart and Melim, 2000). The elevated Mg and Fe (discussed more below) suggest that at some point, there was a time of non-deposition, in which the bottom half of core 4 was likely exposed to large amounts of meteoric flushing, consistent with previous studies of Bahamian hardgrounds (Swart and Melim, 2000).

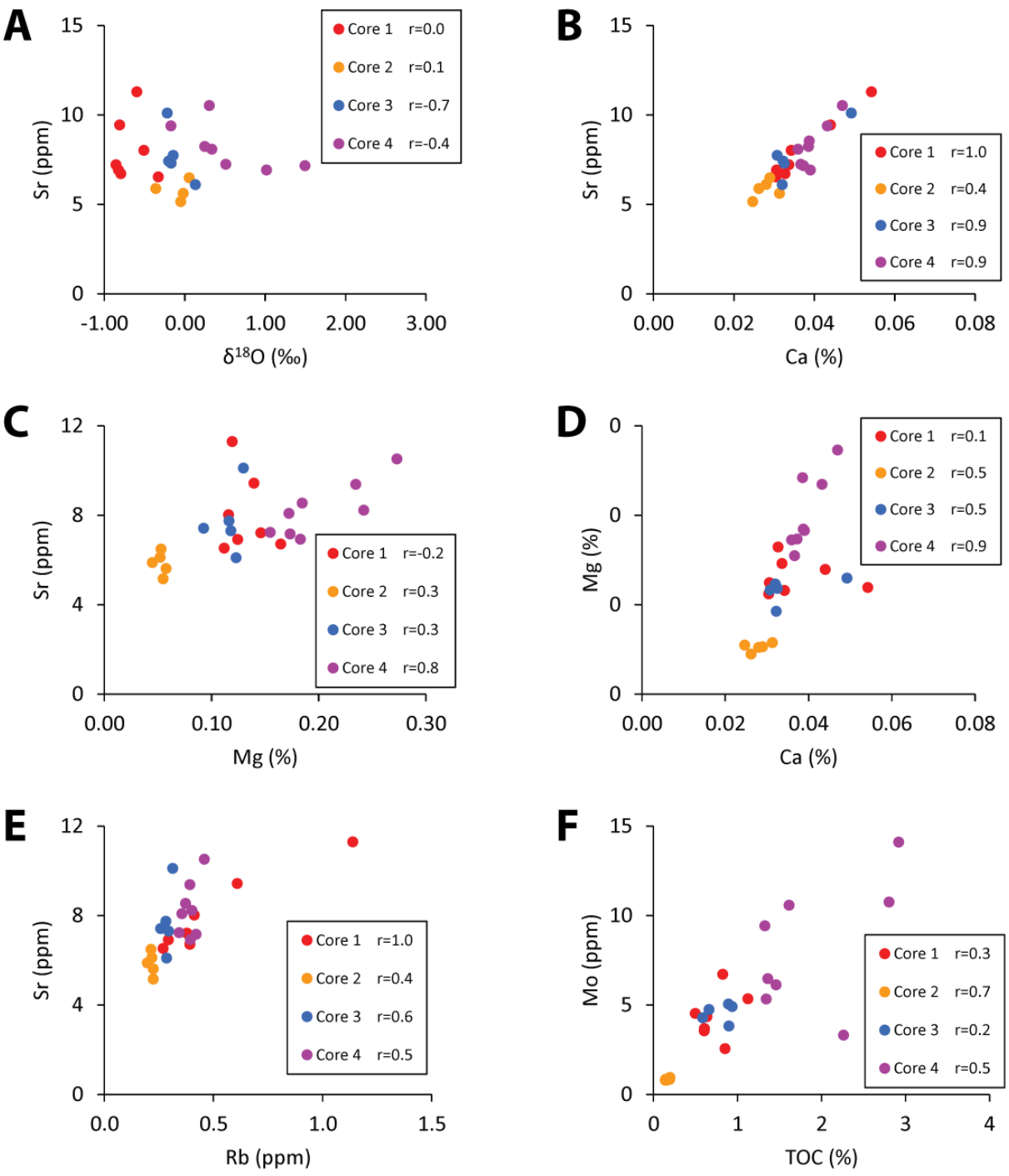

Figure 3.9 Cross plots showing relationships between various attributes of the exchangeable phase of the cores. (A) Sr versus $\delta^{18}O_{VPDB}$. (B) Sr versus Ca. (C) Sr versus Mg. (D) Mg versus Ca. (E) Sr versus Rb (F) Mo versus TOC. (G) U versus TOC. (H) Mo versus $\delta^{13}C_{org}$. (I) U versus $\delta^{13}C_{org}$. (J) Mo versus U. (K) Mo versus V (L) Mo versus $\delta^{34}S_{org}$. (Figure continued)

Exchangeable Phase (continued)

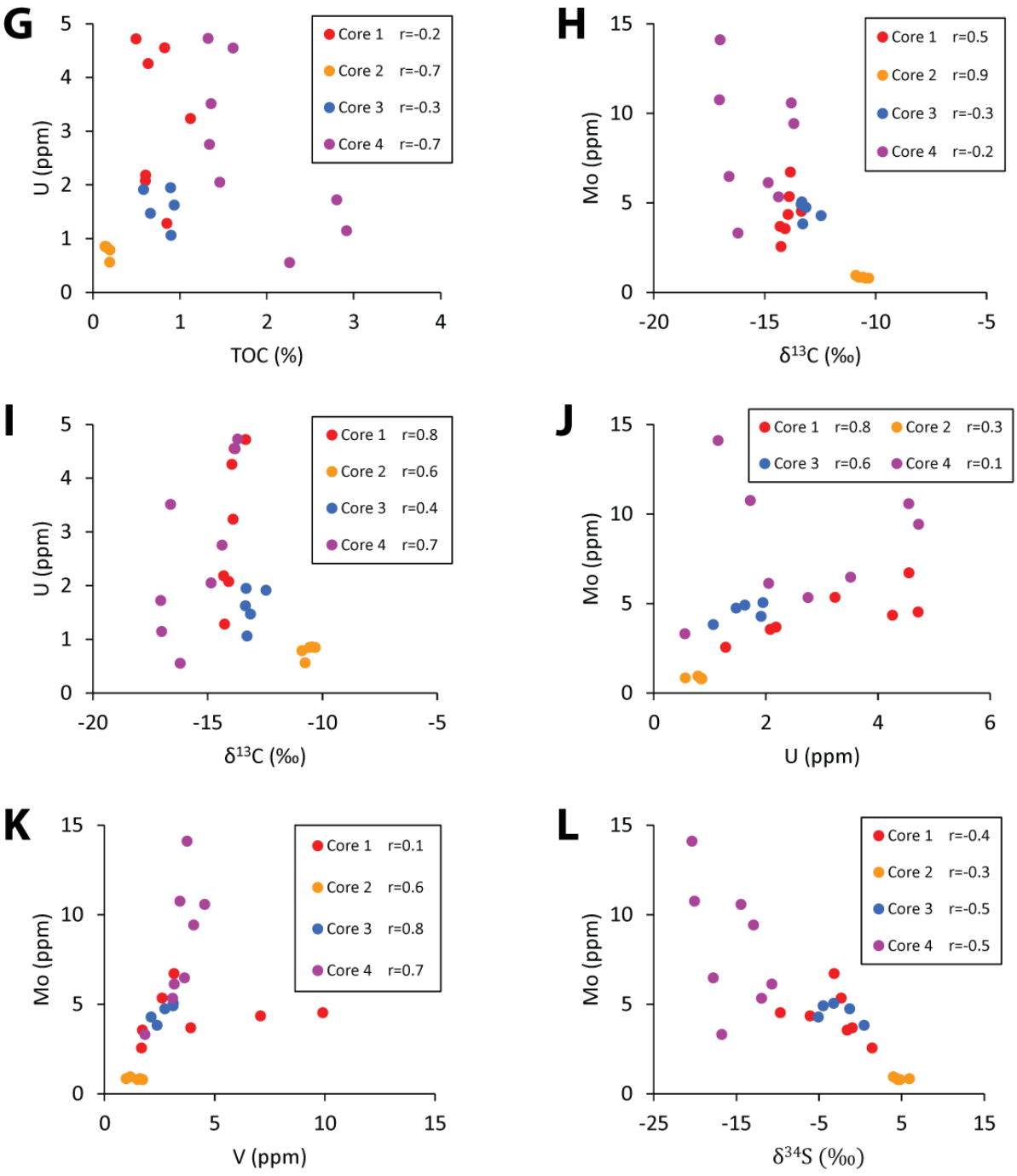

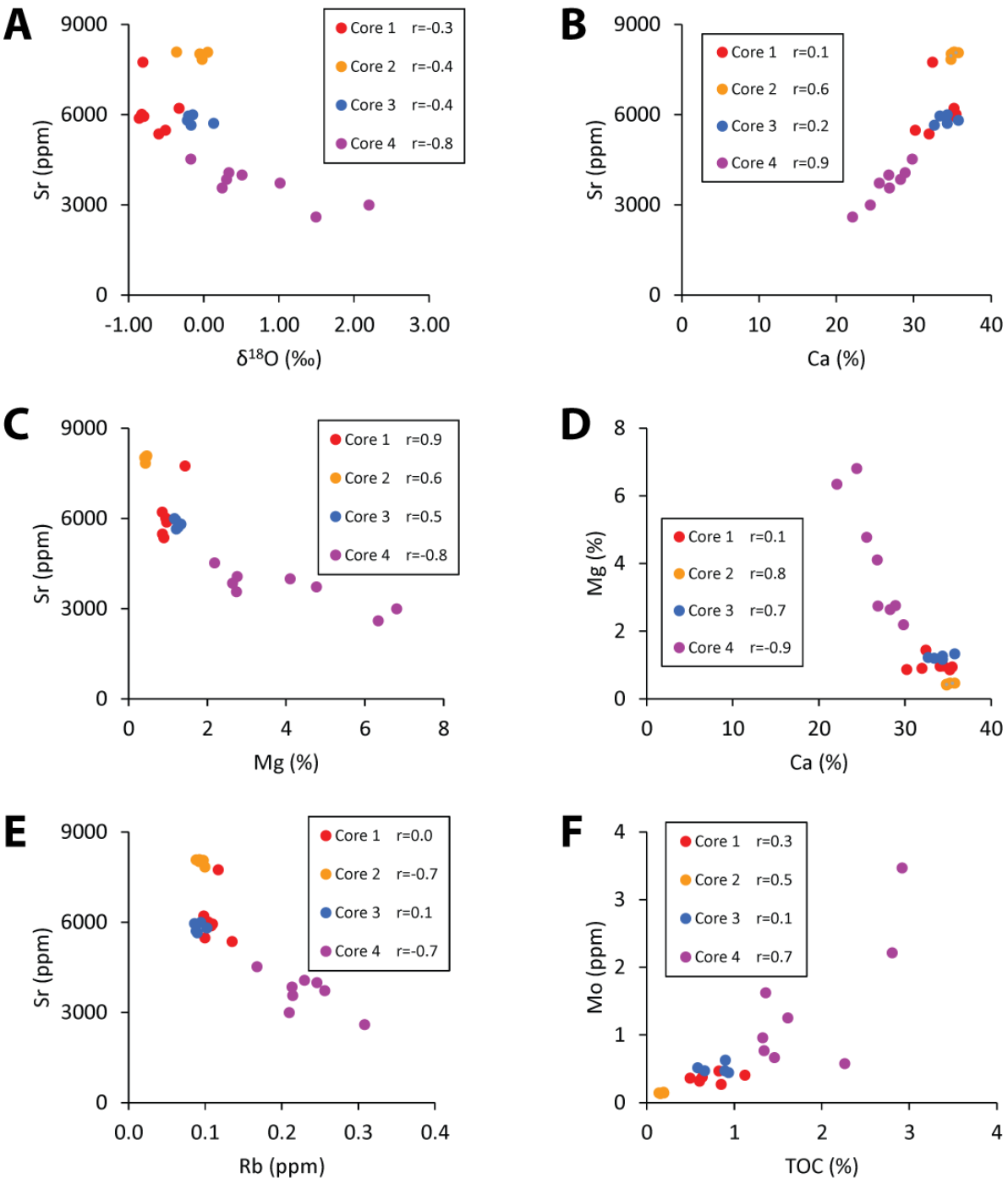

Figure 3.10 Cross plots showing relationships between various attributes of the carbonate phase of the cores. (A) Sr versus $\delta^{18}O_{VPDB}$. (B) Sr versus Ca. (C) Sr versus Mg. (D) Mg versus Ca. (E) Sr versus Rb (F) Mo versus TOC. (G) U versus TOC. (H) Mo versus $\delta^{13}C_{org}$. (I) U versus $\delta^{13}C_{org}$. (J) Mo versus U. (K) Mo versus V (L) Mo versus $\delta^{34}S_{org}$. (Figure continued)

Carbonate Phase (continued)

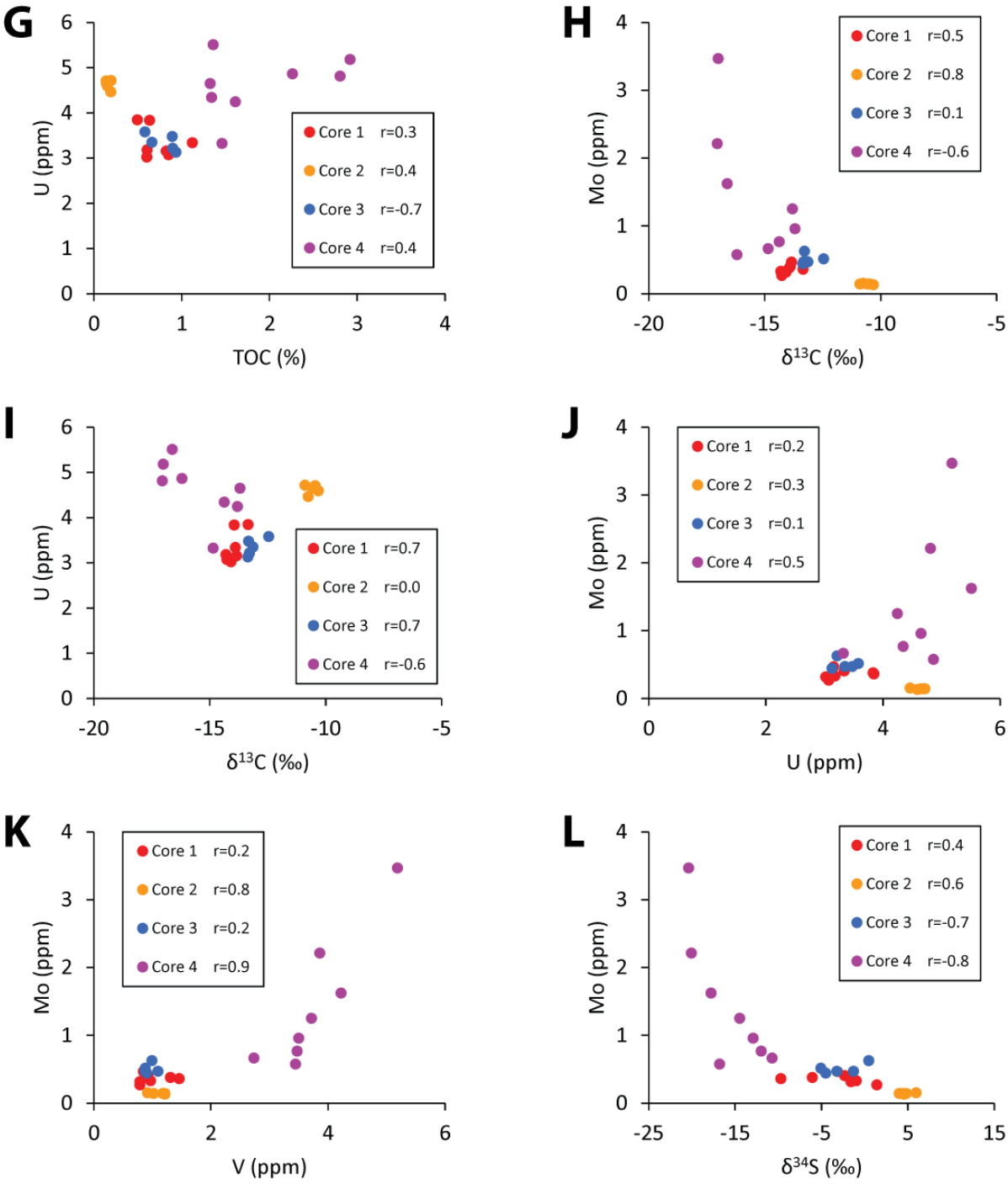

Oxide Phase

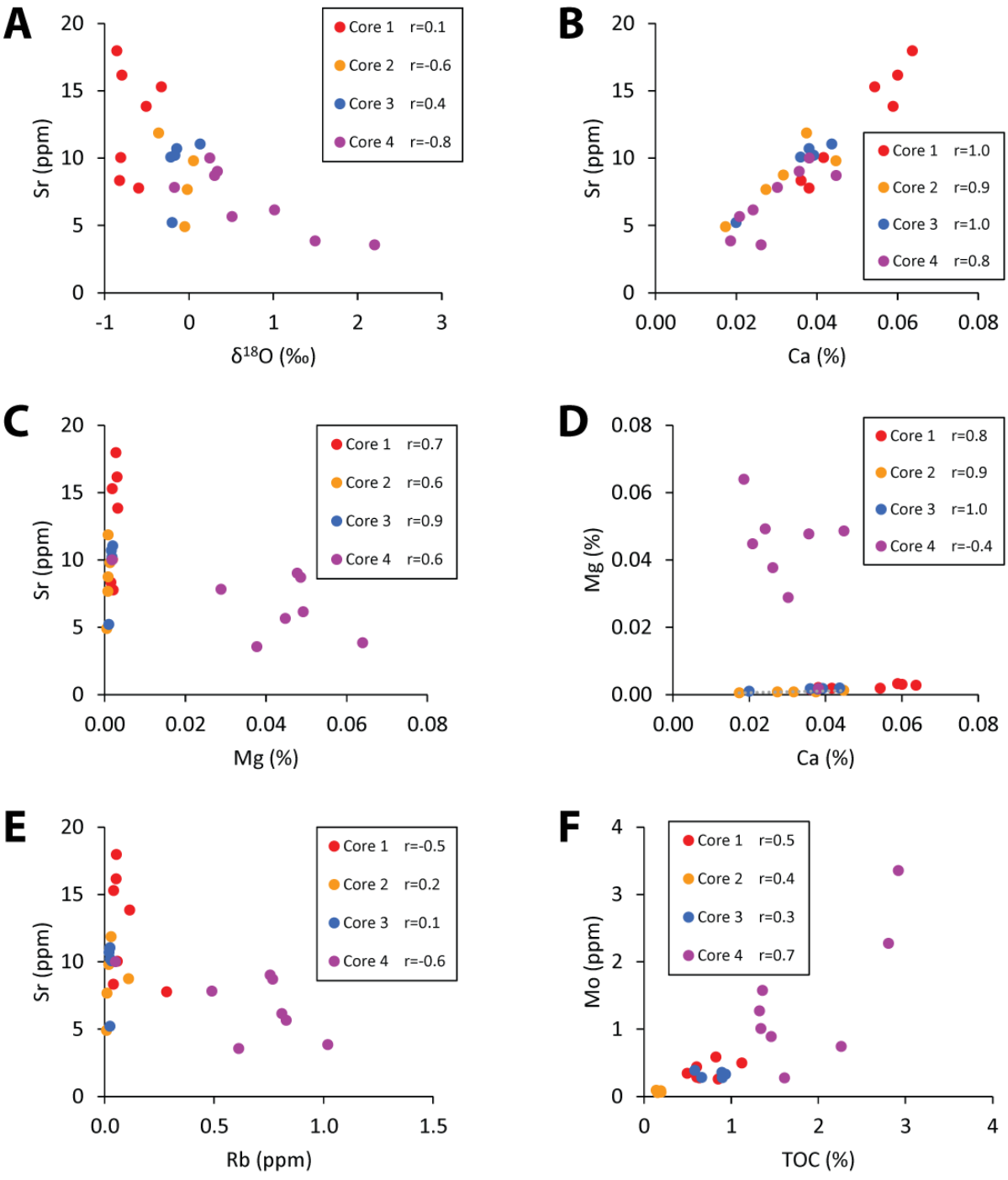

Figure 3.11 Cross plots showing relationships between various attributes of the oxide phase of the cores. (A) Sr versus $\delta^{18}O_{VPDB}$. (B) Sr versus Ca. (C) Sr versus Mg. (D) Mg versus Ca. (E) Sr versus Rb (F) Mo versus TOC. (G) U versus TOC. (H) Mo versus $\delta^{13}C_{org}$. (I) U versus $\delta^{13}C_{org}$. (J) Mo versus U. (K) Mo versus V (L) Mo versus $\delta^{34}S_{org}$. (Figure continued)

Oxide Phase (continued)

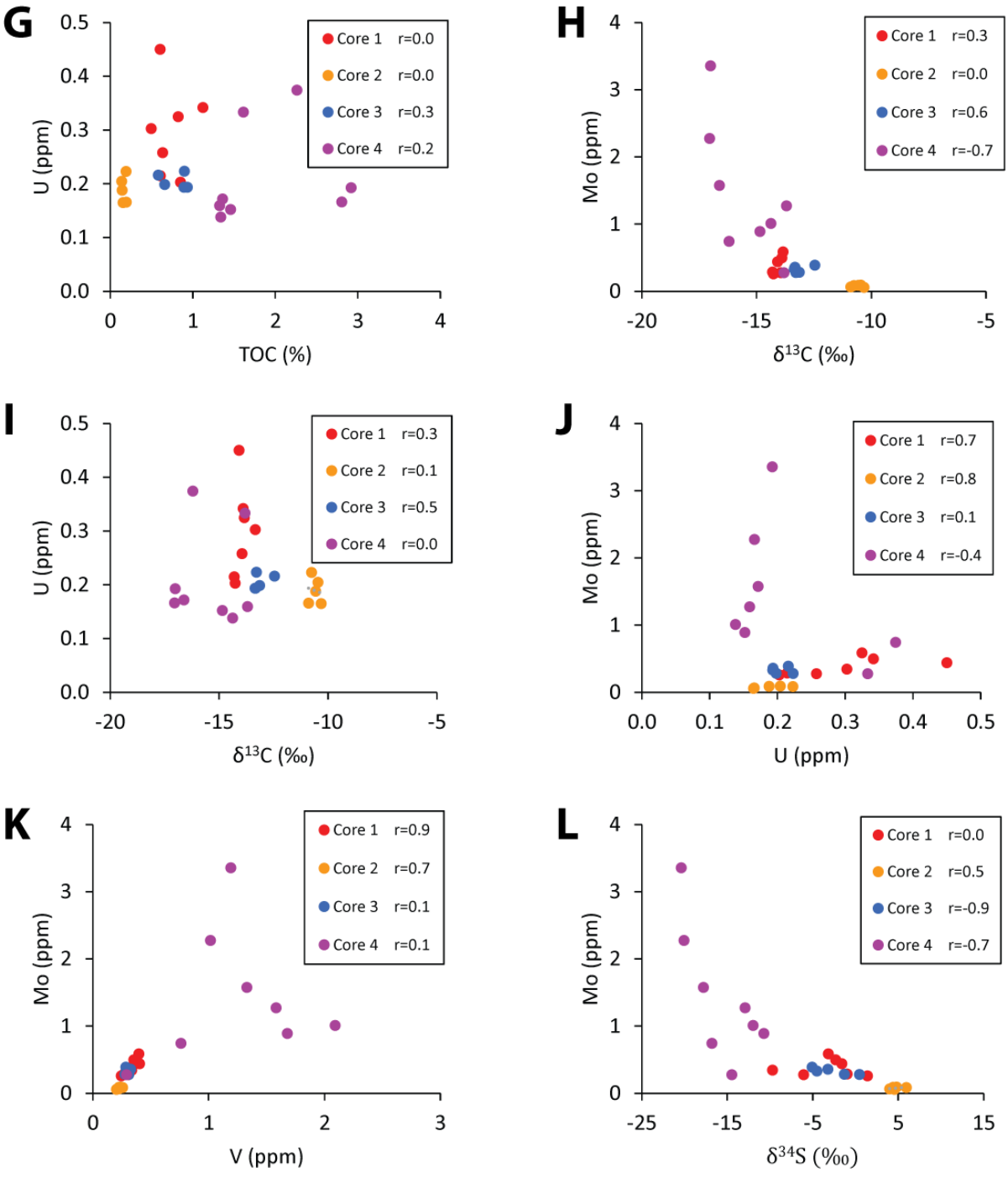

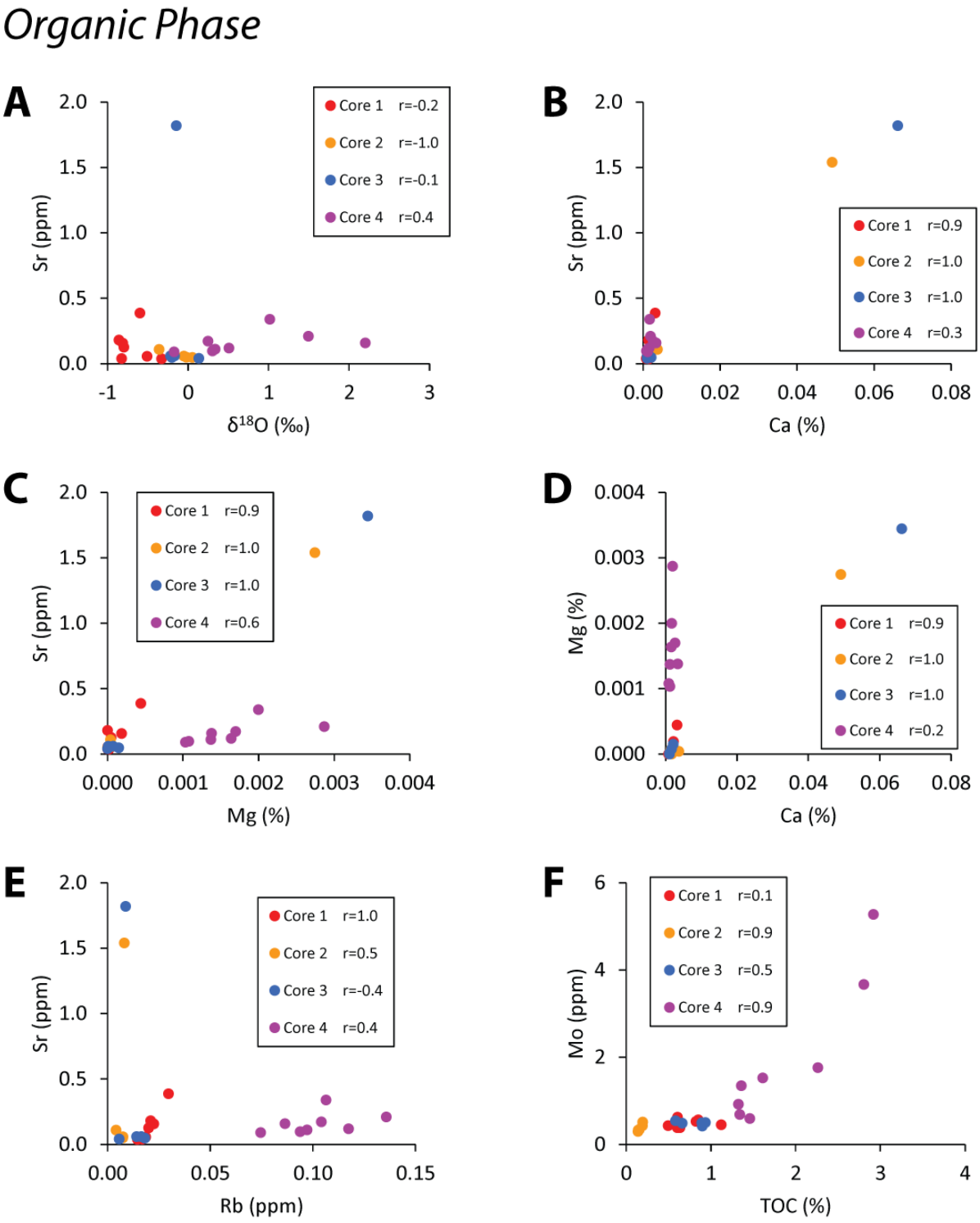

Figure 3.12 Cross plots showing relationships between various attributes of the organic phase of the cores. (A) Sr versus $\delta^{18}O_{VPDB}$. (B) Sr versus Ca. (C) Sr versus Mg. (D) Mg versus Ca. (E) Sr versus Rb (F) Mo versus TOC. (G) U versus TOC. (H) Mo versus $\delta^{13}C_{org}$. (I) U versus $\delta^{13}C_{org}$. (J) Mo versus U. (K) Mo versus V (L) Mo versus $\delta^{34}S_{org}$. (Figure continued)

Organic Phase (continued)

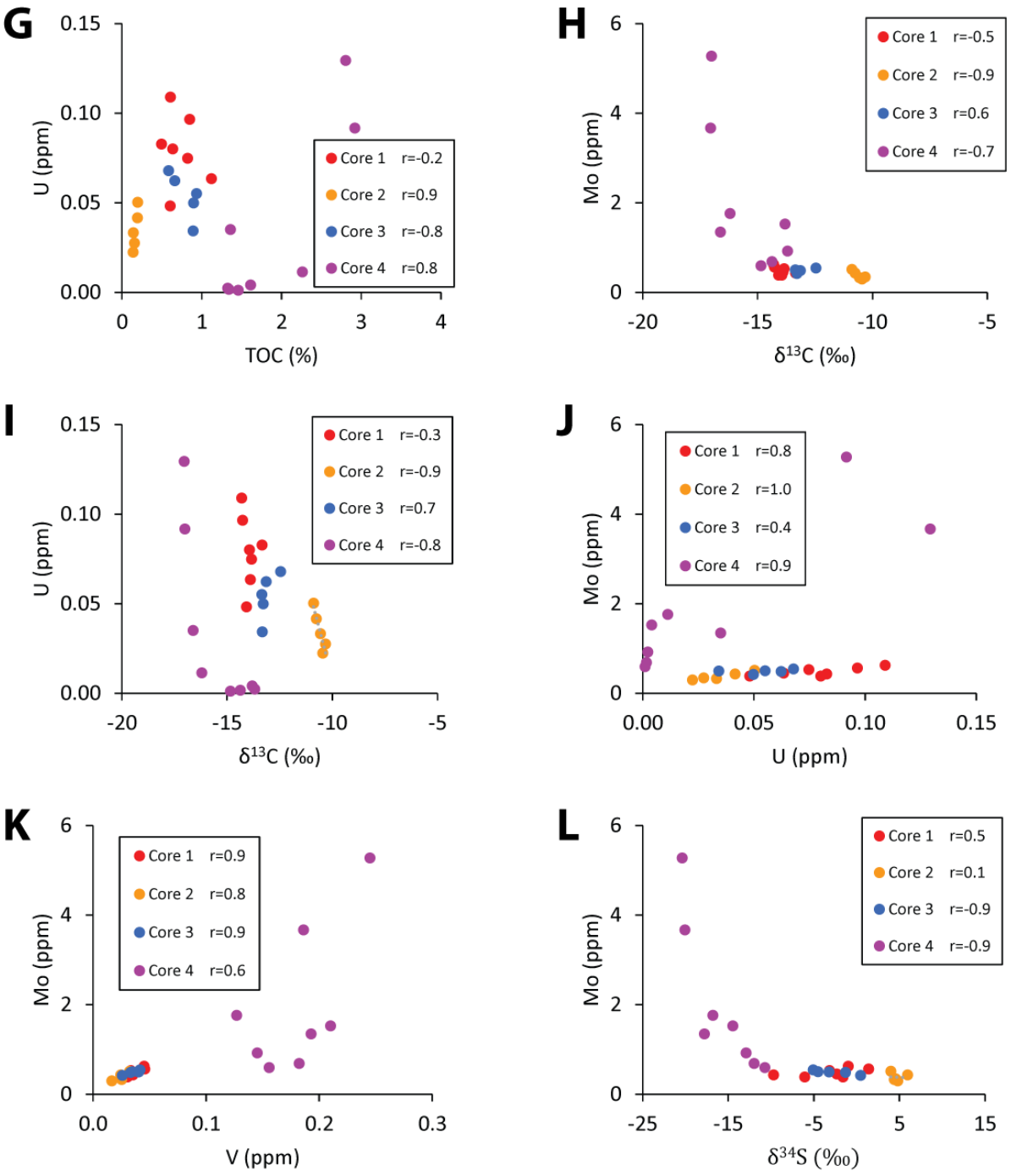

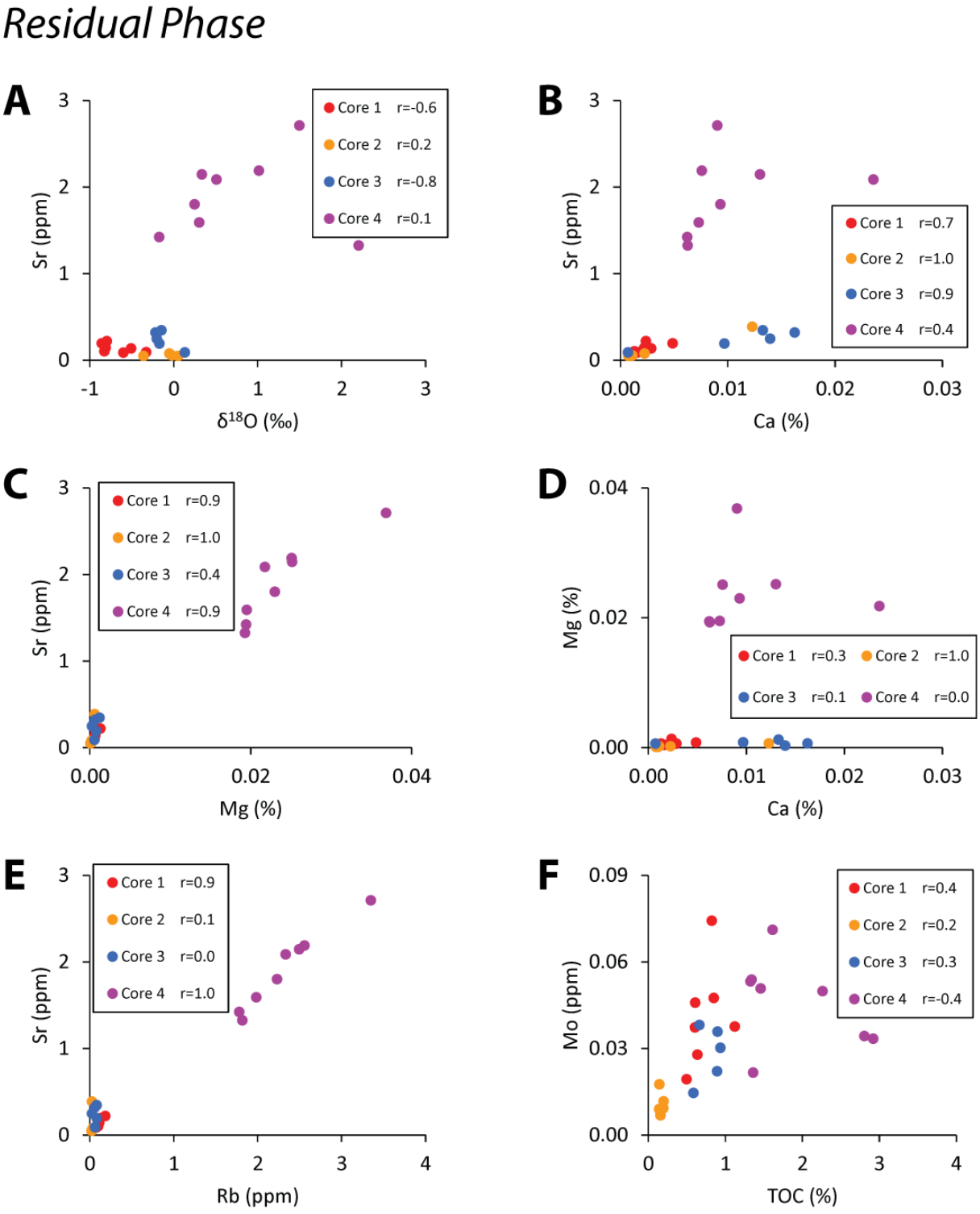

Figure 3.13 Cross plots showing relationships between various attributes of the residual phase of the cores. (A) Sr versus $\delta^{18}O_{VPDB}$. (B) Sr versus Ca. (C) Sr versus Mg. (D) Mg versus Ca. (E) Sr versus Rb (F) Mo versus TOC. (G) U versus TOC. (H) Mo versus $\delta^{13}C_{org}$. (I) U versus $\delta^{13}C_{org}$. (J) Mo versus U. (K) Mo versus V (L) Mo versus $\delta^{34}S_{org}$. (Figure continued)

Residual Phase (continued)

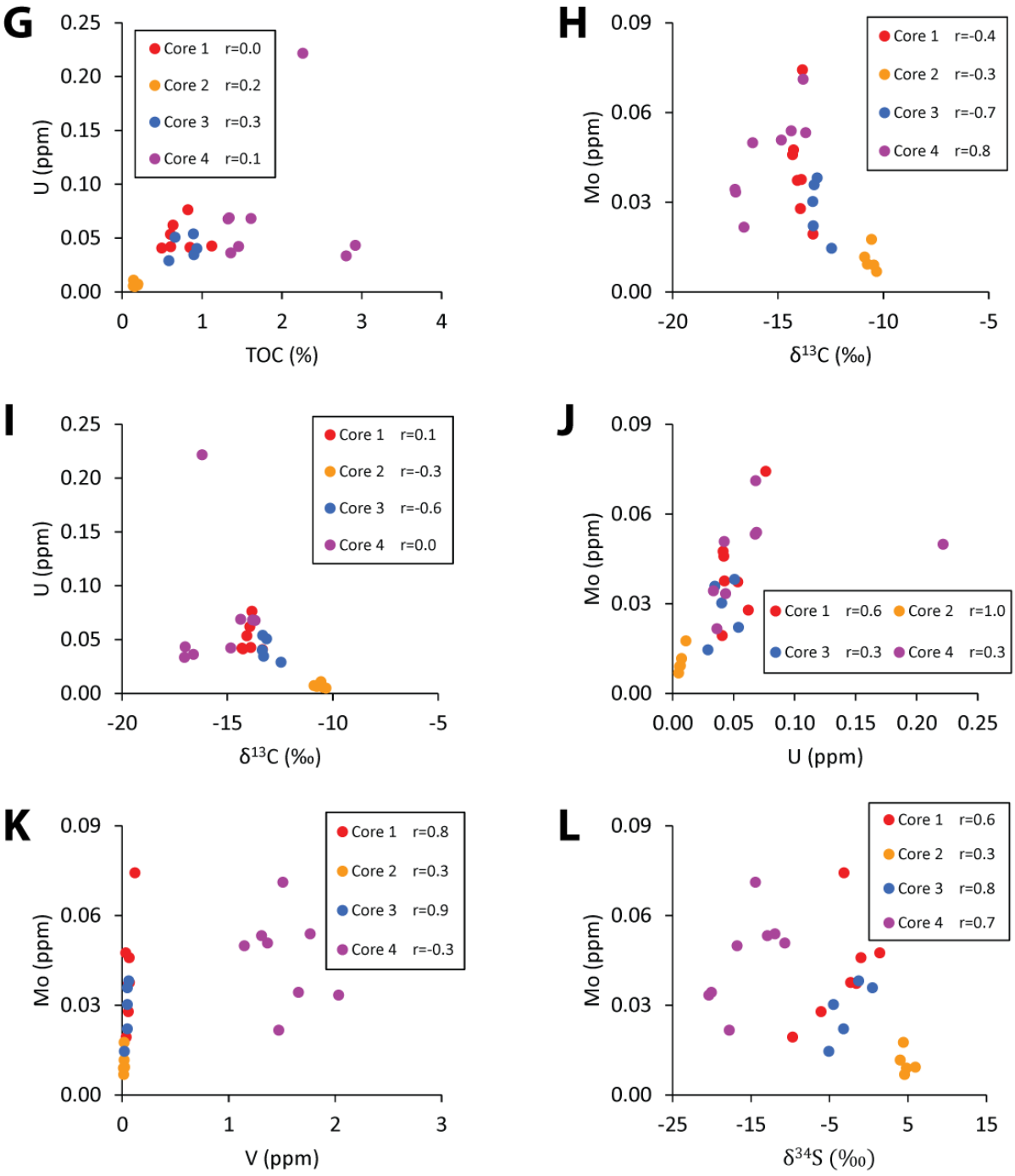

3.4.5 REE + Y

3.4.5.1 Chemistry of REE + Y in seawater

Rare earth elements consist of fourteen elements forming the Lanthanide series. Y is often included with REEs due to its similar chemical properties to Ho. The oxidation state of REE+Y (typically +3) and ionic radius, along with other chemical properties, result in predictable distributions in oceans and sediment (Bau and Dulski, 1996; Elderfield and Greaves, 1982). REEs are supplied to the ocean by riverine input, hydrothermal vents, or through Aeolian dust, and removed through particle scavenging to the sediments (Elderfield and Greaves, 1982; Tostevin et al., 2016). Absolute concentrations of REEs are often (and in this study) normalized to Post Archean Australian Shale (PAAS) (McLennan, 1989) to provide smooth, comparable patterns. Hydrothermal vents and riverine input carry flat shale-normalized (SN) patterns. Once freshwater interacts with saline waters however, patterns quickly acquire seawater characteristics with negative Ce anomalies and HREE enrichments (low Ce/Ce* and Nd_{SN}/Yb_{SN} ratios) (Elderfield and Greaves, 1982). Ce is unlike other REEs in that it occurs naturally in a 3+ or 4+ valance state, and can be readily removed to the sediment in the oxidized Ce(IV) state (Bau and Dulski, 1996; Tostevin et al., 2016). This results in the marine negative Ce anomaly in oxidized oceans and can be used to track redox conditions. Open marine environments contain Y/Ho mass ratios of >36, with ratios up to 40-80 in open marine settings and 33-40 among nearshore or restricted environments (De Baar et al., 1985; Tostevin et al., 2016).

3.4.5.2 REE+Y in the Bahamian cores

In the carbonate phase, PAAS normalized REE's express slightly negative Ce anomalies and positive La anomalies in cores 1, 2, and 3, consistent with seawater values (Fig . 3.14, 3.15) (Bau and Dulski, 1996; Osborne et al., 2015; Piper and Bau, 2013; Webb and Kamber, 2000). Y/Ho ratios are ~50 – 60 for cores 1, 2, and 3, signifying little to no detrital input, as expected in Bahamian samples (Webb and Kamber, 2000). Previous work has shown Light REE's (LREE) are enriched in Bahamian soils due to Aeolian dust input, however, there is no significant LREE enrichment, as reflected in Nd/Yb ratios of ~ 0.55 in cores 1, 2, and 3, suggesting that the REE contribution from terrestrial soils are minimal in these

sections (Muhs et al., 2007). The ΣREY do not strongly correlate with Ca, Sr, $\delta^{18}O$, or Fe (Fig. 3.16), suggesting that there is not a strong diagenetic control or fractionation to oxides (Li and Jones, 2014; Tostevin et al., 2016). The seawater-type distribution of REEs and lack of covariation among diagenetic sensitive elements suggests that seawater REE values are preserved in the carbonate phase of cores 1, 2, and 3 (Fig. 3.14-16). This indicates that REE values are not significantly impacted, even during diagenesis under reducing pore water conditions, consistent with previous studies of REE incorporation into carbonate sediments (Liu, 2018; Webb et al., 2009).

Core 4 has REE patterns unlike those of Cores 1, 2, and 3. Core 4 shows no Ce or La anomaly (Fig. 3.15), moderate HREE enrichment (Nd/Yb average of 0.73, standard deviation of 0.03), and decreased Y/Ho ratios (average of 44.48, standard deviation of 2.55). The decreased Y/Ho ratio and flattened HREE enrichment (Fig. 3.14) suggest increased terrestrial input, consistent with stable isotope. Negative Ce anomalies are indicative of sediment forming under oxic conditions, however the lack of a Ce anomaly, as in Core 4 (Fig. 3.15), does not necessarily prove an increase in reducing conditions during carbonate formation (Tostevin et al., 2016). Factors such as being in a restrictive environment or deposition nearshore can both result in a lack of Ce anomaly, which core 4 being deposited in a restricted salt pond, represents both scenarios (Tostevin et al., 2016). Previously reported pH values (Romaniello et al., 2013) indicate that pore waters were not more reducing than in the subtidal section, thus the Ce anomaly reflects the restriction and terrestrial input to the pond. As with cores 1, 2, and 3, ΣREY do not strongly correlate with diagenesis-sensitive indicators (Fig. 3.16), suggesting that carbonate of core 4 records the REE values of water in which it formed (Li and Jones, 2014).

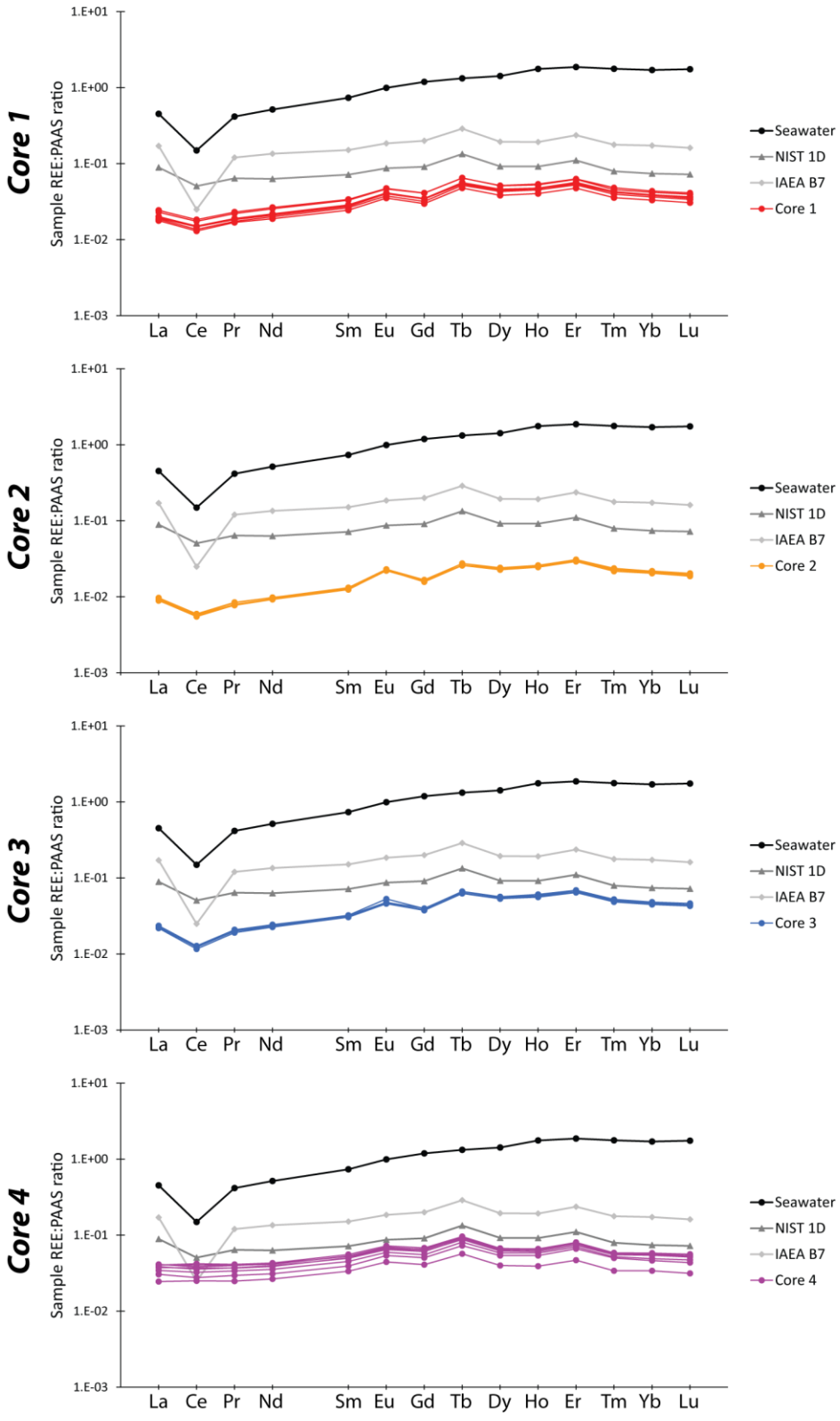

Figure 3.14 REE profile of the carbonate phases of samples from the four cores compared with seawater. Seawater data is from Osborne et al. (2015), surface water from location 200-2.

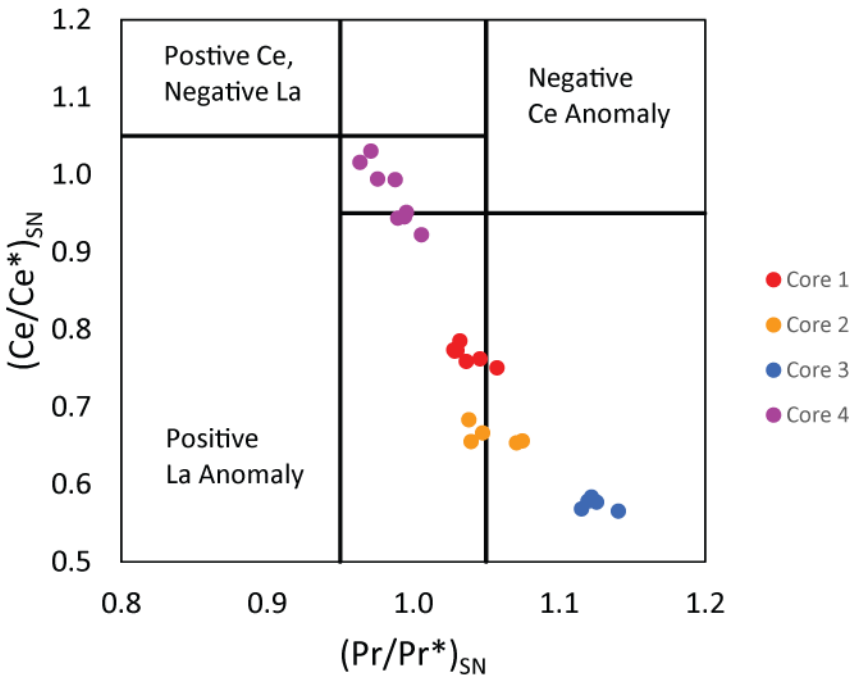

Figure 3.15 Ce and La anomalies, as calculated from $(Ce/Ce^*)_{SN} - (Pr/Pr^*)_{SN}$ variations, after Bao and Dulski (1996). Typical seawater values have positive Ce and La anomalies.

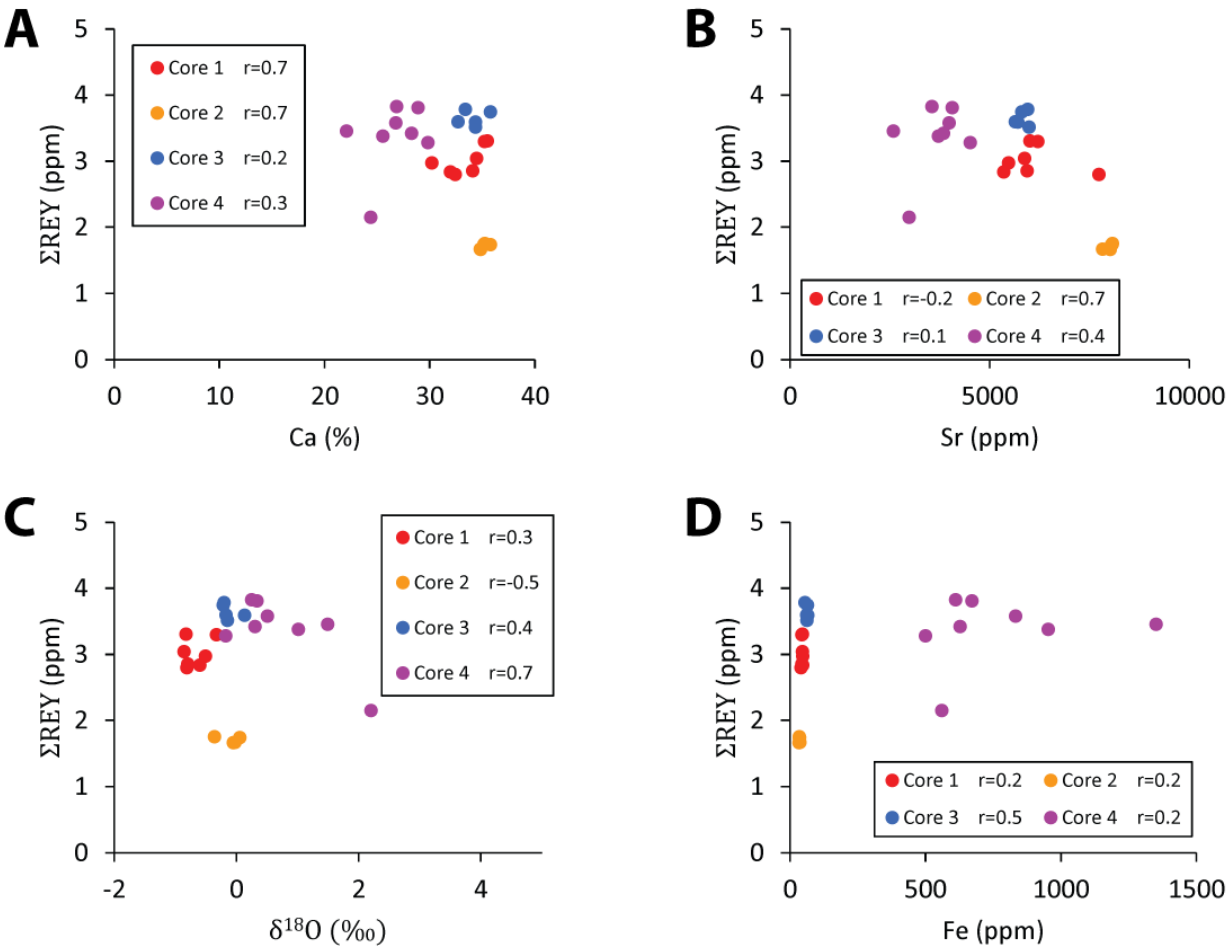

Figure 3.16 Cross plots of the sum of REEs + Y (ΣREY) and various diagenetic indicators. (A) ΣREY versus Ca. (B) ΣREY versus Sr. (C) ΣREY versus $\delta^{18}O_{carb}$. (D) ΣREY versus Fe.

3.4.6 Authigenic Accumulation of U

3.4.6.1 Geochemistry of U

The geochemistry of U in marine environments is highly redox sensitive. In seawater, U(VI) binds to carbonate ions, forming $UO_2(CO_3)_3^{4-}$ and $Ca_2UO_2(CO_3)_3$(aq) (Chen et al., 2016). In reducing environments, soluble U(VI) is reduced to U(IV) and may be scavenged to the sediment, either as an adsorbed species or as a precipitate such as uraninite (UO_2) (Calvert and Pedersen, 1993; Klinkhammer and Palmer, 1991; Tribovillard et al., 2006). The accumulation of authigenic U is in part controlled by bacterial sulphate reduction reactions, as it accelerates the U reduction (McManus et al., 2005; Tribovillard et al., 2006). U may be re-oxidized in the sediment through oxygen penetration, erasing or

potentially masking an original signature (McManus et al., 2005; Morford et al., 2001; Tribovillard et al., 2006).

3.4.6.2 U in Bahamian Cores

Sequential extractions performed for this study show that all chemical phases remain essentially constant downcore with respect to U (±0.5 ppm), with the exception of the exchangeable fraction (Fig. 3.5). The exchangeable fraction increases in concentration from ~ 1.3 to ~ 4.5 ppm in Core 1, and 1.0 to 1.9 ppm in Core 3 (Fig. 3.5), and also increases the percentage of U contribution to the sample; suggesting the exchangeable phase hosts the majority of authigenically accumulated U.

In the carbonate phase, there is little covariation between U-TOC or U-$\delta^{13}C_{org}$ (Fig. 3.10), indicating that carbonate bound U is not effected by the amount of the amount of organic material, or remineralization of such material, and thus is likely a primary precipitate source, such as U directly incorporated in calcareous green algae. There are low concentrations of U (< 1 ppm) hosted in oxide and residual phases, and do not covary well with TOC or U-$\delta^{13}C_{org}$ (Fig. 3.11 and 3.13). The organic phase contains low concentrations of U (< 0.15 ppm), though is correlated with TOC in core 2 and 4, suggesting a minor contribution of U adsorbed to organics (Fig. 3.12).

Authigenic accumulation of U can be in part controlled through BSR reactions due to the fact that sulfate reducing organisms may use U for electron transport (Lovley et al., 1991). This is confirmed to be a driving factor in the exchangeable phase (where authigenic U accumulates) through strong negative covariation of U-$\delta^{34}S$ in cores 1, 2, and 3 (Fig. 3.17). Core 4 shows no covariation between U-$\delta^{34}S$; a result of the meteoric induced dolomitization (detailed in section 4.3) in which oxic waters flushed through the sediment, re-oxidizing and mobilizing authigenic U (McManus et al., 2005).

The accumulation of U downcore in Cores 1 and 3 in the exchangeable phase, along with reducing pore water conditions conducive to precipitation of mononuclear U(IV) suggests an authigenic accumulation of mononuclear U(IV). The remaining chemical phases, other than exchangeable, sum to a concentrations of U between ~ 3 and 5 ppm, similar to primary precipitates (Romaniello et al., 2013), indicating that authigenically accumulated U is quantitatively removed in the bicarbonate phase.

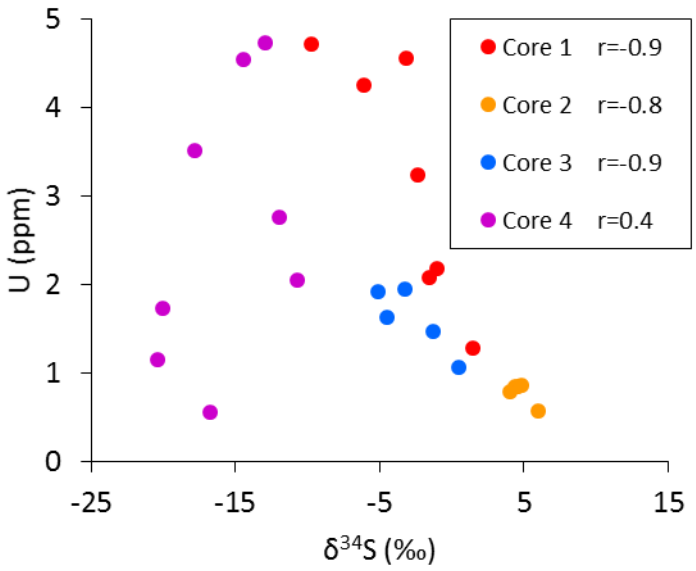

Figure 3.17 Cross plot of $\delta^{34}S$ versus U of the exchangeable phase.

3.4.7 Authigenic contribution of Mo

3.4.7.1 Geochemistry of Mo

Similar to U, Mo is sensitive to shifts to marine redox conditions. Respiration of organic matter during sulfate reduction drives pore water conditions in which free H_2S exceeds ~11 μM, then soluble molybdate (MoO_4^{2-}) is converted to a particle reactive thio-molybdate ($MoO_{4-x}S_x^{2-}$) (Erickson and Helz, 2000). Given sustained euxinic conditions, molybdate may be converted to tetrathio-molybdate (MoS_4^{2-}) and quantitatively removed from sediment, such as what is thought to happen in restrictive, organic rich environments (Algeo and Lyons, 2006).

3.4.7.2 Mo in Bahamian Cores

Mo concentrations, like U, are higher in shallow Bahamian sediment than the primary precipitates that make up the sediment. In the shallow cores analyzed presently, Mo concentrations are variable (< 0.1 – 30 ppm), while modern primary skeletal and non-skeletal precipitates are generally lower (0.005 – 0.17 ppm) (Romaniello et al., 2016; Voegelin et al., 2009). A large percentage of the total concentration of Mo is soluble in the sodium bicarbonate phase of the sequential extraction (Fig. 3.6). Carbonate phase Mo in cores 1, 2, and 3 has a concentration similar to that of primary precipitates (~ 0.1 ppm) and is

generally constant downcore, suggesting that the carbonate phase may retain Mo which coprecipitated with primary precipitates.

Core 4 incorporates progressively more Mo with depth, primarily into the exchangeable phase, but also into carbonate, oxide, and organic phases. As stable isotopes have shown, core 4 experiences dolomitization, effecting the preservation and uptake of trace metals. While much of the total Mo abundance occurs in the exchangeable phase, it is unlikely that remaining phases of core 4 consist only of Mo from primary precipitates as the concentration is much higher (~ 3-5 ppm) than those measured in primary precipitates.

Authigenic enrichment of Mo is mediated by the amount of free H_2S in the pore waters, supplied through organic matter respiration during sulfate reduction (Burdige and Zimmerman, 2002). As such, the exchangeable phase (in which authigenic Mo accumulates) moderately covaries with $\delta^{34}S$ in all cores (Fig. 3.9). Mo covaries poorly with TOC or $\delta^{13}C$ in all phases (Fig. 3.9-13), suggesting that uptake of Mo is not related linearly to an increase in organic matter or reducing conditions, consistent with a stepwise sulfurization of thimolybdates (MoO_xS_{4-x}) (Erickson and Helz, 2000; Romaniello et al., 2016).

3.4.8 Authigenic accumulation of V

Vanadium is present as V(V), forming vanadate oxyanions in oxic waters and may readily adsorb onto Mn- and Fe-oxyhydroxides (Tribovillard et al., 2006). Reducing conditions result in the reduction of V(V) to V(IV), and the formation of hydroxyl species of the vanadyl ions which may form organometallic ligands or adsorb onto particles (Calvert and Pedersen, 1993; Emerson and Huested, 1991). Further reducing conditions, such as in the presence of H_2S formed through BSR in pore waters, can lead to the precipitation of a solid oxide (V_2O_3) or hydroxide phase $V(OH)_3$ (Breit and Wanty, 1991; Wanty and Goldhaber, 1992). Unlike Mo, V is probably not trapped in solid solution by Fe-sulfides, and may be removed from waters (Wanty and Goldhaber, 1992).

In the Bahamian cores, V is present primarily in the exchangeable phase of cores 1, 2, and 3 (Fig. 3.5). It covaries with Mo in the exchangeable phase in cores 2 and 3 (Fig. 3.10), suggesting that free H_2S in pore waters drives the uptake of V, similarly to Mo. V may be taken up in organic complexes or as

hydroxides, thus the presence of organics in cores 1, 2, and 3 may aid in V uptake. In core 1, V concentrations increase with depth in the exchangeable phase not reflected in similar changes in Mo concentration, indicating that Mo may have been quantitatively removed from pore waters, as evidenced previous studies showing δ^{98}Mo decreasing in the lower 20 cm of core 1 (Romaniello et al., 2016). In core 4, V is present primarily in the residual phase. This suggests remobilization of the exchangeable V, likely due to a flushing of oxygenated waters. While V concentrations are low in all cores (up to 12 ppm compared to average carbonates of 20 ppm) the increase with depth in the exchangeable phase and covariation with Mo suggests a redox controlled uptake in The Bahamas sections (Turekian and Wedepohl, 1961)

3.4.9 Diagenetic environments and their effect on sediment geochemistry

The cores may be divided into three diagenetic environments. Core 2, collected in a shallow tidal flat, periodically exposed to elements like rain and meteoric flushing, core 1 and 3, collected from slightly deeper, subtidal flats, and core 4, collected from a tidally connected pond, in which two phases of deposition are present, one in the upper 14 cm of the core, and one in the lower 16 cm (Fig. 3.18).

Tidal Flat

The tidal flat measured in core 2 has low TOC (~0.2%), and a lack of covariation between TOC and $\delta^{13}C_{org}$ indicate little organic input. Any organics that are input into the environment are quickly remineralized. Bacterial sulfate reduction occurs (as indicated by measured pore water H_2S; Romaniello et al., 2013), though $\delta^{34}S$ are higher than in the deeper subtidal flat, suggesting it occurs at a lower rate in the tidal flat. An absence of U in the exchangeable phase suggests periodic flushing of oxidized water, consistent with the section location. REY values reflect sea water values, suggesting that the meteoric flushing does not alter the REY signatures of the carbonates. Sr is elevated in this section, with respect to other sections, indicating that less of the original aragonite is being dissolved and reprecipitated.

Subtidal Flat

Cores from the slightly deeper, subtidal regime (cores 1 and 3) have elevated TOC with respect to the tidal flat (~0.8%). This area is also represented by a slight decrease in Sr relative to the tidal flat,

indicative of aragonite dissolution and recrystallization into LMC. The dissolution is driven by acid production through bacterial respiration of organic matter (Walter et al., 1993). Pore waters which are reducing (evidenced by elevated pore water H_2S with respect to tidal flat; Romaniello et al., 2013) and more insulated from meteoric input than the tidal flat, support the sulfurization of Mo and V and the incorporation of reduced U into the loosely bound exchangeable phase (Fig. 3.18). Covariations of $\delta^{13}C_{org}$ and TOC show a mixed input of terrestrial and marine organics into the sediment. REY values of the subtidal realm, like those of the tidal flat, reflect seawater values, suggesting that despite the dissolution and reprecipitation of carbonates, original sweater values are preserved in the carbonate phase.

Tidal Pond

The tidal pond has the highest concentration of TOC, the lightest $\delta^{13}C_{org}$ values representing a large contribution of terrestrial organic input (Fig. 3.18). The pond concentrates terrestrial input, unlike the other settings investigated, evidenced by elevated Fe_T concentrations. Windblown dust supply Fe to the surrounding island, as runoff carries it into and concentrates in the pond. The tidal pond study section has two distinct geochemical signatures, one in the top 14 cm, and one in the bottom 16 cm. In the top 14 cm, bacterial respiration in the pore waters drive reducing conditions allowing for the sulfurization of Mo and V and the incorporation of reduced U into the loosely bound exchangeable phase, similar to enrichments seen in the subtidal flat. In the lower 16 cm, however, Sr and Mg negatively covary, with a significant increase in Mg. This is likely due to a time period of nondeposition, where meteoric water flushed through the system, dolomitizing the sediment (Swart and Melim, 2000). This is supported by elevated levels of Fe in the lower 16 cm of core 4. Flushing of oxic waters remobilized U and V, decreasing concentrations in the exchangeable phase with respect to the overlaying 14 cm. Mo is incorporated into oxide and organic phases during diagenesis. REYs of the sediment record an increase in terrestrial input (Y/Ho and Ce anomalies).

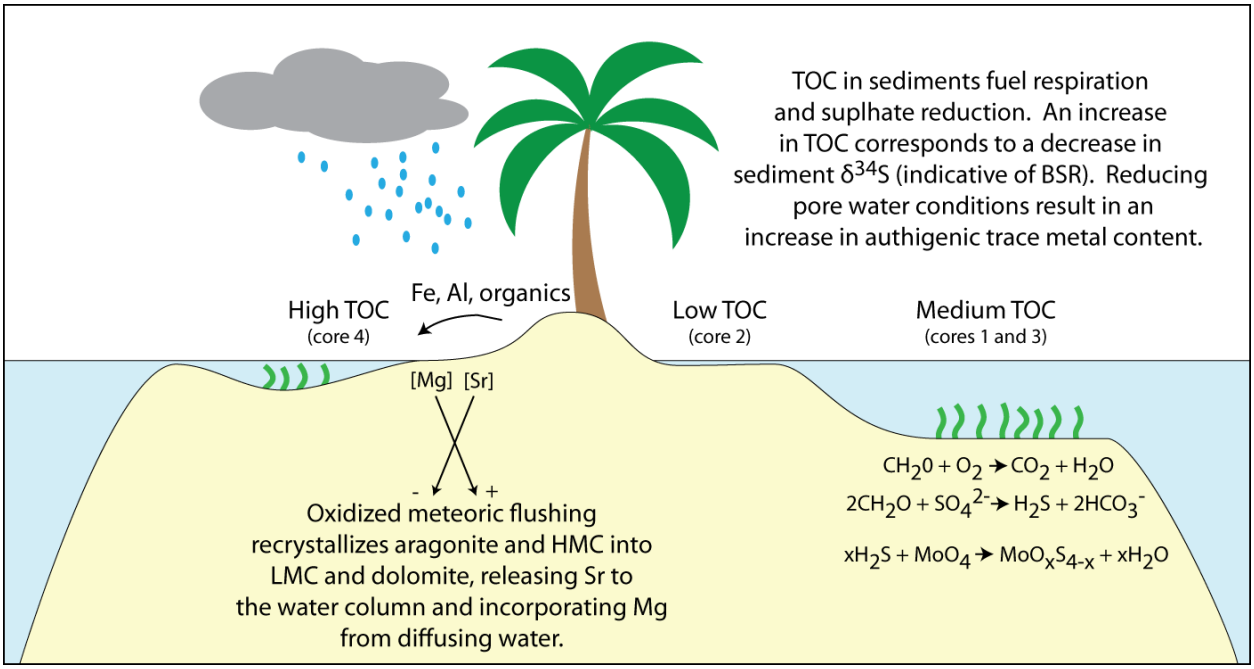

Figure 3.18 A schematic model of the different processes occurring in the different environments represented by the four cores. Mo, U, and V are taken up in reducing environments with medium and high TOC, but not enriched in the low TOC environment. Meteoric flushing causes dolomitization in the lower half of core 4, as seen by the increase in Mg, decrease in Sr, and decrease in the oxidizable U. Mo is incorporated into oxides and organics in this environment as well. Stable isotopes provide evidence of diagenesis, though they are not in the same field as meteoric diagenesis from Oehlert and Swart (2014), likely due to the restricted nature of the pond.

3.4.10 Paleoredox applications

Reduction of U(VI) to U(IV) provides the largest known natural fractionation of $^{238}U/^{235}U$, making it a potentially interesting proxy for ocean redox conditions (Brennecka et al., 2011; Romaniello et al., 2013; Weyer et al., 2008). Due to the long ocean residence time of U (~350 KA) compared to ocean mixing timescales (~1.5 KA), the composition of open seawater should theoretically reflect the globally uniform $^{238}U/^{235}U$ values of the time, giving a global view of redox conditions (Dunk et al., 2002). Romaniello et al. (2013) has shown that while primary precipitates incorporate the $^{238}U/^{235}U$ values of seawater, early diagenesis imparts an authigenic signature creating a bulk heavier $^{238}U/^{235}U$ value with depth of 0.2 – 0.4 ‰. From this, they suggest an authigenic accumulation of isotopically heavy U downcore. Until recently, authigenic accumulations of U were generally thought to be the

product of microbial of chemical reduction and take the form of uraninite, though it is rarely found in nature (Alessi et al., 2014; Alessi et al., 2012; Romaniello et al., 2013).

U precipitated under reducing conditions has been shown to be isotopically heavy (Rolison et al., 2017; Stirling et al., 2007; Weyer et al., 2008). An authigenic accumulation of non-crystalline U(IV) under reducing pore waters could contribute a heavier isotopic signature to bulk carbonate values, consistent with observations by Romaniello et al (2013). Thus, instead of applying a correction factor to $\delta^{238}U$ values of carbonates (Elrick et al., 2017; Romaniello et al., 2013; Song et al., 2017), it may be more effective to chemically remove mononuclear U(IV) using sodium bicarbonate in order to isotopically analyze the remaining sediment.

Estimates for $\delta^{238}U$ values of the isotopically heavier mononuclear U(IV) are possible. Assuming that non-authigenic U records $\delta^{238}U$ values of seawater, and any increase above that is due to authigenic enrichment, a two end member mixing equation can be set up.

$$\delta^{238}U_{bulk} = \delta^{238}U_{exchang} * (f_{exchang}) + \delta^{238}U_{sum-exchang} * (1 - f_{exchang})$$

where:

$$f_{exchang} = \frac{U\ ppm\ from\ exchangeable\ phase}{Sum\ of\ U\ ppm\ from\ all\ phases}$$

Using $\delta^{238}U_{bulk}$ values from Romaniello et al. (2013) and setting $\delta^{238}U_{sum\text{-}exchang}$ to that of seawater (-0.4 ‰), $\delta^{238}U_{exchang}$ ranges from 0.03 – 0.63 ‰ (average 0.31 ‰, standard deviation 0.15 ‰) in Cores 1 and 3 where authigenic enrichment is observed. Slightly higher $\delta^{238}U_{exchang}$ values of 0.89 – 1.86 ‰ (average 1.36 ‰, standard deviation 0.36 ‰) would be required in Core 3 where very little U is measured. This range is similar to that proposed by Romaniello et al. (2013) (0.6 – 1.2 ‰) and consistent with studies of $\delta^{238}U$ fractionation in reducing environments (Clarkson et al., 2018; Rolison et al., 2017; Romaniello et al., 2013; Stirling et al., 2007; Weyer et al., 2008).

Mo, like U, has a long residence time in the open ocean (~700 KA) with respect to ocean mixing time, making it too an attractive proxy for potentially recording a globally integrated redox state (Anbar, 2004). Recent studies have demonstrated its utility in black shales in which Mo can potentially be

quantitatively removed (Dahl et al., 2011; Herrmann et al., 2012; Siebert et al., 2005), however these shales do not constitute all of geologic history and may be biased towards restrictive epicontinental seas (Arthur and Sageman, 1994). Furthermore, it is difficult to prove quantitative removal of Mo, which could have unintended fractionation effects (Gordon et al., 2009; Herrmann et al., 2012; Siebert et al., 2006). Recent work has suggested that Mo isotopic signatures may be preserved in carbonate sediments (Bura-Nakić et al., 2018; Kendall et al., 2017; Voegelin et al., 2009), however authigenic Mo may be isotopically light, resulting in bulk values shifting away from seawater (Romaniello et al., 2016).

Erickson and Helz (2000) predict a "switching" point of 11 μM H_2S_{aq}, after which MoO_4^{2-} is rapidly converted to MoS_4^{2-}. Further studies and modelling have suggested a step-wise conversion of MoO_4^{2-} to MoS_4^{2-}, with a series of intermediates, $MoO_xS_{4-x}^{2-}$, and associated isotopic fractionations (Dahl et al., 2010; Herrmann et al., 2012; Romaniello et al., 2016). Sediments under which there is a quantitative conversion of MoO_4^{2-} to MoS_4^{2-} are thought to capture seawater Mo isotopic compositions, though it is unclear if shallow sediments (such as those found in The Bahamas) are capable of such conditions (Dahl et al., 2010; Gordon et al., 2009; Herrmann et al., 2012; Neubert et al., 2008; Romaniello et al., 2016). Voegelin et al (2009) show that non-skeletal carbonate primary precipitates preserve seawater Mo isotopic values. By chemically removing the authigenic fraction of bulk sediment using sequential extractions, it may be possible to mitigate the complexities of stepwise Mo fractionation occurring in pore waters and capture original seawater isotopic values through the non-exchangeable phases. Since the majority of bulk sediment Mo is found in the exchangeable phase (~ 50-85%), a mass balance of non-exchangeable phases could result in a wide range of isotopic values, requiring further study to determine the potential for directly recording seawater values.

3.5. Summaries

In the shallow, modern Bahamian cores studied, syndepositional diagenesis drives variable trace metal uptake. Sequential extractions indicate that authigenic accumulation of trace metals are hosted in the exchangeable phase, while BSR reactions drive their uptake. In cores with little organic material and no evidence of BSR reactions (core 2), there was little to no uptake of authigenic trace metals. Cores with

terrestrial input of carbon, driving production of H_2S through BSR (cores 1 and 3; evidenced by stable isotopes), authigenic enrichments of 2 - 3 ppm U, 3 – 6 Mo, and up to 12 ppm V were common. The carbonate phase retained concentrations of Mo and U similar to that expected for primary precipitates (~0.1 and ~3-4 ppm respectively). In an environment which appears to be diagenetically altered through meteoric waters (core 4; evidenced by an increase in Mg and decrease in Sr), in combination with increased organics driving reducing conditions, Mo is authigenically enriched, while U and V appear to be removed due to re-oxidation. Future work should be carried out to analyze trace metal isotopes, as carbonate phase elemental concentrations indicate they may preserve sweater values.

PAAS normalized REY values of cores 1, 2, and 3 reflect sweater characteristics, regardless of specific diagenetic circumstances. Each core retained Y/Ho ratios of ~50 – 60 (indicating that sediments were free of terrestrial REY influence), negative Ce anomalies (typical of oxidized seawater), and light REE depletion (Nd_{SN}/Yb_{SN} ~0.5). Core 4 REY values show evidence of terrestrial influence, with higher Y/Ho ratios (~44), and neutral Ce anomalies (indicative of being near shore, restricted environment, or reducing waters at the time of carbonate precipitation). The lack of correlation between ΣREY and diagenesis-sensitive stable isotope and elements ($\delta^{18}O$, Sr, and Mg) indicate that meteoric diagenesis had little to no impact on the REY distribution pattern of the carbonate phase.

3.6. References

Alessi, D.S., Lezama-Pacheco, J.S., Stubbs, J.E., Janousch, M., Bargar, J.R., Persson, P., Bernier-Latmani, R., 2014. The product of microbial uranium reduction includes multiple species with U (IV)–phosphate coordination. Geochimica et Cosmochimica Acta 131, 115-127.

Alessi, D.S., Uster, B., Veeramani, H., Suvorova, E.I., Lezama-Pacheco, J.S., Stubbs, J.E., Bargar, J.R., Bernier-Latmani, R., 2012. Quantitative separation of monomeric U (IV) from UO2 in products of U (VI) reduction. Environmental science & technology 46, 6150-6157.

Algeo, T.J., Lyons, T.W., 2006. Mo–total organic carbon covariation in modern anoxic marine environments: Implications for analysis of paleoredox and paleohydrographic conditions. Paleoceanography 21.

Anbar, A.D., 2004. Molybdenum stable isotopes: observations, interpretations and directions. Reviews in Mineralogy and Geochemistry 55, 429-454.

Andersen, M., Romaniello, S., Vance, D., Little, S., Herdman, R., Lyons, T., 2014. A modern framework for the interpretation of 238 U/235 U in studies of ancient ocean redox. Earth and Planetary Science Letters 400, 184-194.

Arthur, M.A., Sageman, B.B., 1994. Marine black shales: depositional mechanisms and environments of ancient deposits. Annual Review of Earth and Planetary Sciences 22, 499-551.

Baker, P.A., Kastner, M., 1981. Constraints on the formation of sedimentary dolomite. Science 213, 214-216.

Bau, M., Dulski, P., 1996. Distribution of yttrium and rare-earth elements in the Penge and Kuruman iron-formations, Transvaal Supergroup, South Africa. Precambrian Research 79, 37-55.

Bentley, S., Nittrouer, C., 1997. Environmental influences on the formation of sedimentary fabric in a fine-grained carbonate-shelf environment: Dry Tortugas, Florida Keys. Geo-Marine Letters 17, 268-275.

Bentley Sr, S.J., Nittrouer, C.A., 2012. Accumulation and intense bioturbation of bioclastic muds along a carbonate-platform margin: Dry Tortugas, Florida. Marine Geology 315, 44-57.

Bhattacharyya, A., Campbell, K.M., Kelly, S.D., Roebbert, Y., Weyer, S., Bernier-Latmani, R., Borch, T., 2017. Biogenic non-crystalline U (IV) revealed as major component in uranium ore deposits. Nature communications 8, 15538.

Böhm, L., Fütterer, D., Kaminski, E., 1978. Algal calcification in some Codiaceae (Chlorophyta): ultrastructure and location of skeletal deposits. Journal of Phycology 14, 486-493.

Breit, G.N., Wanty, R.B., 1991. Vanadium accumulation in carbonaceous rocks: a review of geochemical controls during deposition and diagenesis. Chemical Geology 91, 83-97.

Brennecka, G.A., Herrmann, A.D., Algeo, T.J., Anbar, A.D., 2011. Rapid expansion of oceanic anoxia immediately before the end-Permian mass extinction. Proceedings of the National Academy of Sciences 108, 17631-17634.

Bura-Nakić, E., Andersen, M.B., Archer, C., de Souza, G.F., Marguš, M., Vance, D., 2018. Coupled Mo-U abundances and isotopes in a small marine euxinic basin: Constraints on processes in euxinic basins. Geochimica et Cosmochimica Acta 222, 212-229.

Burdige, D.J., Zimmerman, R.C., 2002. Impact of sea grass density on carbonate dissolution in Bahamian sediments. Limnology and Oceanography 47, 1751-1763.

Calvert, S., Pedersen, T., 1993. Geochemistry of recent oxic and anoxic marine sediments: implications for the geological record. Marine geology 113, 67-88.

Canfield, D.E., Boudreau, B.P., Mucci, A., Gundersen, J.K., 1998. The early diagenetic formation of organic sulfur in the sediments of Mangrove Lake, Bermuda. Geochimica et Cosmochimica Acta 62, 767-781.

Chen, X., Romaniello, S.J., Herrmann, A.D., Wasylenki, L.E., Anbar, A.D., 2016. Uranium isotope fractionation during coprecipitation with aragonite and calcite. Geochimica et Cosmochimica Acta 188, 189-207.

Clarkson, M.O., Stirling, C.H., Jenkyns, H.C., Dickson, A.J., Porcelli, D., Moy, C.M., von Strandmann, P.A.P., Cooke, I.R., Lenton, T.M., 2018. Uranium isotope evidence for two episodes of deoxygenation during Oceanic Anoxic Event 2. Proceedings of the National Academy of Sciences, 201715278.

Cloern, J.E., Canuel, E.A., Harris, D., 2002. Stable carbon and nitrogen isotope composition of aquatic and terrestrial plants of the San Francisco Bay estuarine system. Limnology and oceanography 47, 713-729.

Dahl, T.W., Anbar, A.D., Gordon, G.W., Rosing, M.T., Frei, R., Canfield, D.E., 2010. The behavior of molybdenum and its isotopes across the chemocline and in the sediments of sulfidic Lake Cadagno, Switzerland. Geochimica et Cosmochimica Acta 74, 144-163.

Dahl, T.W., Canfield, D.E., Rosing, M.T., Frei, R.E., Gordon, G.W., Knoll, A.H., Anbar, A.D., 2011. Molybdenum evidence for expansive sulfidic water masses in~ 750Ma oceans. Earth and Planetary Science Letters 311, 264-274.

De Baar, H.J., Bacon, M.P., Brewer, P.G., Bruland, K.W., 1985. Rare earth elements in the Pacific and Atlantic Oceans. Geochimica et Cosmochimica Acta 49, 1943-1959.

Derry, L.A., 2010. A burial diagenesis origin for the Ediacaran Shuram–Wonoka carbon isotope anomaly. Earth and Planetary Science Letters 294, 152-162.

Dunk, R., Mills, R., Jenkins, W., 2002. A reevaluation of the oceanic uranium budget for the Holocene. Chemical Geology 190, 45-67.

Elderfield, H., Greaves, M.J., 1982. The rare earth elements in seawater. Nature 296, 214-219.

Elrick, M., Polyak, V., Algeo, T.J., Romaniello, S., Asmerom, Y., Herrmann, A.D., Anbar, A.D., Zhao, L., Chen, Z.-Q., 2017. Global-ocean redox variation during the middle-late Permian through Early Triassic based on uranium isotope and Th/U trends of marine carbonates. Geology 45, 163-166.

Emerson, S.R., Huested, S.S., 1991. Ocean anoxia and the concentrations of molybdenum and vanadium in seawater. Marine Chemistry 34, 177-196.

Erickson, B.E., Helz, G.R., 2000. Molybdenum (VI) speciation in sulfidic waters:: stability and lability of thiomolybdates. Geochimica et Cosmochimica Acta 64, 1149-1158.

Furukawa, Y., Bentley, S.J., Shiller, A.M., Lavoie, D.L., Van Cappellen, P., 2000. The role of biologically-enhanced pore water transport in early diagenesis: An example from carbonate sediments in the vicinity of North Key Harbor, Dry Tortugas National Park, Florida. Journal of Marine Research 58, 493-522.

Gordon, G., Lyons, T., Arnold, G.L., Roe, J., Sageman, B., Anbar, A., 2009. When do black shales tell molybdenum isotope tales? Geology 37, 535-538.

Herrmann, A.D., Kendall, B., Algeo, T.J., Gordon, G.W., Wasylenki, L.E., Anbar, A.D., 2012. Anomalous molybdenum isotope trends in Upper Pennsylvanian euxinic facies: Significance for use of δ98Mo as a global marine redox proxy. Chemical Geology 324, 87-98.

Higgins, J., Blättler, C., Lundstrom, E., Santiago-Ramos, D., Akhtar, A., Ahm, A.C., Bialik, O., Holmden, C., Bradbury, H., Murray, S., 2018. Mineralogy, early marine diagenesis, and the chemistry of shallow-water carbonate sediments. Geochimica et Cosmochimica Acta 220, 512-534.

Hoffman, P.F., Kaufman, A.J., Halverson, G.P., Schrag, D.P., 1998. A Neoproterozoic snowball earth. science 281, 1342-1346.

Ingalls, A.E., Aller, R.C., Lee, C., Wakeham, S.G., 2004. Organic matter diagenesis in shallow water carbonate sediments. Geochimica et Cosmochimica Acta 68, 4363-4379.

Kendall, B., Dahl, T.W., Anbar, A.D., 2017. The stable isotope geochemistry of molybdenum. Reviews in Mineralogy and Geochemistry 82, 683-732.

Klinkhammer, G., Palmer, M., 1991. Uranium in the oceans: where it goes and why. Geochimica et Cosmochimica Acta 55, 1799-1806.

Knauth, L.P., Kennedy, M.J., 2009. The late Precambrian greening of the Earth. Nature 460, 728-732.

Lajtha, K., Marshall, J., 1994. Sources of variation in the stable isotopic composition of plants, Lajtha K., Michener RH, Stable Isotopes in Ecology and Environmental Science, 1-21. Blackwell Scientific Publications, Oxford.

Lee, D., Carpenter, S.J., 2001. Isotopic disequilibrium in marine calcareous algae. Chemical Geology 172, 307-329.

Li, R., Jones, B., 2013. Heterogeneous diagenetic patterns in the Pleistocene Ironshore Formation of Grand Cayman, British West Indies. Sedimentary Geology 294, 251-265.

Li, R., Jones, B., 2014. Evaluation of carbonate diagenesis: A comparative study of minor elements, trace elements, and rare-earth elements (REE+ Y) between Pleistocene corals and matrices from Grand Cayman, British West Indies. Sedimentary Geology 314, 31-46.

Liu, X., Hardisty, D., Lyons, T. W., Swart, P., 2018. Evaluating the integrity of the cerium paleoredox tracer through analysis of a modern marine carbonate analog. Geochimica et Cosmochimica Acta.

Lovley, D.R., Phillips, E.J., Gorby, Y.A., Landa, E.R., 1991. Microbial reduction of uranium. Nature 350, 413.

Lowenstam, H.A., Epstein, S., 1957. On the origin of sedimentary aragonite needles of the Great Bahama Bank. The Journal of Geology 65, 364-375.

Luo, G., Kump, L.R., Wang, Y., Tong, J., Arthur, M.A., Yang, H., Huang, J., Yin, H., Xie, S., 2010. Isotopic evidence for an anomalously low oceanic sulfate concentration following end-Permian mass extinction. Earth and Planetary Science Letters 300, 101-111.

McLennan, S.M., 1989. Rare earth elements in sedimentary rocks; influence of provenance and sedimentary processes. Reviews in Mineralogy and Geochemistry 21, 169-200.

McManus, J., Berelson, W.M., Klinkhammer, G.P., Hammond, D.E., Holm, C., 2005. Authigenic uranium: relationship to oxygen penetration depth and organic carbon rain. Geochimica et Cosmochimica Acta 69, 95-108.

Meyers, P.A., 1994. Preservation of elemental and isotopic source identification of sedimentary organic matter. Chemical geology 114, 289-302.

Morford, J., Russell, A., Emerson, S., 2001. Trace metal evidence for changes in the redox environment associated with the transition from terrigenous clay to diatomaceous sediment, Saanich Inlet, BC. Marine Geology 174, 355-369.

Morin, G., Mangeret, A., Othmane, G., Stetten, L., Seder-Colomina, M., Brest, J., Ona-Nguema, G., Bassot, S., Courbet, C., Guillevic, J., 2016. Mononuclear U (IV) complexes and ningyoite as major uranium species in lake sediments. Geochemical Perspectives Letter 2, 95-105.

Muhs, D.R., Budahn, J.R., Prospero, J.M., Carey, S.N., 2007. Geochemical evidence for African dust inputs to soils of western Atlantic islands: Barbados, the Bahamas, and Florida. Journal of Geophysical Research: Earth Surface 112.

Neubert, N., Nägler, T.F., Böttcher, M.E., 2008. Sulfidity controls molybdenum isotope fractionation into euxinic sediments: Evidence from the modern Black Sea. Geology 36, 775-778.

Oehlert, A.M., Swart, P.K., 2014. Interpreting carbonate and organic carbon isotope covariance in the sedimentary record. Nature Communications 5.

Osborne, A.H., Haley, B.A., Hathorne, E.C., Plancherel, Y., Frank, M., 2015. Rare earth element distribution in Caribbean seawater: Continental inputs versus lateral transport of distinct REE compositions in subsurface water masses. Marine Chemistry 177, 172-183.

Patterson, W.P., Walter, L.M., 1994. Depletion of 13C in seawater ΣC02 on modern carbonate platforms: Significance for the carbon isotopic record of carbonates. Geology 22, 885-888.

Phillips, E.J., Landa, E.R., Lovley, D.R., 1995. Remediation of uranium contaminated soils with bicarbonate extraction and microbial U (VI) reduction. Journal of Industrial Microbiology 14, 203-207.

Piper, D.Z., Bau, M., 2013. Normalized rare earth elements in water, sediments, and wine: identifying sources and environmental redox conditions. American Journal of Analytical Chemistry 4, 69.

Rolison, J.M., Stirling, C.H., Middag, R., Rijkenberg, M.J., 2017. Uranium stable isotope fractionation in the Black Sea: Modern calibration of the 238U/235U paleo-redox proxy. Geochimica et Cosmochimica Acta 203, 69-88.

Romaniello, S.J., Herrmann, A.D., Anbar, A.D., 2013. Uranium concentrations and 238 U/235 U isotope ratios in modern carbonates from the Bahamas: Assessing a novel paleoredox proxy. Chemical Geology 362, 305-316.

Romaniello, S.J., Herrmann, A.D., Anbar, A.D., 2016. Syndepositional diagenetic control of molybdenum isotope variations in carbonate sediments from the Bahamas. Chemical Geology 438, 84-90.

Sahoo, S.K., Planavsky, N.J., Kendall, B., Wang, X., Shi, X., Scott, C., Anbar, A.D., Lyons, T.W., Jiang, G., 2012. Ocean oxygenation in the wake of the Marinoan glaciation. Nature 489, 546-549.

Sharp, J.O., Lezama-Pacheco, J.S., Schofield, E.J., Junier, P., Ulrich, K.-U., Chinni, S., Veeramani, H., Margot-Roquier, C., Webb, S.M., Tebo, B.M., 2011. Uranium speciation and stability after reductive immobilization in aquifer sediments. Geochimica et Cosmochimica Acta 75, 6497-6510.

Siebert, C., Kramers, J., Meisel, T., Morel, P., Nägler, T.F., 2005. PGE, Re-Os, and Mo isotope systematics in Archean and early Proterozoic sedimentary systems as proxies for redox conditions of the early Earth. Geochimica et Cosmochimica Acta 69, 1787-1801.

Siebert, C., McManus, J., Bice, A., Poulson, R., Berelson, W.M., 2006. Molybdenum isotope signatures in continental margin marine sediments. Earth and Planetary Science Letters 241, 723-733.

Song, H., Song, H., Algeo, T.J., Tong, J., Romaniello, S.J., Zhu, Y., Chu, D., Gong, Y., Anbar, A.D., 2017. Uranium and carbon isotopes document global-ocean redox-productivity relationships linked to cooling during the Frasnian-Famennian mass extinction. Geology 45, 887-890.

Stehli, F.G., Hower, J., 1961. Mineralogy and early diagenesis of carbonate sediments. Journal of Sedimentary Research 31.

Stirling, C.H., Andersen, M.B., Potter, E.-K., Halliday, A.N., 2007. Low-temperature isotopic fractionation of uranium. Earth and Planetary Science Letters 264, 208-225.

Šurija, B., Branica, M., 1995. Distribution of Cd, Pb, Cu and Zn in carbonate sediments from the Krka river estuary obtained by sequential extraction. Science of the total environment 170, 101-118.

Swart, P.K., 2015. The geochemistry of carbonate diagenesis: The past, present and future. Sedimentology 62, 1233-1304.

Swart, P.K., Melim, L.A., 2000. The origin of dolomites in Tertiary sediments from the margin of Great Bahama Bank. Journal of Sedimentary Research 70, 738-748.

Swart, P.K., Oehlert, A.M., 2018. Revised interpretations of stable C and O patterns in carbonate rocks resulting from meteoric diagenesis. Sedimentary Geology 364, 14-23.

Tedesco, L.P., Wanless, H.R., 1991. Generation of sedimentary fabrics and facies by repetitive excavation and storm infilling of burrow networks, Holocene of South Florida and Caicos Platform, BWI. Palaios, 326-343.

Tessier, A., Campbell, P.G., Bisson, M., 1979. Sequential extraction procedure for the speciation of particulate trace metals. Analytical chemistry 51, 844-851.

Tostevin, R., Shields, G.A., Tarbuck, G.M., He, T., Clarkson, M.O., Wood, R.A., 2016. Effective use of cerium anomalies as a redox proxy in carbonate-dominated marine settings. Chemical Geology 438, 146-162.

Tribovillard, N., Algeo, T.J., Lyons, T., Riboulleau, A., 2006. Trace metals as paleoredox and paleoproductivity proxies: an update. Chemical geology 232, 12-32.

Turekian, K.K., Wedepohl, K.H., 1961. Distribution of the elements in some major units of the earth's crust. Geological Society of America Bulletin 72, 175-192.

Vahrenkamp, V.C., Swart, P.K., 1990. New distribution coefficient for the incorporation of strontium into dolomite and its implications for the formation of ancient dolomites. Geology 18, 387-391.

Veizer, J., Hoefs, J., 1976. The nature of O18/O16 and C13/C12 secular trends in sedimentary carbonate rocks. Geochimica et Cosmochimica Acta 40, 1387-1395.

Voegelin, A.R., Nägler, T.F., Samankassou, E., Villa, I.M., 2009. Molybdenum isotopic composition of modern and Carboniferous carbonates. Chemical Geology 265, 488-498.

Walter, L.M., Bischof, S.A., Patterson, W.P., Lyons, T.W., 1993. Dissolution and recrystallization in modern shelf carbonates: evidence from pore water and solid phase chemistry. Phil. Trans. R. Soc. Lond. A 344, 27-36.

Walter, L.M., Burton, E.A., 1990. Dissolution of recent platform carbonate sediments in marine pore fluids. American Journal of Science 290, 601-643.

Walter, L.M., Ku, T.C., Muehlenbachs, K., Patterson, W.P., Bonnell, L., 2007. Controls on the δ13C of dissolved inorganic carbon in marine pore waters: An integrated case study of isotope exchange during syndepositional recrystallization of biogenic carbonate sediments (South Florida Platform, USA). Deep Sea Research Part II: Topical Studies in Oceanography 54, 1163-1200.

Wanty, R.B., Goldhaber, M.B., 1992. Thermodynamics and kinetics of reactions involving vanadium in natural systems: Accumulation of vanadium in sedimentary rocks. Geochimica et Cosmochimica Acta 56, 1471-1483.

Webb, G.E., Kamber, B.S., 2000. Rare earth elements in Holocene reefal microbialites: a new shallow seawater proxy. Geochimica et Cosmochimica Acta 64, 1557-1565.

Webb, G.E., Nothdurft, L.D., Kamber, B.S., Kloprogge, J., ZHAO, J.X., 2009. Rare earth element geochemistry of scleractinian coral skeleton during meteoric diagenesis: a sequence through neomorphism of aragonite to calcite. Sedimentology 56, 1433-1463.

Weyer, S., Anbar, A., Gerdes, A., Gordon, G., Algeo, T., Boyle, E., 2008. Natural fractionation of 238 U/235 U. Geochimica et Cosmochimica Acta 72, 345-359.

Wilbur, K.M., Colinvaux, L.H., Watabe, N., 1969. Electron microscope study of calcification in the alga Halimeda (order Siphonales). Phycologia 8, 27-35.

CHAPTER 4 HISTORICAL TRENDS OF SEDIMENT TRACE METAL UPTAKE AND STABLE ISOTOPE VARIATION IN NORTHERN GULF OF MEXICO HYPOXIC ZONE

4.1. Introduction

Anthropogenically driven hypoxic zones, such as the "Dead Zone" of the Northern Gulf of Mexico (GOM), are of increasing concern worldwide (Diaz, 2001; Diaz and Rosenberg, 2008; Turner et al., 2008; Vaquer-Sunyer and Duarte, 2008). Elevated production of organic material due to an increase in nutrients, and the subsequent remineralization of the organic matter, consume oxidants in the water column and can set up hypoxic bottom water conditions (Gooday et al., 2009; Rabalais et al., 2002). This process, known as eutrophication (Gray et al., 2002), combined with thermo-haline stratification on the northern shelf of the GOM, near the mouth of the Mississippi River, result in seasonally hypoxic bottom waters with < 2 mg/L dissolved oxygen (Rabalais et al., 2002). This condition occurs both naturally and anthropogenically forced in many modern environments such as oxygen minimum zones, fjords, basins, or restricted bays. In the northern GOM, hypoxia occurs primarily on the Louisiana and Texas upper continental shelf during summer months, when the Mississippi River has the greatest nutrient load and bottom waters are most stratified. "Dead Zones" like the one in the northern GOM are stimulated through N and P fertilizer water contamination and exhaust emissions, and constitute a key stressor on marine ecosystems (Diaz and Rosenberg, 2008).

Low oxygen bottom waters were first reported in the northern GOM in the 1970's (Diaz and Rosenberg, 2008), however the phenomenon was not vigorously studied until the mid-1980's with the deployment of several instrument clusters, capable of continuous logs of oxygen, temperature, and salinity. The hypoxic conditions are driven by nutrient loads derived from exhaust emissions and excess fertilizer used for agriculture in the central and Midwestern United States, carried to the GOM by the Mississippi River (Rabalais et al., 2002). The increase in nutrients fuel primary productivity of surface algae, which then die and sink to the ocean floor. Oxidation of the algal organic matter by bacteria consumes oxygen, resulting in dysoxic conditions (Diaz and Rosenberg, 2008). The Mississippi River delivers the most nutrients during the summer months, when farms receive the bulk of their fertilizers.

Summer months are also when the GOM experiences thermohaline stratification where bottom water consumption of oxygen outstrips resupply, allowing oxygen-poor conditions to persist. The high nutrient delivery and stratification combine to create the second largest hypoxic zone in the world, topping more 15,000 km^2 (Rabalais et al., 2007), with size of the hypoxic zone being tightly coupled with nitrate and nitrite N loading of the Mississippi (Turner et al., 2007). Hypoxic conditions have a varied duration and may depend on several factors such as rainfall or ocean mixing, but typically persist for several months. Benthic organisms capable of moving out of the hypoxic zone typically will, however less mobile fauna can experience stress or death.

Studies have demonstrated the ability of certain redox sensitive elements (such as U, Mo, and V) to record the redox state of overlying ocean bodies during sediment deposition of similar modern (Helz and Adelson, 2013; Jilbert and Slomp, 2013) and ancient systems (Hardisty et al., 2016) with a high degree of resolution capable of determining onset, duration, and intensity of hypoxic events. Using high resolution sampling and modified Tessier sequential extractions carried out in an anoxic environment, we investigate the mode of uptake for redox sensitive trace metals, as well as chemical speciation of partitioning of rare earth elements (REE). Trace metal concentrations and REEs document the effects and history of anthropogenic influence in the GOM hypoxic zone and allow for a deeper understanding of the nutrient feedback cycles.

4.1.1 Core description

The 21 cm core exhibited little visual variation down core. The top ~2 cm were dark grey, and poorly consolidated. The lower 19 cm had no visual changes downcore. The lower 19 cm was a medium gray, fine silt to clay grain size. There were no obvious shells or signs of bioturbation. There were no laminations.

4.2. Materials and Methods

4.2.1 Sampling

A shallow core (~20 cm) was collected using a multi-corer deployed near the decimal degree coordinates 28.86907, -90.48217, approximately 150 km west of the mouth of the Mississippi River, at a

depth of ~17 m (Fig. 4.1). This location was chosen due to the persistence of hypoxia every season. Cores were extruded and sliced on cm intervals. Samples were immediately bagged and placed on ice for the duration of the cruise and transportation back to the laboratory to minimize oxidation of redox sensitive elements. Upon delivery, samples were frozen until chemical extractions were carried out.

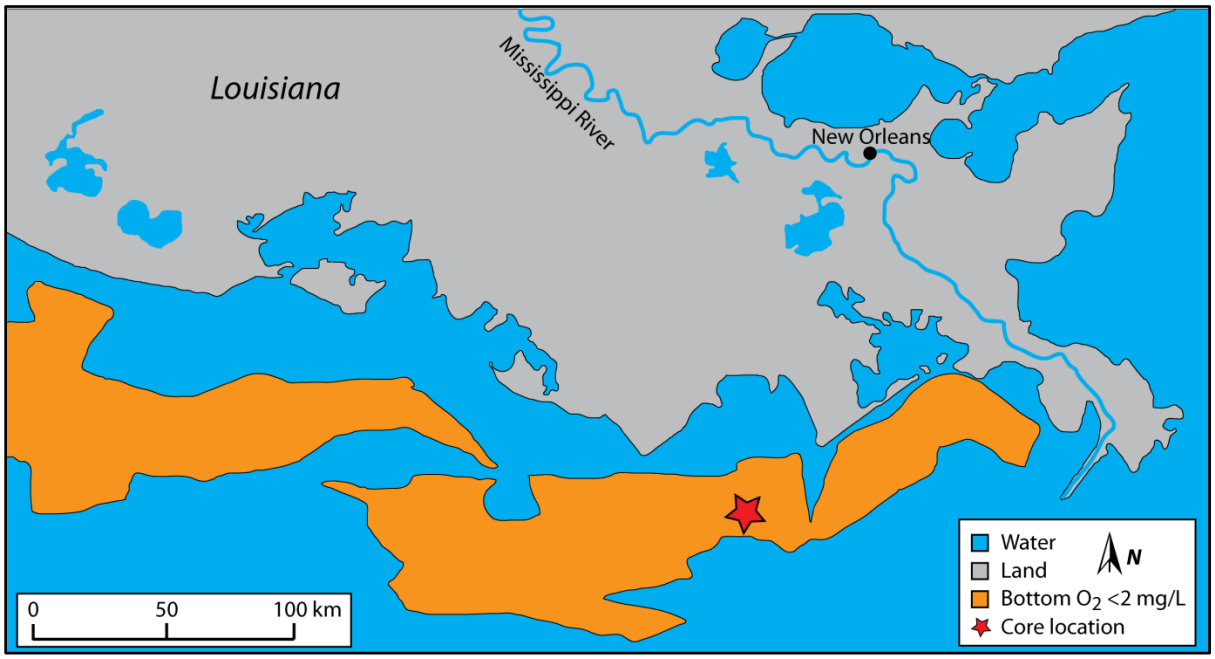

Figure 4.1 Map of core location. The red star is the approximate location the core was taken at (28.86907, -90.48217 decimal degree coordinates). The orange shaded area is the approximate extent of July 2015 dysoxia (bottom water <2 mg/L; modified after Turner and Rabalais, 2017).

4.2.2 Organic Nitrogen, Carbon, and Sulfur elements and isotope analysis

Portions of dried samples were homogenized and decalcified using 1 N hydrochloric acid. The remaining organic sample was washed 5 times with de-ionized water and dried overnight in a 50 ^{0}C oven. Samples were then weighed out in ~50 mg portions to combustible tin capsules, then sealed. The Oxy-Anion Stable Isotope Consortium (OASIC) at Louisiana State University performed measurements of all stable isotopes using an Isoprim100 IRMS, coupled with a Micro Vario Cube elemental analyzer.

$\delta^{15}N$ reported in ‰ variation from air in standard deltaic notation, where $\delta^{15}N_{air}=((((^{15}N/^{14}N)_{sample}/(^{15}N/^{14}N)_{standard})-1)\times1000)$. Elemental content was calibrated using mass

calibration curve while glycine standards (high with $\delta^{15}N_{air}$ = +40.83 ‰ and low with $\delta^{15}N_{air}$ = +1.35 ‰) used to calibrate the mass spectrometer during analysis. Analytical precision was < 0.1‰.

Carbon isotopic values are reported as $\delta^{13}C_{org}$ in ‰ VPDB variation. Glycene standards are used for isotopic value calibration (high with $\delta^{13}C_{VPDB}$ = –0.67 ‰ and low with $\delta^{13}C_{VPDB}$ = –40.81 ‰). Analytical precision is < 0.1‰.

$\delta^{34}S$ measurements are reported in ‰ deviations from VCDT. Isotopic value calibrations are performed using two barium sulfate and two silver sulfide in house standards (LSU-Ag2S-1: -4.3‰; LSU-Ag2S-2: +20.2‰; LSU-BaSO4-1: -4.5‰; LSU-BaSO4-2: +38.5‰). Analytical precision for $\delta^{34}S$ is < 0.2‰.

4.2.3 Major elements XRF analysis

Dried samples were homogenized first using a benchtop vibrating ball mill, then using a McCrone Micronising Mill. Homogenized samples were fused into small glass beads using a borate flux for analysis. Samples were analyzed by a Bruker S2 Puma XRF with 12 sample carousel. Two standards were run with the XRF measurements (NIST1d and USGS SCO1), values were within 5% of certified values for major elements such as Ca, Si, and Al (Jochum et al., 2005).

4.2.4 Sequential Extractions

Frozen samples were transferred to a nitrogen filled glove box where they were partially thawed in order to subsample. Portions of ~ 0.2 g were transferred to nitrogen purged centrifuge tubes for sequential extractions. Any portion of sample that appeared oxidized (black material turned gray or green from iron oxidation) was scraped off and discarded. Separate portions of ~ 0.5 g were transferred to centrifuge tubes, dried, and homogenized to determine amount of pore water, stable isotope makeup, and total digests. A modified Tessier sequential extraction was carried out (at room temperature unless otherwise noted) with the following steps: 1) 1 M sodium bicarbonate for 12 hours targeting loosely bound, non-crystalline fraction; 2) 1 M sodium acetate buffered to pH 5 with acetic acid for 24 hours targeting carbonates; 3) 1 M nitric acid for 30 minutes targeting apatite bound elements; 4) 1 M hydroxylamine hydrochloride in 30 % (w/w) acetic acid for 12 hours at 95 ^{0}C targeting hydrous oxides;

5) 30 % hydrogen peroxide with 0.02 M nitric acid for 24 hours at 85 ^{0}C targeting organic phases; 6) Concentrated nitric acid at 95 ^{0}C for 48 hours targeting any residuals. Samples were washed twice with de-ionized water after each extraction. Extracts were collected and dried down to remove the liquid portion of reagents, then brought back up in 2 % nitric acid for ICP-MS analysis. Modifications from the original Tessier method include the addition of an apatite phase and the substitution of sodium bicarbonate solution during the exchangeable phase, used to target mononuclear U (Morin et al., 2016; Šurija and Branica, 1995; Tessier et al., 1979). Two USGS shale standards (SGR and SDO-1), procedural blanks, and reagent blanks were collected to check for successful chemical and analytical techniques.

4.2.5 ICP-MS

Elemental concentrations of extracts were determined using a Thermo iCAP Q quadrapole inductively coupled mass spectrometer at Louisiana State University. Each chemical phase of the sequential extraction was run individually to reduce matrix complications. Internal standards and check standards were used to correct for suppression or instrument drift.

4.3. Results

4.3.1 C, N, and S Stable Isotopes and Concentrations

Organic carbon isotopes generally increase upcore from ~-23.5 to -22.8‰ in the bottom 5 cm (21-16 cm; Fig. 4.2). After the initial enrichment of ^{13}C, values oscillate from ~-23.2 to -22.8‰ for the upper 16 cm of the core. Nitrogen isotopic values steadily increase upcore from ~5 to 6.8‰. Total organic carbon (TOC) varies from ~1-1.5%, generally decreasing upcore. Molar C/N ratios steadily decrease upcore from ~16-11. Sulfur isotopes become more enriched with depth, with δ^{34}S values of ~ -20‰ to ~ -14‰.

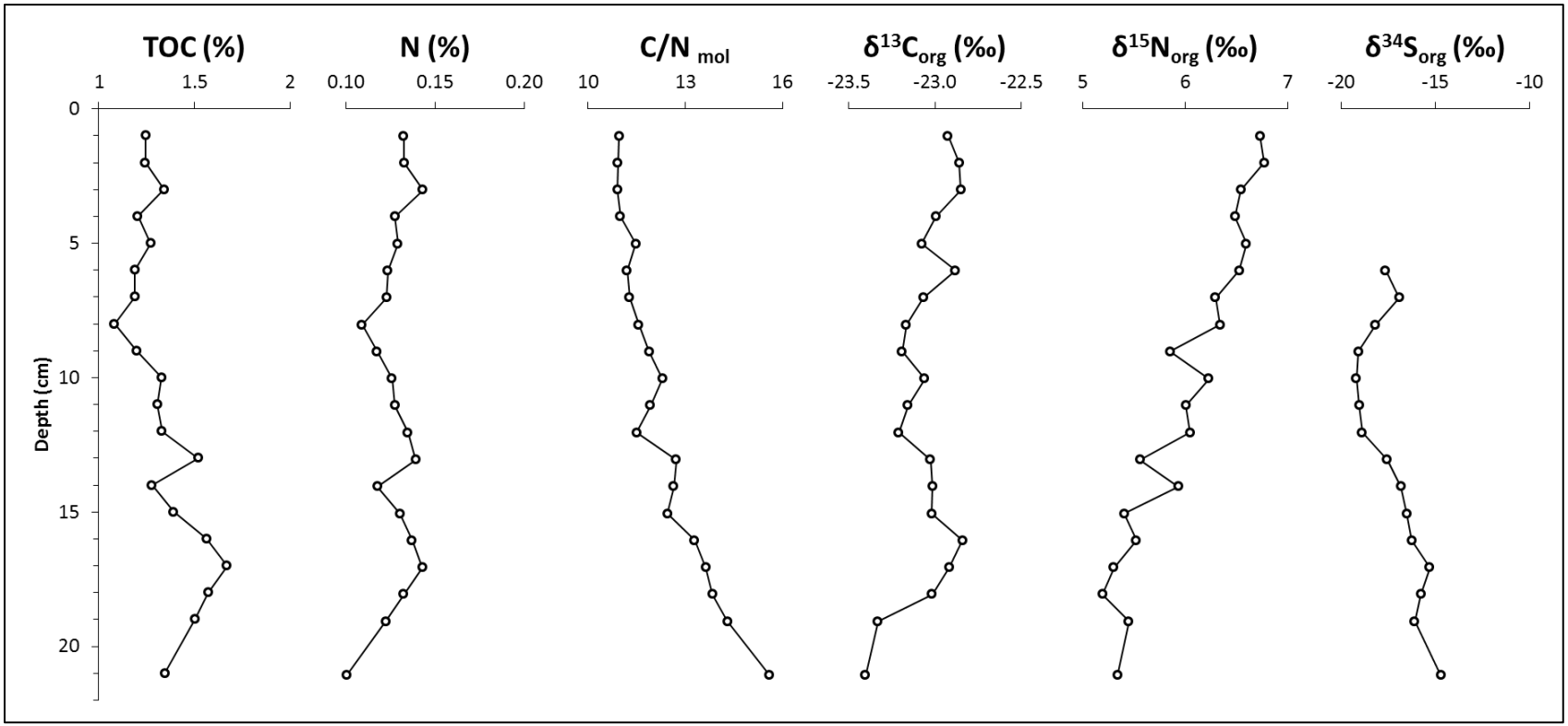

Figure 4.2 Depth profiles of organic carbon, nitrogen, and stable isotopes. C/N_{mol} is the molar ratio of the organic carbon and nitrogen.

4.3.2 Major Elements

Major elements, as measured by XRF, yield important information on temporal evolution trends during deposition of the core and may be used to normalize trace metal enrichment for rate of deposition. Ca (measured as an oxide) is steady throughout the core at ~2%, with the exception of the 2 cm sample, which has ~3.5% (Fig. 4.3). Fe_2O_3 decreases upcore from ~5 to 3.5%. SiO_2 varies from ~55 to 70%, though generally increases upcore. Al_2O_3 is ~17% from 12-22 cm and decreases to ~15% in the upper 11 cm.

4.3.3 Trace Metals

Enrichment factors (EFs) were calculated as: $X_{EF} = (X/Al)_{sample}/(X/Al)_{PAAS}$, where X is the element of inteterest from a sequential extraction phase, Al_{sample} uses the bulk sediment Al measured using XRF, and PAAS is the Post Archean Australian Shale (McLennan, 2001).

U_{EF} varied from ~0.5 – 5, with no discernable trend along core for carbonate, apatite, oxide, and organic phases, and slightly decreasing with depth in the exchangeable phase (Fig. 4.4). The greatest percentage of total U resides in the exchangeable and residual phases (~35 and 25% respectively; Fig. 4.5). The remaining phases contain ~10% or less of the total U present.

Mo_{EF} varied from 5 - 15 in exchangeable and organic phases, while remaining roughly constant and less than 3 in residual and oxide, and close to zero in carbonate and apatite, with the exception of the 13 cm sample, which has Mo_{EF} of ~10 in the residual phase as well (Fig. 4.4). There are no depth trends for carbonate, apatite, oxide, or residual phases, however there is a slight decrease in Mo_{EF} with depth in the organic and exchangeable phases. Exchangeable and organic phases each contain ~45% of all Mo present, with the exception of the 13 cm in which exchangeable and organic phases each contain ~30% and residual contains ~40% and the uppermost sample (1 cm) in which the organic phase contains ~25% of total Mo and Exchangeable contains ~55% (Fig. 4.5).

Enrichment factors of V are generally constant with depth for carbonate (~0.1), apatite (~0.2), oxide (~0.3), organic (~0.3), and residual (~2), however decrease with depth in the exchangeable phase (

0.3 to 0.1). The majority of V (50 – 75%) residing in the residual phase (Fig. 4.4, 4.5). 5 - 20% reside in exchangeable, oxide, and organic phases, with <1% in carbonate and apatite phases.

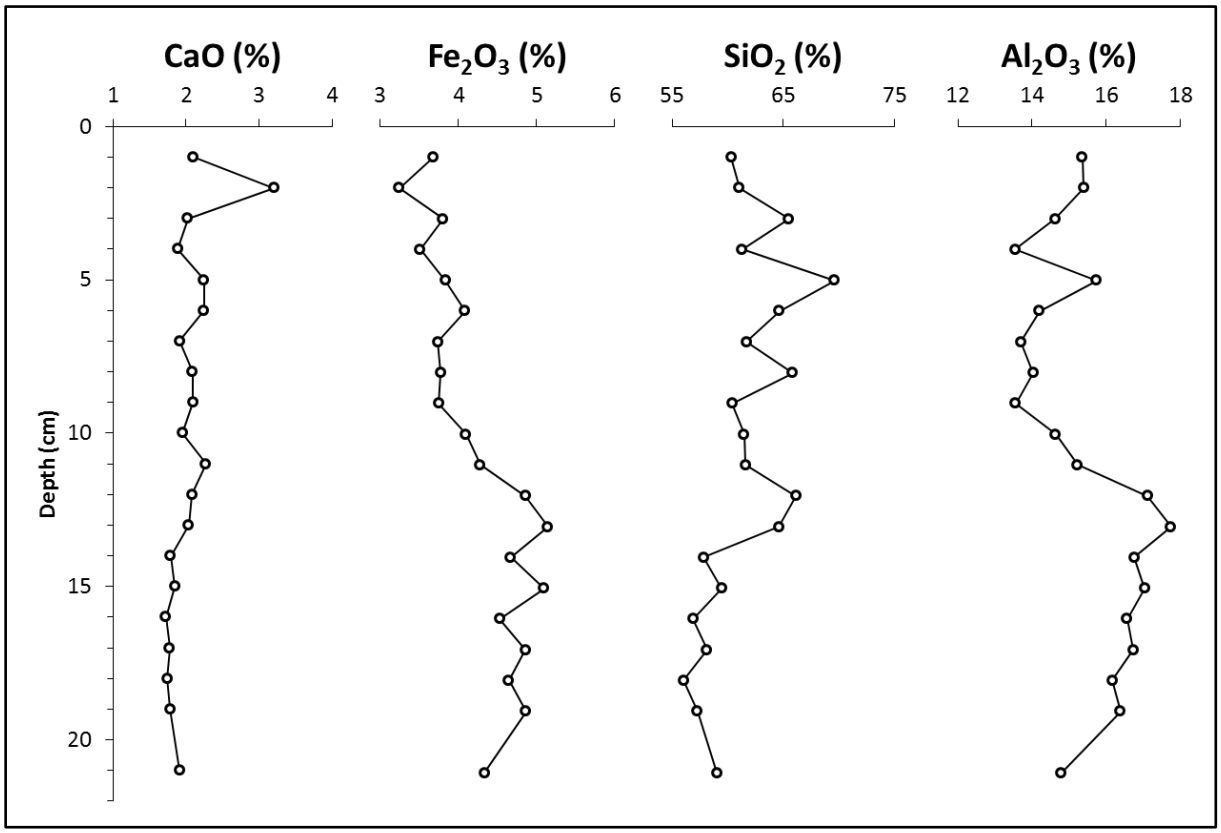

Figure 4.3 Depth profile of major elements as oxides.

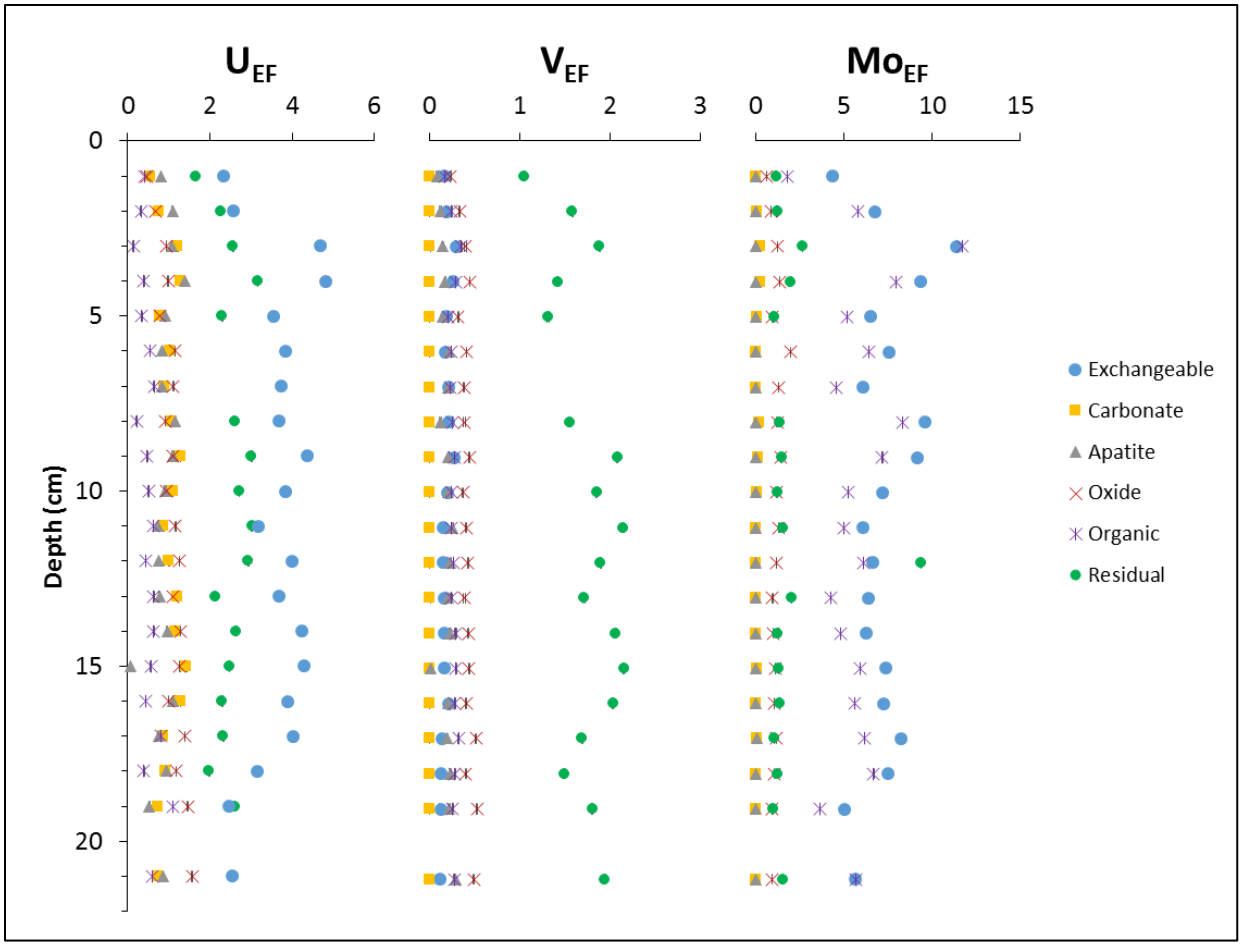

Figure 4.4 Trace metal depth profiles of sequential extraction.

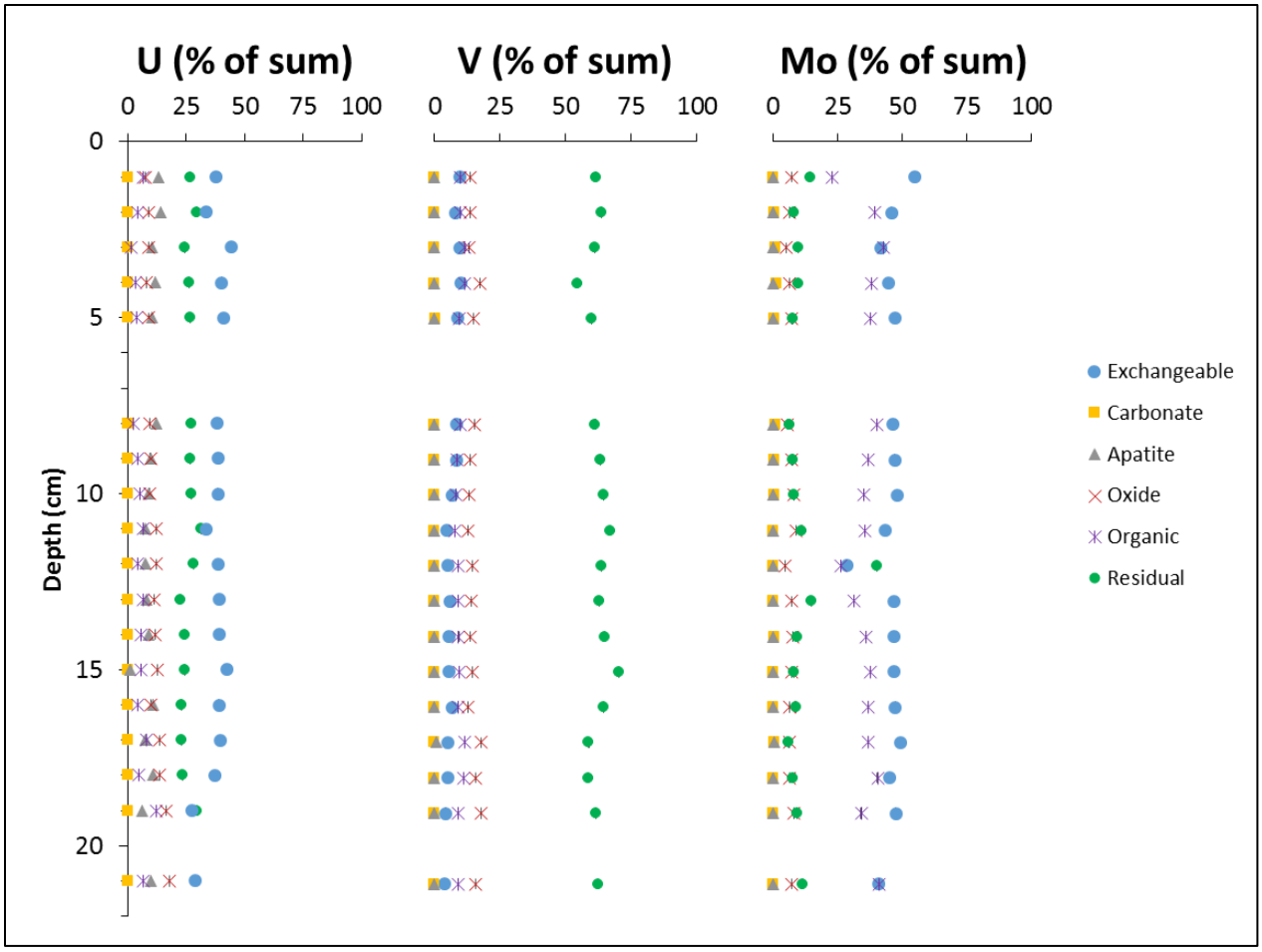

Figure 4.5 Trace metals represented of the percentage of each phase (i.e. trace metal abundance in a phase divided by the sum of the abundance in all phases)

4.3.4 REEs

REEs are normalized using Post Archean Australian Shale values (PAAS) (McLennan, 2001)(Fig. 4.6). The distribution of REEs reveal partitioning of elements by chemical phases. The exchangeable phase contained low concentrations of REEs, at or near the limit of quantification for the ICP-MS, and thus are not plotted. The organic phase contains a slight negative Ce anomaly (Fig. 7), and heavy REE (HREE) enrichment as evidenced by Nd/Yb ratios (average of 0.86, standard deviation of 0.05). Ce anomalies and La anomalies are described by $(Ce/Ce^*)_{SN}$ and $(Pr/Pr^*)_{SN}$ respectively, and defined after Bau and Dulski (1996) as:

$$(Ce/Ce^*)_{SN} = \frac{2 * Ce_{SN}}{La_{SN} + Pr_{SN}}$$

and

$$(Pr/Pr^*)_{SN} = \frac{2 * Pr_{SN}}{Nd_{SN} + Ce_{SN}}$$

Carbonate, apatite, and oxide phases are generally smooth, with elevated normalized middle REEs with respect to surrounding REEs. Elevated middle REE are described by the bell shaped index (BSI or MREE/MREE*), defined by:

$$BSI = \frac{2 * (Sm_{SN} + Gd_{SN} + Dy_{SN})/3}{\frac{La_{SN} + Pr_{SN} + Nd_{SN}}{3} + \frac{Ho_{SN} + Er_{SN} + Tm_{SN} + Yb_{SN} + Lu_{SN}}{5}}$$

after Haley et al., 2004. BSI values above 1 are considered a convex anomaly. Carbonate has BSI values of ~1.5 – 1.7, apatite ~1.6 – 1.7, oxide 1.4 – 1.5, residual 1.3 – 1.4, and oxide 1.1 - 1.3. The residual phase has a unique distribution of REEs, with a general MREE enrichment, though more variation than other phases in elemental concentrations. Carbonate, apatite, oxide, organic, and residual phases have low Y/Ho ratios (~37 for carbonate, ~26 for apatite, and ~23 for oxide, organic, and residual phases).

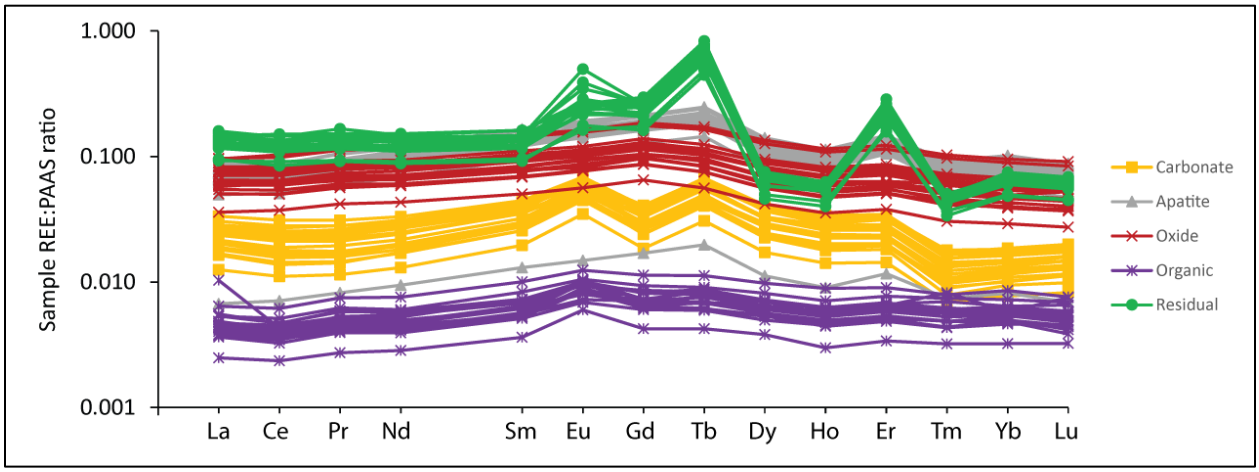

Figure 4.6 REE profiles, colored by chemical phase.

4.4. Discussion

4.4.1 Eutrophication, its role in supplying organics to sediment

Hypoxic zones develop under vertically stratified water columns where the benthic oxygen demand outstrips supply. Oxygen demand is stimulated through a supply of organic matter to the sediment, usually as a result of increased primary productivity. Evidence of eutrophication, or an increase

in primary productivity and carbon accumulation, and thus a record of hypoxia may be recorded by stable isotopes, though it is important to first establish what controls the isotopic signatures, whether it is in situ marine production or a result of riverine terrestrial delivery (Rabalais et al., 2014; Wang et al., 2004).

Terrestrial C3 and C4 plant organics typically have elevated C_{org}/N molar ratios (>20) with respect to marine or lacustrine algal organics (C_{org}/N between 4 and 10) (Meyers, 1994). Wang et al. (2004) performed a survey of particulate organic carbon (POC) from the mouth of the Mississippi River and waters surrounding it, and found that near the river C_{org}/N ratios were measured to be ~10-17, while further offshore C_{org}/N ratios were lower (~6-10). $\delta^{13}C$ values for POC of the northern Gulf of Mexico range from -23.9 –25.0‰ near the mouth of the Mississippi River to more depleted values of -18.7—22.5‰ in shelf and slope waters (Wang et al., 2004). $\delta^{15}N$ values of nitrate near the mouth of the Mississippi have been measured to range between 9.4 and 3.4‰, dependent on the season and nitrate load (Battaglin et al., 2001).

The core studied presently contains molar C_{org}/N ratios between ~ 11 and 16, an average $\delta^{13}C$ value of -23.1‰ (standard deviation of 0.15), and $\delta^{15}N$ values ranging from 5.0-6.6‰ (Fig. 2). The relatively high C_{org}/N ratio and average $\delta^{13}C$ value that falls between riverine POC and offshore POC indicate that organics are a blend of in situ marine organics and terrestrial vascular C3 plants (consistent with previous studies) (Hedges and Parker, 1976; Sackett, 1964; Wang et al., 2004). $\delta^{15}N$ values often reflect isotopic values in the water column (Battaglin et al., 2001), and the core values reflect those of nitrate supplied by the river (~ 5.5-6.5‰), confirming the incorporation of Mississippi derived N into marine production.

4.4.2 Historical eutrophication – evolution over core

^{210}Pb dating from previous studies reveal sedimentations rates of 0.5-1.5 cm yr^{-1} within 50 km of the Mississippi River mouth, decreasing with distance from the mouth to 0.41 cm yr^{-1} at a core ~ 300 km to the west of the mouth (Turner et al., 2004; Turner and Rabalais, 1994). The core used in this study was collected from the western shelf, approximately 150 km from the mouth of the Mississippi, suggesting the

sedimentation rate should be between 0.41 and 0.5 cm yr^{-1}. The core collected is 21 cm long, spanning the past ~40-50 yrs.

4.4.2.1 Carbon and Sulphur

A general, though small, increase of $\delta^{13}C$ values upcore (~ -23.5 - -22.75‰) provides evidence of increased in situ marine productivity over the past 40-50 yrs. Additionally, $\delta^{34}S$ decreases upcore (from ~ -15 to -20‰; uppermost portion of the core was not measured). Sulfur-reducing bacteria incorporate isotopically light S (Peterson et al., 1985, 1986), indicating a greater proportion of bacterial sulphate reduction in samples upcore. This provides evidence for increased in situ organic production, as well as reducing environment intensity.

4.4.2.2 Nitrogen cycles in the GOM

$\delta^{15}N$ values steadily increase upcore in the same interval. Variations in $\delta^{15}N$ reflect variations in water column. Water column $\delta^{15}N$ values are effected by the composition of the freshwater delivered by the Mississippi (which can be variable), assimilatory uptake, N fixation, and denitrification (Bateman and Kelly, 2007; Brandes and Devol, 2002; Sigman et al., 1999; Voss et al., 2001). Nitrate in the Mississippi are heavily influenced by fertilizer and pollutant runoff; most synthetic fertilizer has $\delta^{15}N$ values of ~ 0‰, while organic fertilizers (manure) and sewage runoff are have typically elevated $\delta^{15}N$ values (~ 8-15‰) (Bateman and Kelly, 2007). Assimilatory uptake can result in a positive fractionation of ~ 5‰, though is usually dominant in low productivity zones (Sigman et al., 1999). N fixation converts gaseous N_2 to bioavailable nitrate, but typically lowers seawater $\delta^{15}N$ values due to nitrate $\delta^{15}N$ values of ~ 0‰ (Voss et al., 2001). Denitrification can result in positive $\delta^{15}N$ waters owing to bacteria selectively removing light N, leaving behind waters enriched in ^{15}N, and can result in seawater nitrate fractionation of >15‰ (Brandes and Devol, 2002; Voss et al., 2001). The increase in $\delta^{15}N$ values observed upcore of ~1.5‰ could be the result of evolving Mississippi delivery, representing a higher delivery of sewage or organic manure, or increased denitrification in or near the mouth of the river, resulting in increased $\delta^{15}N$ values as

waters migrate further from the mouth in the freshwater plume. The corresponding increase in marine productivity suggests the latter is most likely.

Denitrification occurs when three conditions are satisfied: nitrate is available, oxygen concentrations are reduced, and electron donors are available (Seitzinger et al., 2006). Nitrate provided through fertilizer runoff supplied much of the nutrients requited to set up eutrophication and fuel the hypoxic zone. Unfortunately, as the nitrate load increases in the Mississippi River, the efficiency of nitrate removal through denitrification in the river system decreases (Mulholland et al., 2008). The rate of denitrification depends largely on residence time, allowing for estuaries at the mouth of the Mississippi River to become an active site for denitrification (Saunders and Kalff, 2001). While denitrification is occurring in the riverine and estuarine environments, it occurs at a much lower rate than that seen in upwelling oxygen minimum zones, which help to control the global N budget of the oceans and are evidenced by large $\delta^{15}N$ excursions (~4 - 6‰), much greater than seen in the GOM sediments (Groffman et al., 2006).

4.4.3 REE+Y

4.4.3.1 REE + Y Background

Geochemical properties of REE +Y (REY) enable them to be tracers of many aspects of marine environments. Their use ranges from studies to estuaries, to hydrothermal systems, to diagenesis and redox proxies (Bau et al., 1995; Haley et al., 2004; Hoyle et al., 1984; Klinkhammer et al., 1983; Tostevin et al., 2016). REEs consists of the Lanthanide series, and are commonly paired with Y due to its similar geochemical characteristics to Ho. REYs are supplied to marine environments by hydrothermal vents, Aeolian dust, and by riverine input and removed from marine systems by particle scavenging (Elderfield et al., 1990; Tostevin et al., 2016). Due to the relative increase in stability of elements with even atomic numbers, compared to those with odd atomic numbers, the concentration of REEs with positive atomic numbers exist in higher concentrations in nature than due REEs with negative atomic numbers (Oddo-Harkins rule). By normalizing REEs to PAAS, the distribution of REEs typically form a smooth, predictable pattern that allows for comparison between different samples.

REY's typically exist in a single oxidation state (+3) which limits their fractionation in sediment during weathering and transport (Elderfield et al., 1990). In dissolved loads, however, Ce can be oxidized to a highly insoluble 4+ state, resulting in negative Ce anomalies in some river systems and in oxic open marine settings (De Baar et al., 1985; Sholkovitz et al., 1994). In seawater, REEs readily form complexes with carbonates, with an increasing stability with increasing atomic number (Lee and Byrne, 1993). This results in a seawater distribution with enriched heavy REEs and a negative Ce anomaly. Seawater is also characterized by large Y/Ho mass ratios (> 36) (De Baar et al., 1985; Tostevin et al., 2016). This is due to complexation of REY with organic and inorganic particles, which are less stable for Y than Ho, resulting in increased concentration of Y in the ocean with respect to Ho (Bau et al., 1997; Byrne and Lee, 1993).

Riverine water REE profiles typically reflect the source rocks which have weathered in the drainage basin (Elderfield et al., 1990). While many times, this creates a flat REE pattern, weathering of phosphates can create REE distributions with enriched middle REEs (high BSI) (Haley et al., 2004; Martin et al., 2010). Clays and other material carried in the rivers can have a diverse set of patterns and are largely dependent on their source. Y/Ho ratios of rivers are generally lower than 36, owing to fact that the residence time is lower than that in the ocean and Ho has not complexed with particles and been removed to sediment (Bau et al., 1997; De Baar et al., 1985).

Redox cycling can have an effect on the distribution of REY as well. In Fe- and Mn- reducing conditions, Ho preferentially sorbs with respect to Y onto Fe and Mn oxide particles (Bau et al., 1997). These particles may subsequently dissolve under anoxic conditions, releasing Ho to the water column. The result is decreased Y/Ho ratios in anoxic bottom waters. In addition, it has been shown that anoxic pore waters with Fe in solution may result in elevated BSI values (~ 1.5) (Haley et al., 2004).

4.4.3.2 REE+Y in the Gulf of Mexico

Sequential extractions allow the investigation of the chemical speciation of REYs and further understanding of the environment of deposition. Carbonates have been shown to incorporate REYs of the surrounding water during precipitation (Piper and Bau, 2013; Tostevin et al., 2016). Y/Ho ratios of the

carbonate phase of the Gulf of Mexico core are indicative of a near shore or restricted setting (Y/Ho ~ 33-40) (Bau et al., 1997; De Baar et al., 1985; Webb and Kamber, 2000). The carbonate phase also exhibits neutral to negative Ce anomalies ($(Ce/Ce^*)_{SN}$ ~ 0.9 -1.0; Fig. 4.7) and pronounced middle REE enrichment (BSI ~1.6; Fig. 4.8), indicative of riverine waters (Tostevin et al., 2016). Carbonates of the core studied reflect riverine influence and do not share seawater REY characteristics, indicating a fluvial dominated environment, which is expected and confirms the riverine input on the hypoxic zone.

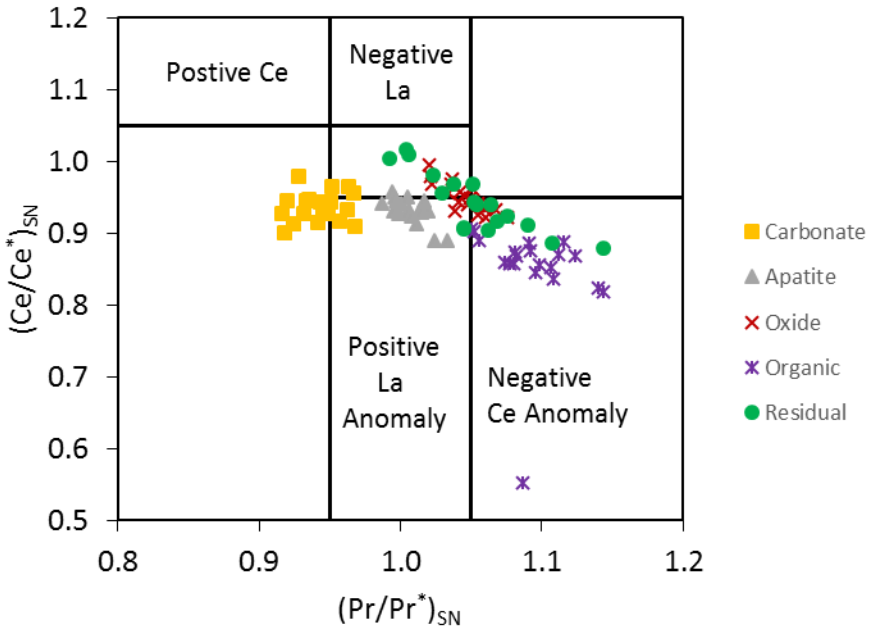

Figure 4.7 Ce and La anomalies of chemical phases, as calculated from $(Ce/Ce^*)_{SN} - (Pr/Pr^*)_{SN}$ variations, after Bao and Dulski (1996).

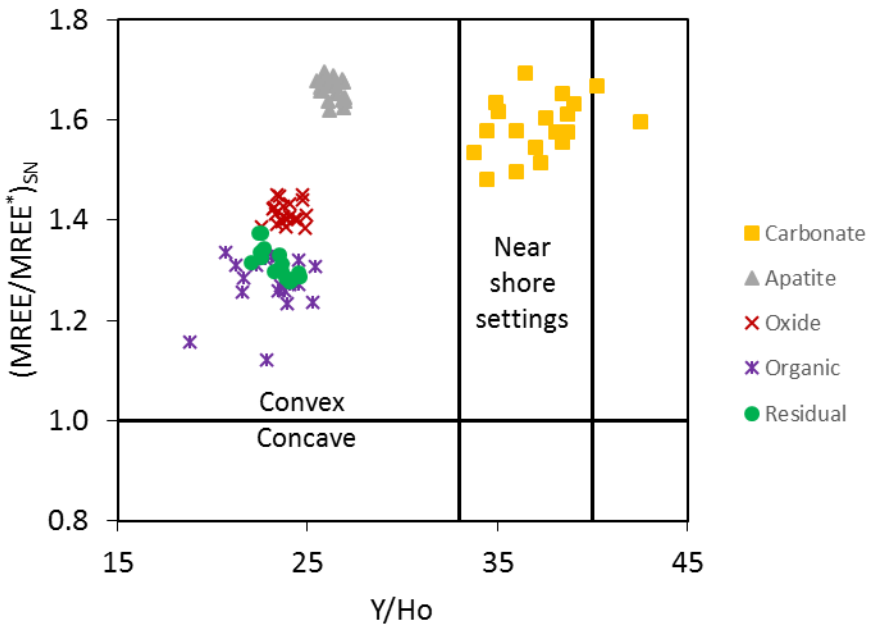

Figure 4.8 Cross plot of Y/Ho mass ratios to BSI $(MREE/MREE^*)_{SN}$

REY characteristics have no discernable depth trends, with the exception of middle REE enrichment (BSI) in the apatite phase (Fig. 4.9). BSI increases upcore consistently from ~1.6 to 1.7 in the apatite phase, suggesting that it is tied to evolving water mass characteristics, and consistently high indicating Fe-reducing conditions (Haley et al., 2004). Y/Ho ratios are low for the apatite phase (~25 – 30), suggesting precipitation in reducing waters (Bau et al., 1997). Ce anomalies are neutral to slightly negative in apatites, in agreement that reducing conditions may be possible (Fig. 4.7). BSI in the apatite phase covaries closely with the TOC/N_{mol} ratio (Fig. 4.10). A covariation between BSI and organic type shows that as the proportion of more labile marine organics increased in the sediment, Fe-oxide reduction increases as well, resulting in the rising BSI (Haley et al., 2004). Precipitation of apatite under reducing conditions indicates that the apatite phase authigenically accumulates in the sediment, consistent with previous studies of apatite on the Mississippi delta and incorporation of the incorporation of the REE of surrounding waters into apatite (Ruttenberg and Berner, 1993; Wright et al., 1987).

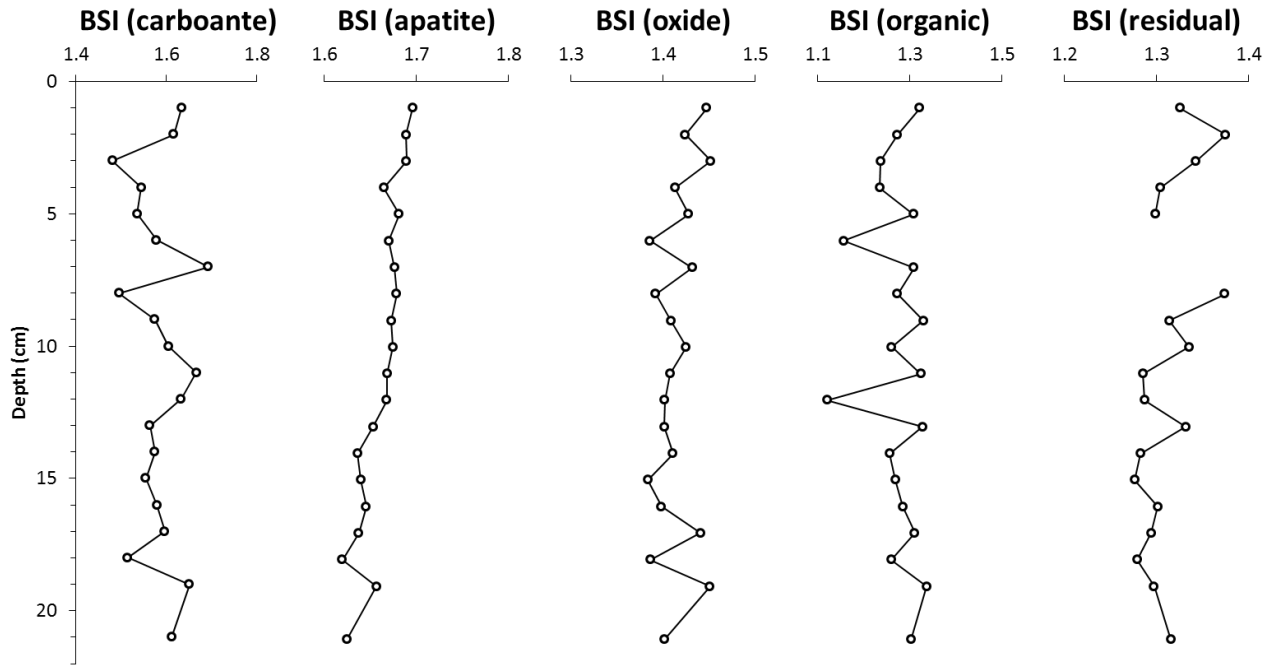

Figure 4.9 Depth plot of BSI (MREE/MREE*) from the apatite phase.

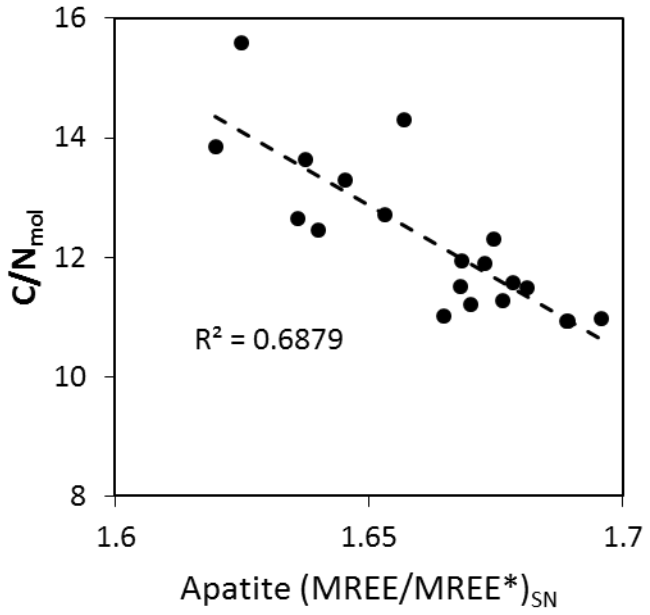

Figure 4.10 Cross plot of TOC/N molar ratios with the BSI (MREE/MREE*) of the apatite phase.

The oxide and organic phases have enriched middle REEs, low Y/Ho ratios (Fig. 4.8), and moderate negative Ce anomalies (Fig. 4.7), reflecting the suspended fraction of seawater (Piper and Bau, 2013; Sholkovitz et al., 1994). Adsorpition to organics and oxides result in fractionation of REEs from seawater forming the bell shape distribution (Haley et al., 2004). The residual phase reflects a terrestrial driven signature, rather than a smooth marine distribution, and is the result of weathering and transport into the Gulf of Mexico.

4.4.4 Trace Metals (V, Mo, and U)

4.4.4.1 Trace Metals (V, Mo, and U) Geochemistry Background

Redox sensitive trace metals, such as U, Mo, and V can provide historical context for the evolution of the redox state of the bottom waters during deposition. Under reducing environments, soluble U(VI) is reduced to insoluble U(IV), and may be exported to the sediment (Calvert and Pedersen, 1993; Tribovillard et al., 2006). Reduction of U(VI) occurs under chemical ranges similar to Fe(III) reduction to Fe(II) (Algeo and Maynard, 2004). Authigenic enrichment of U takes place in pore water, as reduced U is adsorbed onto particles or precipitates directly as uraninite or mononuclear U (Alessi et al., 2012; Klinkhammer and Palmer, 1991).

Mo is present in seawater primarily as soluble molybdate (MoO_4). Under reducing conditions, with sufficient concentrations of free H_2S, molybdate is reduced to particle reactive thiomolybdate (MoO_xS_{4-x}) (Erickson and Helz, 2000; Helz et al., 1996; Zheng et al., 2000). The level of free H_2S required (~11 µM) for the conversion of molybdate to thiomolybdate is referred to by Helz et al. (1996) as the “switching point”. Under permanently euxinic bottom waters, such as the Black Sea, molybdates are completely converted to tetrathiomolybdates (MoS_4) (Erickson and Helz, 2000). Mo is captured in the water column by Mn-oxyhydroxides and delivered to the sediment, where under reducing conditions it is released to pore waters where thimolybdates may form, then scavenged by Fe- or S-rich particles (Calvert and Pedersen, 1993; Helz et al., 1996).

In oxic waters, V forms vanadate and readily adsorbs onto both Mn- and Fe-oxyhydroxides (Calvert and Piper, 1984). Under mildly reducing conditions, V(V) is reduced to V(IV) and may be

removed to the sediment through surface adsorptions or by forming organometallic ligands (Emerson and Huested, 1991; Tribovillard et al., 2006). In the presence of free H_2S (euxinic conditions), V is further reduced to V(III) and may precipitate as oxides (Breit and Wanty, 1991).

4.4.4.2 Trace Metals (V, Mo, and U) in the Gulf of Mexico

As discussed above, in reducing environments, an increase in authigenic trace metal uptake by the sediment should be recorded in geochemical profiles. The authigenic uptake will be reflected by increased enrichment factors of V, Mo, and U. Thus, if authigenic accumulation takes place, there should be a positive covariation between the trace metal enrichment factors in the sediment. The sequential extraction carried out allows for the comparison of chemical phases in order to determine in which chemical phase authigenic enrichment of trace metals is hosted. Of the six chemical phases (exchangeable, carbonate, apatite, oxide, organic, and residual), only the exchangeable phase has a significant covariation between the three redox sensitive trace metals (Fig. 4.11-13). U_{EF} and V_{EF} covary in the oxide phase due to the fact that U is reduced in similar geochemical conditions as Fe, and V is tied closely to the Fe- and Mn-oxyhydroxide cycling (Algeo and Maynard, 2004; Tribovillard et al., 2006). This suggests that the exchangeable phase of the Gulf of Mexico sediment records variations in bottom water redox conditions. While the hypoxic zone of the Gulf of Mexico is seasonal, the trace metal enrichment will be tied to processes controlling the water chemistry year round. While the water column is reducing, trace metal enrichment may be intensified, especially through processes like particle shuttles. Under oxic water columns, the sediment may still be enriched in redox-sensitive trace metals through diffusion if the pore water is reducing. There is little oxygen penetration into the sediment, as evidenced by the U enrichment, which is easily re-oxidized and would be remobilized in the presence of O_2.

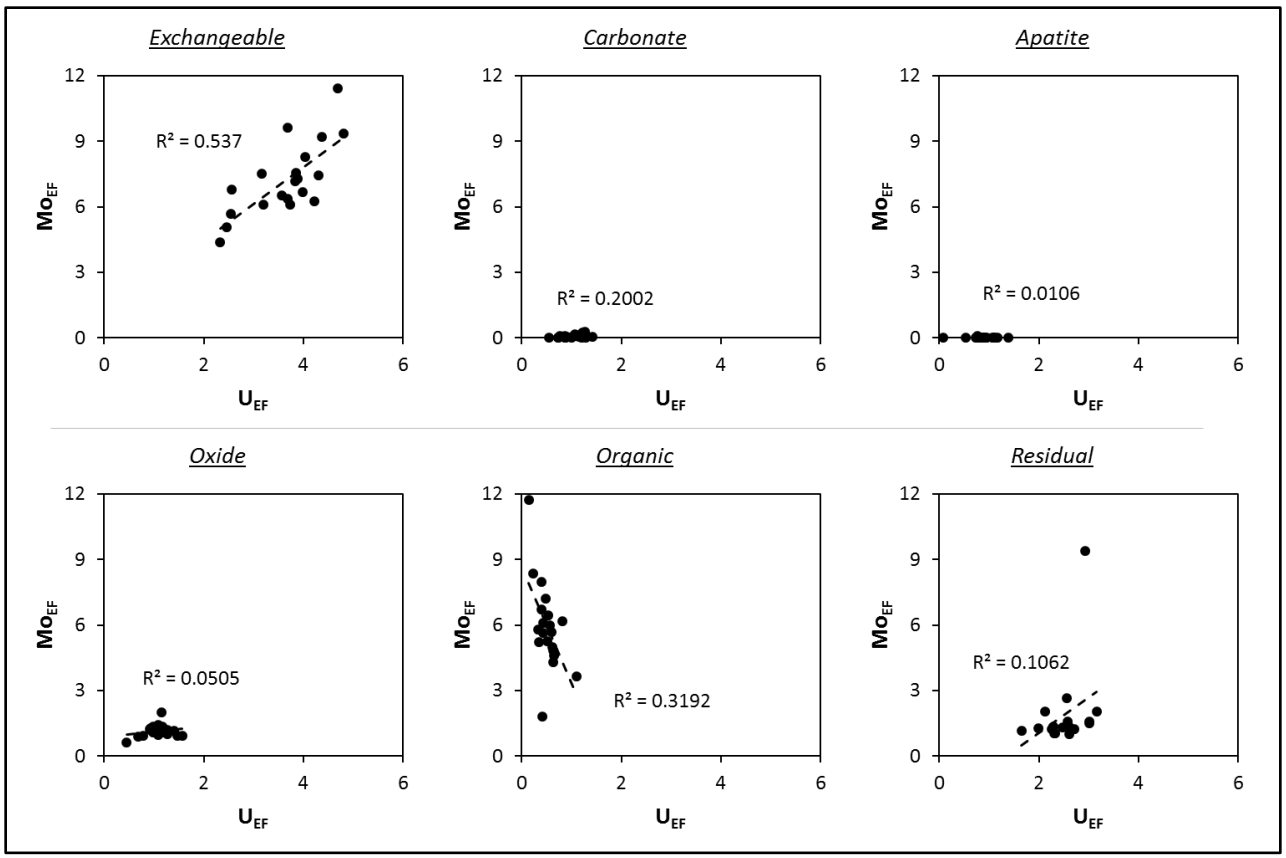

Figure 4.11 Cross plots of Mo_{EF} and U_{EF} of each chemical phase.

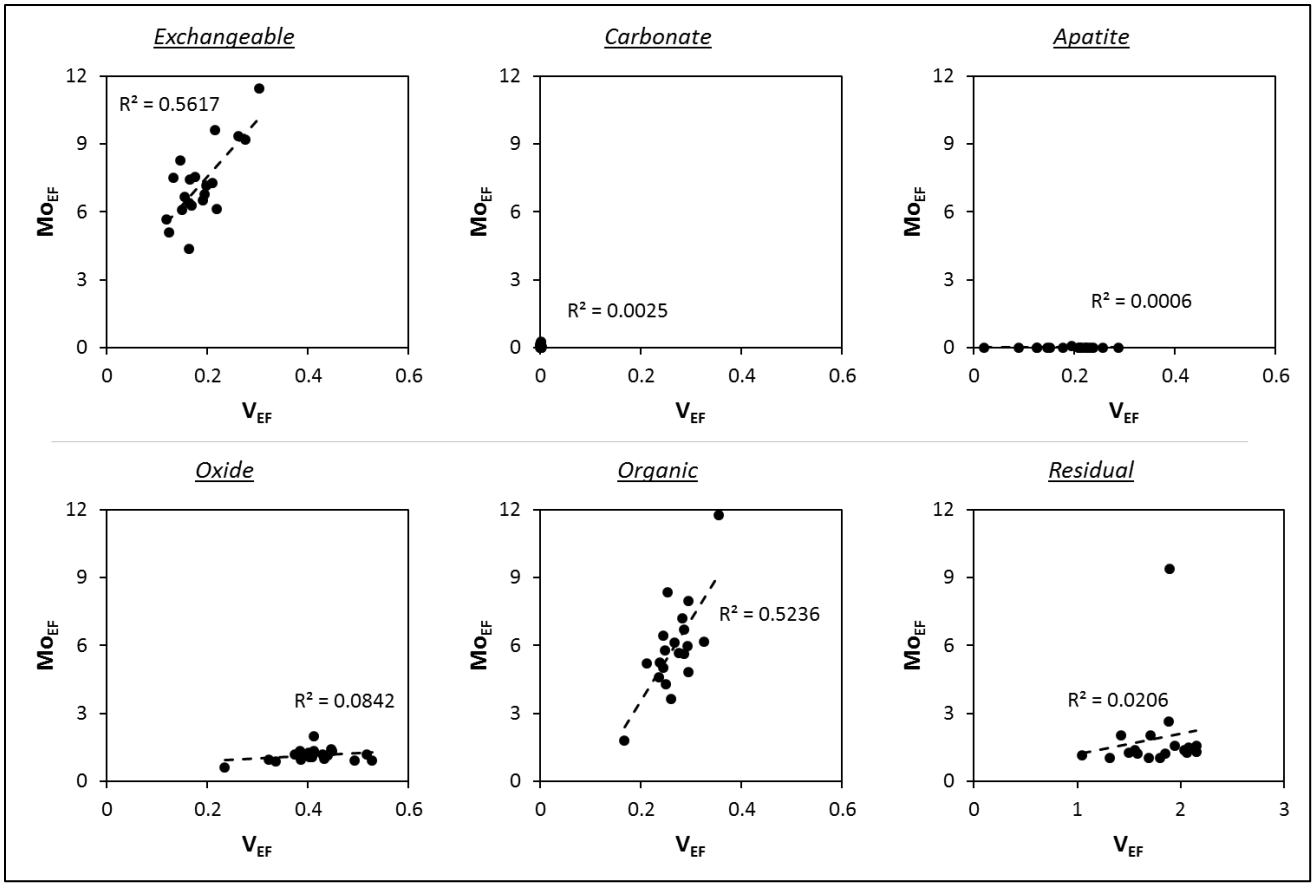

Figure 4.12 Cross plots of Mo_{EF} and V_{EF} of each chemical phase.

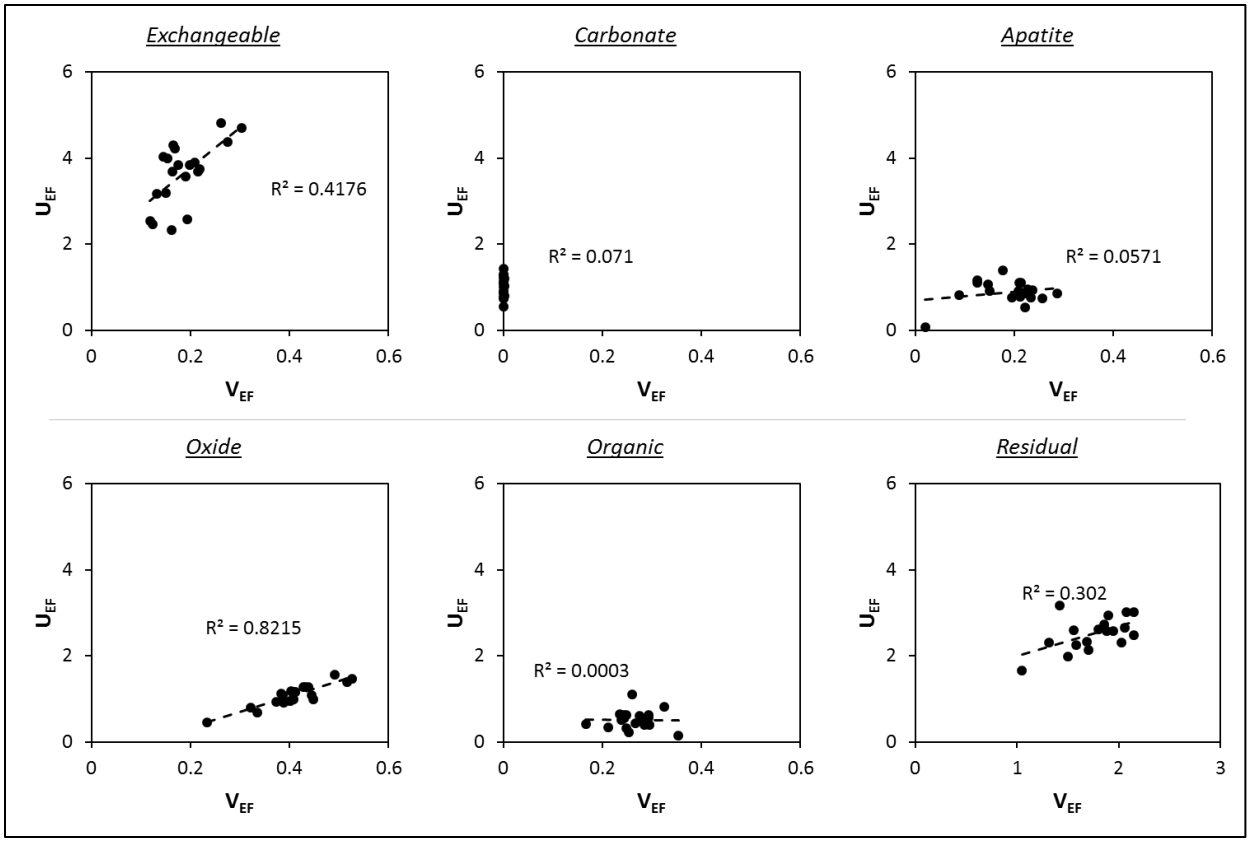

Figure 4.13 Cross plots of U_{EF} and V_{EF} of each chemical phase.

Previous studies have used redox sensitive trace elements as proxy records of hypoxic zones in both ancient marine systems and recent coastal zones (Helz and Adelson, 2013; Herrmann et al., 2012; Jilbert and Slomp, 2013). Trace element enrichment of sediment can correspond to historic O_2 depletion in bottom waters (Helz and Adelson, 2013). Developing proxies which track coastal hypoxia is an ongoing field of research (Gooday et al., 2009; Helz and Adelson, 2013), and sequential extractions have allowed the isolation of the chemical species in which authigenic uptake is hosted. In the case of V, the authigenic signature would have been obscured by the residual phase in a bulk analyses. Comparing depth profiles of the exchangeable phase of trace metals with the historic record of bottom water O_2 from the location (when available) and the aerial extent of the Gulf of Mexico hypoxic zone (as a proxy for hypoxic zone intensity where O_2 data is unavailable), approximate correlations may be made (Fig. 14). An exact covariation between trace metal enrichment and historical records is challenging for a few reasons: (1) U and V may be remobilized during oxic conditions, (2) sedimentation rates are not constant,

as evidenced by Al variation up core, (3) sampling the core by height may cause annual variation to be averaged out over multiple samples, and (4) storms or other high energy events may rework the sediment, distorting the original sedimentary structure. The decrease of trace metal enrichment with depth in the exchangeable phase and covariation between trace metals show that they do track historic O_2 depletion and reflect the intensity of hypoxia.

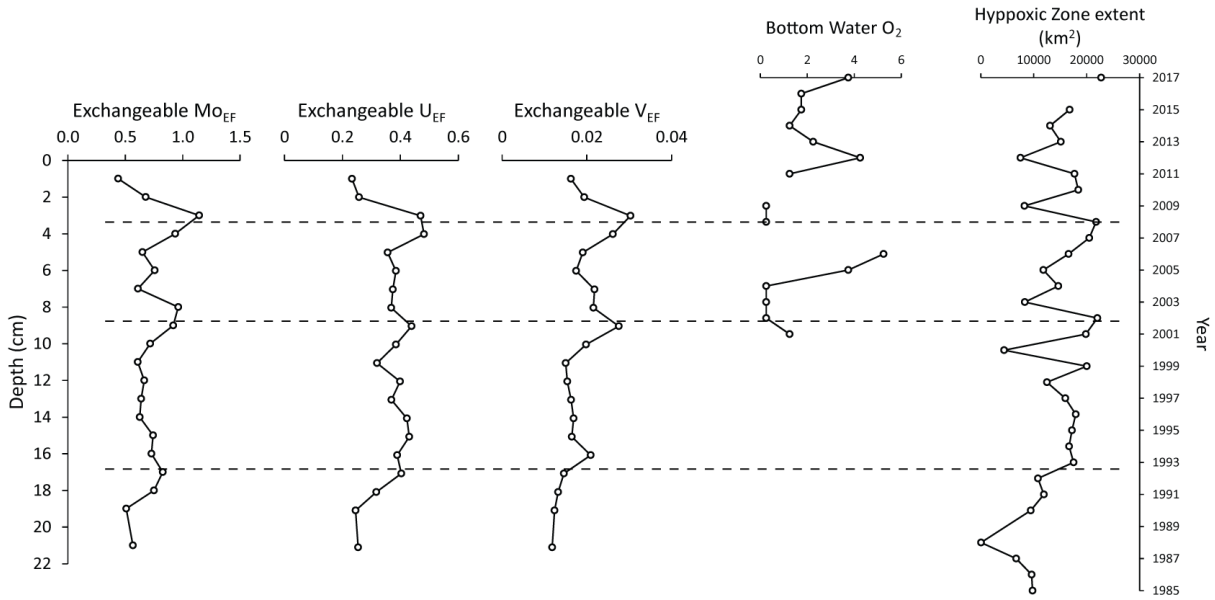

Figure 4.14 Depth profiles of V_{EF}, Mo_{EF}, and U_{EF} compared to the bottom water O_2 data available from the core location since 2001 and the aerial extent of annual hypoxic zones of the Gulf of Mexico. Dashed lines represent approximate correlation. Bottom Water O_2 data: National Oceanic and Atmospheric Administration, Southeast Area Monitoring and Assessment Program (https://ncddc.noaa.gov). Hypoxic zone aerial extent data source: Nancy N. Rabalais, LUMCON and R. Eugene Turner, LSU (https://gulfhypoxia.net).

4.5. Summaries

Sediment geochemistry in the Gulf of Mexico records the historical hypoxia trends. Stable isotopes of C, N, and S, as well as their elemental concentrations in the sediment show an increasing abundance of marine sourced organics, stimulated by an increased anthropogenic input of nutrients. The sediment documents a shift in N isotopes, attributable wither to intensified denitrification occurring near the river mouth, or an evolving riverine N load reflecting more organic waste in the water mass. S isotopes document a negative shift, indicative of increased bacterial sulphate reduction, stimulated by the

labile marine organics delivered to the sediment. REY are consistent with reducing environments and riverine influence, with enriched middle REE (high BSI) and relatively low Y/Ho ratios.

The intensity of the hypoxic zone is recorded in authigenic trace metal uptake in the exchangeable phase of the sediment. Covariations between V, Mo, and U in the exchangeable phase reflect the increase of anthropogenic loading, and hence the increased intensity of hypoxia over time. While an exact correlation with historical records of hypoxia extent is challenging, the comparison suggests that sedimentary trace metal enrichment of the Gulf of Mexico sediment reflects annual variations in hypoxia intensity.

4.6. References

Alessi, D.S., Uster, B., Veeramani, H., Suvorova, E.I., Lezama-Pacheco, J.S., Stubbs, J.E., Bargar, J.R., Bernier-Latmani, R., 2012. Quantitative separation of monomeric U (IV) from UO2 in products of U (VI) reduction. Environmental science & technology 46, 6150-6157.

Algeo, T.J., Maynard, J.B., 2004. Trace-element behavior and redox facies in core shales of Upper Pennsylvanian Kansas-type cyclothems. Chemical geology 206, 289-318.

Bateman, A.S., Kelly, S.D., 2007. Fertilizer nitrogen isotope signatures. Isotopes in environmental and health studies 43, 237-247.

Battaglin, W.A., Kendall, C., Chang, C.C., Silva, S.R., Campbell, D., 2001. Chemical and isotopic evidence of nitrogen transformation in the Mississippi River, 1997–98. Hydrological Processes 15, 1285-1300.

Bau, M., Dulski, P., Moller, P., 1995. Yttrium and holmium in South Pacific seawater: vertical distribution and possible fractionation mechanisms. Oceanographic Literature Review 11, 955.

Bau, M., Möller, P., Dulski, P., 1997. Yttrium and lanthanides in eastern Mediterranean seawater and their fractionation during redox-cycling. Marine Chemistry 56, 123-131.

Brandes, J.A., Devol, A.H., 2002. A global marine-fixed nitrogen isotopic budget: Implications for Holocene nitrogen cycling. Global Biogeochemical Cycles 16.

Breit, G.N., Wanty, R.B., 1991. Vanadium accumulation in carbonaceous rocks: a review of geochemical controls during deposition and diagenesis. Chemical Geology 91, 83-97.

Byrne, R.H., Lee, J.H., 1993. Comparative yttrium and rare earth element chemistries in seawater. Marine chemistry 44, 121-130.

Calvert, S., Pedersen, T., 1993. Geochemistry of recent oxic and anoxic marine sediments: implications for the geological record. Marine geology 113, 67-88.

Calvert, S., Piper, D., 1984. Geochemistry of ferromanganese nodules from DOMES Site A, Northern Equatorial Pacific: Multiple diagenetic metal sources in the deep sea. Geochimica et Cosmochimica Acta 48, 1913-1928.

De Baar, H.J., Bacon, M.P., Brewer, P.G., Bruland, K.W., 1985. Rare earth elements in the Pacific and Atlantic Oceans. Geochimica et Cosmochimica Acta 49, 1943-1959.

Diaz, R.J., 2001. Overview of hypoxia around the world. Journal of environmental quality 30, 275-281.

Diaz, R.J., Rosenberg, R., 2008. Spreading dead zones and consequences for marine ecosystems. science 321, 926-929.

Elderfield, H., Upstill-Goddard, R., Sholkovitz, E., 1990. The rare earth elements in rivers, estuaries, and coastal seas and their significance to the composition of ocean waters. Geochimica et Cosmochimica Acta 54, 971-991.

Emerson, S.R., Huested, S.S., 1991. Ocean anoxia and the concentrations of molybdenum and vanadium in seawater. Marine Chemistry 34, 177-196.

Erickson, B.E., Helz, G.R., 2000. Molybdenum (VI) speciation in sulfidic waters:: stability and lability of thiomolybdates. Geochimica et Cosmochimica Acta 64, 1149-1158.

Gooday, A., Jorissen, F., Levin, L., Middelburg, J., Naqvi, S., Rabalais, N., Scranton, M., Zhang, J., 2009. Historical records of coastal eutrophication-induced hypoxia. Biogeosciences 6, 1707-1745.

Gray, J.S., Wu, R.S.-s., Or, Y.Y., 2002. Effects of hypoxia and organic enrichment on the coastal marine environment. Marine Ecology Progress Series 238, 249-279.

Groffman, P.M., Altabet, M.A., Böhlke, J., Butterbach-Bahl, K., David, M.B., Firestone, M.K., Giblin, A.E., Kana, T.M., Nielsen, L.P., Voytek, M.A., 2006. Methods for measuring denitrification: diverse approaches to a difficult problem. Ecological Applications 16, 2091-2122.

Haley, B.A., Klinkhammer, G.P., McManus, J., 2004. Rare earth elements in pore waters of marine sediments. Geochimica et Cosmochimica Acta 68, 1265-1279.

Hardisty, D.S., Riedinger, N., Planavsky, N.J., Asael, D., Andrén, T., Jørgensen, B.B., Lyons, T.W., 2016. A Holocene history of dynamic water column redox conditions in the Landsort Deep, Baltic Sea. American Journal of Science 316, 713-745.

Hedges, J.I., Parker, P.L., 1976. Land-derived organic matter in surface sediments from the Gulf of Mexico. Geochimica et Cosmochimica Acta 40, 1019-1029.

Helz, G., Miller, C., Charnock, J., Mosselmans, J., Pattrick, R., Garner, C., Vaughan, D., 1996. Mechanism of molybdenum removal from the sea and its concentration in black shales: EXAFS evidence. Geochimica et Cosmochimica Acta 60, 3631-3642.

Helz, G.R., Adelson, J.M., 2013. Trace element profiles in sediments as proxies of dead zone history; rhenium compared to molybdenum. Environmental science & technology 47, 1257-1264.

Herrmann, A.D., Kendall, B., Algeo, T.J., Gordon, G.W., Wasylenki, L.E., Anbar, A.D., 2012. Anomalous molybdenum isotope trends in Upper Pennsylvanian euxinic facies: Significance for use of δ98Mo as a global marine redox proxy. Chemical Geology 324, 87-98.

Hoyle, J., Elderfield, H., Gledhill, A., Greaves, M., 1984. The behaviour of the rare earth elements during mixing of river and sea waters. Geochimica et Cosmochimica Acta 48, 143-149.

Jilbert, T., Slomp, C.P., 2013. Rapid high-amplitude variability in Baltic Sea hypoxia during the Holocene. Geology 41, 1183-1186.

Jochum, K.P., Nohl, U., Herwig, K., Lammel, E., Stoll, B., Hofmann, A.W., 2005. GeoReM: a new geochemical database for reference materials and isotopic standards. Geostandards and Geoanalytical Research 29, 333-338.

Klinkhammer, G., Elderfield, H., Hudson, A., 1983. Rare earth elements in seawater near hydrothermal vents. Nature 305, 185.

Klinkhammer, G., Palmer, M., 1991. Uranium in the oceans: where it goes and why. Geochimica et Cosmochimica Acta 55, 1799-1806.

Lee, J.H., Byrne, R.H., 1993. Complexation of trivalent rare earth elements (Ce, Eu, Gd, Tb, Yb) by carbonate ions. Geochimica et Cosmochimica Acta 57, 295-302.

Martin, E.E., Blair, S.W., Kamenov, G.D., Scher, H.D., Bourbon, E., Basak, C., Newkirk, D.N., 2010. Extraction of Nd isotopes from bulk deep sea sediments for paleoceanographic studies on Cenozoic time scales. Chemical Geology 269, 414-431.

McLennan, S.M., 2001. Relationships between the trace element composition of sedimentary rocks and upper continental crust. Geochemistry, Geophysics, Geosystems 2.

Meyers, P.A., 1994. Preservation of elemental and isotopic source identification of sedimentary organic matter. Chemical geology 114, 289-302.

Morin, G., Mangeret, A., Othmane, G., Stetten, L., Seder-Colomina, M., Brest, J., Ona-Nguema, G., Bassot, S., Courbet, C., Guillevic, J., 2016. Mononuclear U (IV) complexes and ningyoite as major uranium species in lake sediments. Geochemical Perspectives Letter 2, 95-105.

Mulholland, P.J., Helton, A.M., Poole, G.C., Hall, R.O., Hamilton, S.K., Peterson, B.J., Tank, J.L., Ashkenas, L.R., Cooper, L.W., Dahm, C.N., 2008. Stream denitrification across biomes and its response to anthropogenic nitrate loading. Nature 452, 202.

Peterson, B.J., Howarth, R.W., Garritt, R.H., 1985. Multiple stable isotopes used to trace the flow of organic matter in estuarine food webs. Science 227, 1361-1363.

Peterson, B.J., Howarth, R.W., Garritt, R.H., 1986. Sulfur and Carbon Isotopes as Tracers of Salt-Marsh Organic Matter Flow. Ecology 67, 865-874.

Piper, D.Z., Bau, M., 2013. Normalized rare earth elements in water, sediments, and wine: identifying sources and environmental redox conditions. American Journal of Analytical Chemistry 4, 69.

Rabalais, N.N., Cai, W.-J., Carstensen, J., Conley, D.J., Fry, B., Hu, X., Quinones-Rivera, Z., Rosenberg, R., Slomp, C.P., Turner, R.E., 2014. Eutrophication-driven deoxygenation in the coastal ocean. Oceanography 27, 172-183.

Rabalais, N.N., Turner, R.E., Gupta, B.K.S., Platon, E., Parsons, M.L., 2007. Sediments tell the history of eutrophication and hypoxia in the northern Gulf of Mexico. Ecological Applications 17.

Rabalais, N.N., Turner, R.E., Wiseman Jr, W.J., 2002. Gulf of Mexico hypoxia, aka "The dead zone". Annual Review of ecology and Systematics 33, 235-263.

Ruttenberg, K.C., Berner, R.A., 1993. Authigenic apatite formation and burial in sediments from non-upwelling, continental margin environments. Geochimica et cosmochimica acta 57, 991-1007.

Sackett, W.M., 1964. The depositional history and isotopic organic carbon composition of marine sediments. Marine Geology 2, 173-185.

Saunders, D., Kalff, J., 2001. Nitrogen retention in wetlands, lakes and rivers. Hydrobiologia 443, 205-212.

Seitzinger, S., Harrison, J.A., Böhlke, J., Bouwman, A., Lowrance, R., Peterson, B., Tobias, C., Drecht, G.V., 2006. Denitrification across landscapes and waterscapes: a synthesis. Ecological Applications 16, 2064-2090.

Sholkovitz, E.R., Landing, W.M., Lewis, B.L., 1994. Ocean particle chemistry: the fractionation of rare earth elements between suspended particles and seawater. Geochimica et Cosmochimica Acta 58, 1567-1579.

Sigman, D., Altabet, M., McCorkle, D., Francois, R., Fischer, G., 1999. The δ15N of nitrate in the Southern Ocean: Consumption of nitrate in surface waters. Global Biogeochemical Cycles 13, 1149-1166.

Šurija, B., Branica, M., 1995. Distribution of Cd, Pb, Cu and Zn in carbonate sediments from the Krka river estuary obtained by sequential extraction. Science of the total environment 170, 101-118.

Tessier, A., Campbell, P.G., Bisson, M., 1979. Sequential extraction procedure for the speciation of particulate trace metals. Analytical chemistry 51, 844-851.

Tostevin, R., Shields, G.A., Tarbuck, G.M., He, T., Clarkson, M.O., Wood, R.A., 2016. Effective use of cerium anomalies as a redox proxy in carbonate-dominated marine settings. Chemical Geology 438, 146-162.

Tribovillard, N., Algeo, T.J., Lyons, T., Riboulleau, A., 2006. Trace metals as paleoredox and paleoproductivity proxies: an update. Chemical geology 232, 12-32.

Turner, R.E., Milan, C., Rabalais, N., 2004. A retrospective analysis of trace metals, C, N and diatom remnants in sediments from the Mississippi River delta shelf. Marine Pollution Bulletin 49, 548-556.

Turner, R.E., Rabalais, N.N., 1994. Coastal eutrophication near the Mississippi river delta. Nature 368, 619.

Turner, R.E., Rabalais, N.N., 2017. 2017 Forecast: Summer Hypoxic Zone Size Northern Gulf of Mexico. Louisiana State University, Website PDF article. Accessed December 11.

Turner, R.E., Rabalais, N.N., Alexander, R.B., McIsaac, G., Howarth, R., 2007. Characterization of nutrient, organic carbon, and sediment loads and concentrations from the Mississippi River into the Northern Gulf of Mexico. Estuaries and Coasts 30, 773-790.

Turner, R.E., Rabalais, N.N., Justic, D., 2008. Gulf of Mexico hypoxia: Alternate states and a legacy. Environmental Science & Technology 42, 2323-2327.

Vaquer-Sunyer, R., Duarte, C.M., 2008. Thresholds of hypoxia for marine biodiversity. Proceedings of the National Academy of Sciences 105, 15452-15457.

Voss, M., Dippner, J.W., Montoya, J.P., 2001. Nitrogen isotope patterns in the oxygen-deficient waters of the Eastern Tropical North Pacific Ocean. Deep Sea Research Part I: Oceanographic Research Papers 48, 1905-1921.

Wang, X.-C., Chen, R.F., Gardner, G.B., 2004. Sources and transport of dissolved and particulate organic carbon in the Mississippi River estuary and adjacent coastal waters of the northern Gulf of Mexico. Marine Chemistry 89, 241-256.

Webb, G.E., Kamber, B.S., 2000. Rare earth elements in Holocene reefal microbialites: a new shallow seawater proxy. Geochimica et Cosmochimica Acta 64, 1557-1565.

Wright, J., Schrader, H., Holser, W.T., 1987. Paleoredox variations in ancient oceans recorded by rare earth elements in fossil apatite. Geochimica et Cosmochimica Acta 51, 631-644.

Zheng, Y., Anderson, R.F., van Geen, A., Kuwabara, J., 2000. Authigenic molybdenum formation in marine sediments: a link to pore water sulfide in the Santa Barbara Basin. Geochimica et Cosmochimica Acta 64, 4165-4178.

CHAPTER 5 SEQUENTIAL EXTRACTION ANALYSIS OF THE LATE PENNSYLVANIAN NORTH AMERICAN MIDCONTINENT SEA

5.1. Introduction

Waxing and waning of Gondwanan ice sheet drove eustatic highstands which inundated the interior of the Laurentian Craton, flooding a vast expanse (>1 × 10^6 km^2) creating an immense sea known as The Late Pennsylvanian North American Midcontinent Sea (NAMS, Fig. 5.1) (Algeo and Heckel, 2008; Heckel, 1977). The NAMS likely had multiple sources of terrestrial freshwater input in the south, east, and west, and a single connection to the open ocean. The combination of strong freshwater input and upwelling of preconditions, oxygen poor water from the eastern tropical Panthalassic ocean created a strongly stratified water column in which reducing bottom waters circulated freely beneath an oxygenated brackish water mass, termed "superestuarine circulation" (Algeo et al., 2008a).

In chapter 2, bulk geochemical properties were used in order to investigate gyral circulation and general watermass conditions. Chapters 3 and 4 developed a sequential extraction technique in which the chemical phase trace metals are hosted may be investigated. It was determined that authigenic enrichment of trace metals in reducing pore waters (chapter 3) and hypoxic water column (chapter 4) are hosted in the exchangeable phase, allowing for the isolation of enrichment due to redox variation from that of terrestrial, organic, or non-redox related input. In the NAMS, water column conditions in the restricted bottom waters were euxinic (free H_2S), providing more reducing conditions than in the Gulf of Mexico hypoxic zone, and water column euxinia as opposed to pore water H_2S in The Bahamas. Sequential extractions of NAMS sediment allow for a detailed understanding of how trace metal are incorporated under these restricted conditions.

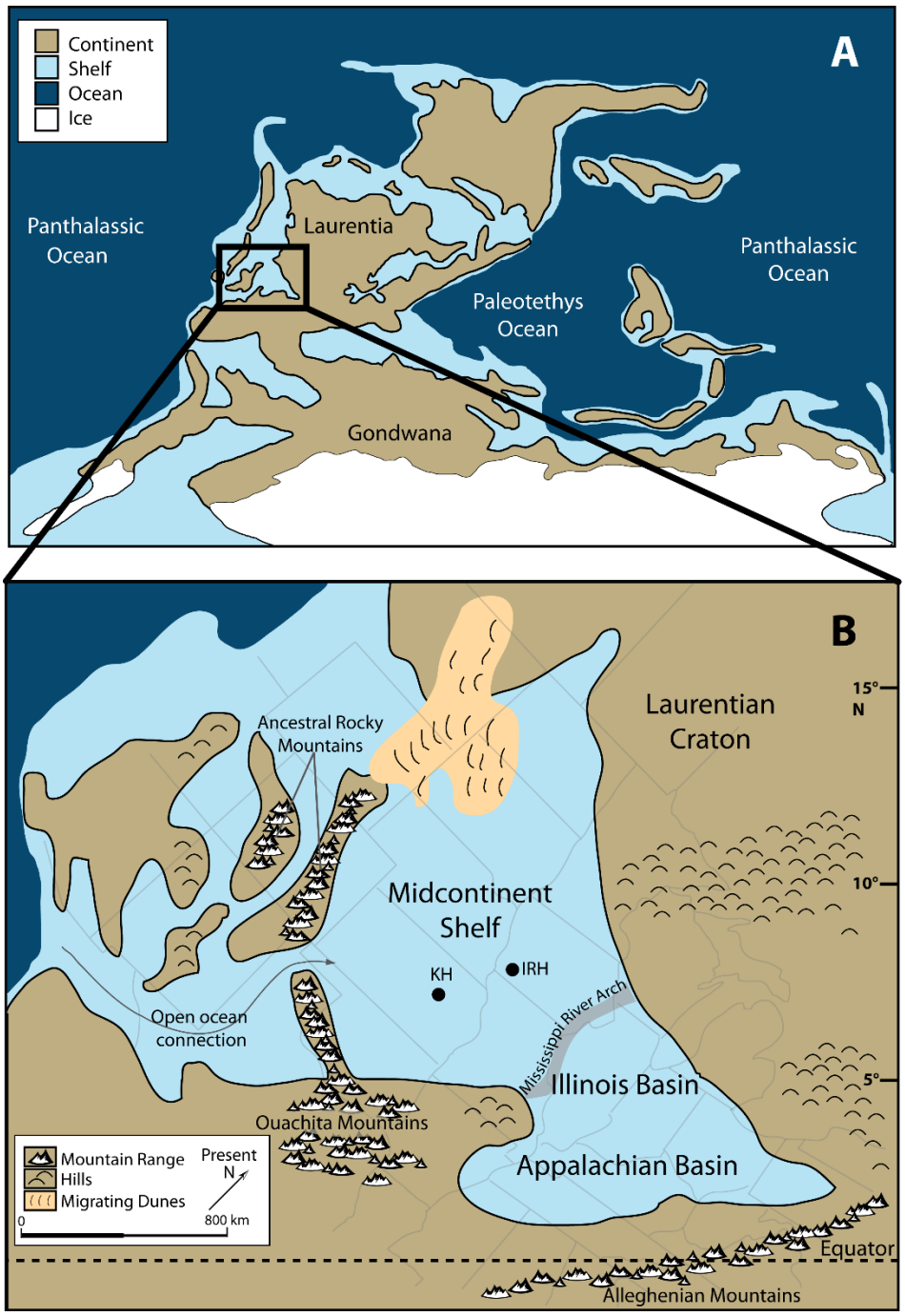

Figure 5.1 Paleogeographic map of study area. Present state outlines provide scale and orientation. Sources: (A) modified from Ron Blakey (https://deeptimemaps.com/); (B) modified from Algeo et al. (2008a).

5.1.1 Geologic Background

The NAMS had landmasses which nearly surrounded it. The Laurentian Craton was to the east, the Alleghenian Mountains to the south, and the Ouachita Mountains to the west. The Alleghenian

Mountain rose due to a large continent-continent collision as Gondwana and Laurentia collide, causing the mountain range to rise to high elevations. The crustal thickening related to the Alleghenian Mountain formation caused the formation of the foreland basin that became the NAMS. The combination of the surrounding mountain ranges and accommodation space created in the basin led to large runoffs of freshwater and sediment into the eastern end of the NAMS, near the Appalachian Basin, where abundant coal swamps are found. The mountain ranges likely led to the creation of a monsoonal climate (Montañez et al., 2007; Poulsen et al., 2007), increasing terrestrial discharge into the NAMS.

Inundation and subsequent drainage of the NAMS was controlled by waxing and waning of the Gondwanan ice sheets. The core shale deposited under sealevel highstands therefor is thought to have been deposited over 100 – 150 thousand year period.

5.1.2 Conceptual model for circulation

In chapter 2, it was asserted that the NAMS likely experienced gyral circulation in a clockwise, basin scale manner. This can be ground proofed through conceptual thought experiments based on current published understandings of wind patterns, freshwater discharge, and bathymetric restrictions. Tabor and Poulsen (2008) propose wind patterns across the NAMS moving from west to east, and monsoonal climates. Algeo et al. (2008a) meanwhile detail large freshwater influxes to the NAMS, with freshwater associated with the foreland basin drainage system similar, but slightly lower than that of the modern Ganges-Brahmaputra (400 – 750 km^3 yr^{-1} vs ~970 km^3yr^{-1} of the Ganges).

Geochemical evidence provided by this study and others (e.g. Algeo et al., 2008) provides evidence for large scale circulation of the brackish water column, which is supplied by the large terrestrial freshwater runoff. This circulation would be affect significantly by wind drag due to the large surface area of the NAMS and low bathymetric relief. The wind patterns proposed by Tabor and Poulsen (2008) (from west to east, across the northern NAMS) combined with the circulation of the brackish water layer, support Ekman Transport of the watermass in a clockwise motion around the NAMS.

5.2. Materials and Methods

This work analyzes two drillcore sections of the lower Gzhelian Heebner Hale Member of the Oread Limestone on the northern Midcontinent Shelf (Fig. 5.1). Eleven samples from each core were chosen to encompass different aspects of water column conditions during deposition. A modified Tessier sequential extraction was carried out. Modifications from the original Tessier method consist of an addition of an apatite phase and the substitution of sodium bicarbonate solution during the exchangeable phase, used to target mononuclear U (Morin et al., 2016; Šurija and Branica, 1995; Tessier et al., 1979). The extraction consists of the following steps (at room temperature unless otherwise noted): 1) 1 M sodium bicarbonate for 12 hours targeting loosely bound, non-crystalline fraction; 2) 1 M sodium acetate buffered to pH 5 with acetic acid for 24 hours targeting carbonates; 3) 1 M nitric acid for 30 minutes targeting apatite bound elements; 4) 1 M hydroxylamine hydrochloride in 30 % (w/w) acetic acid for 12 hours at 95 ^{0}C targeting hydrous oxides; 5) 30 % hydrogen peroxide with 0.02 M nitric acid for 24 hours at 85 ^{0}C targeting organic phases; 6) Concentrated nitric acid at 95 ^{0}C for 48 hours targeting any residuals. Samples were washed twice with de-ionized water after each extraction. Extracts were collected and dried down to remove the liquid portion of reagents, then brought back up in 2 % nitric acid for ICP-MS analysis. Two USGS shale standards (SGR and SDO-1), procedural blanks, and reagent blanks were collected to check for successful chemical and analytical techniques.

Analysis was carried out using a Thermo iCAP Q quadrapole inductively coupled mass spectrometer. Chemical phases were run individually, so as to reduce matrix effects. Instrument drift and suppression were corrected for using internal and check standards.

5.3. Results

5.3.1 Internal correlation of the Heebner Shale across the NAMS

Previous studies have subdivided the shale unit into smaller units based on geochemical traits (Algeo et al., 2008b; Algeo et al., 2004; Herrmann et al., 2015; Herrmann et al., 2012). Using bulk geochemical traits detailed in chapter 2, this study follows in a similar path, though subdivides the core shale into five sub-units: lower black shale-1 (LBS-1), lower black shale-2 (LBS-2), upper black shale-1

(UBS-1), upper black shale-2 (UBS-2), and grey shale (GS) (Fig. 5.2). The lower black shale is delineated by a nitrogen isotopic excursion, the intensification phase is the LBS-1 and the relaxation phase is LBS-2. The boundary between LBS-2 and UBS-1 is recognized as the maximum flooding surface (MFS) (Algeo et al., 2004). UBS-1 is characterized by variable, but elevated organic carbon content (TOC) and molybdenum enrichment factors (Mo_{EF}). UBS-2 has Mo_{EF} near 1 and little variation in TOC (~5-10%). The GS is marked by a decline in TOC (<2.5 %) and little trace metal enrichment.

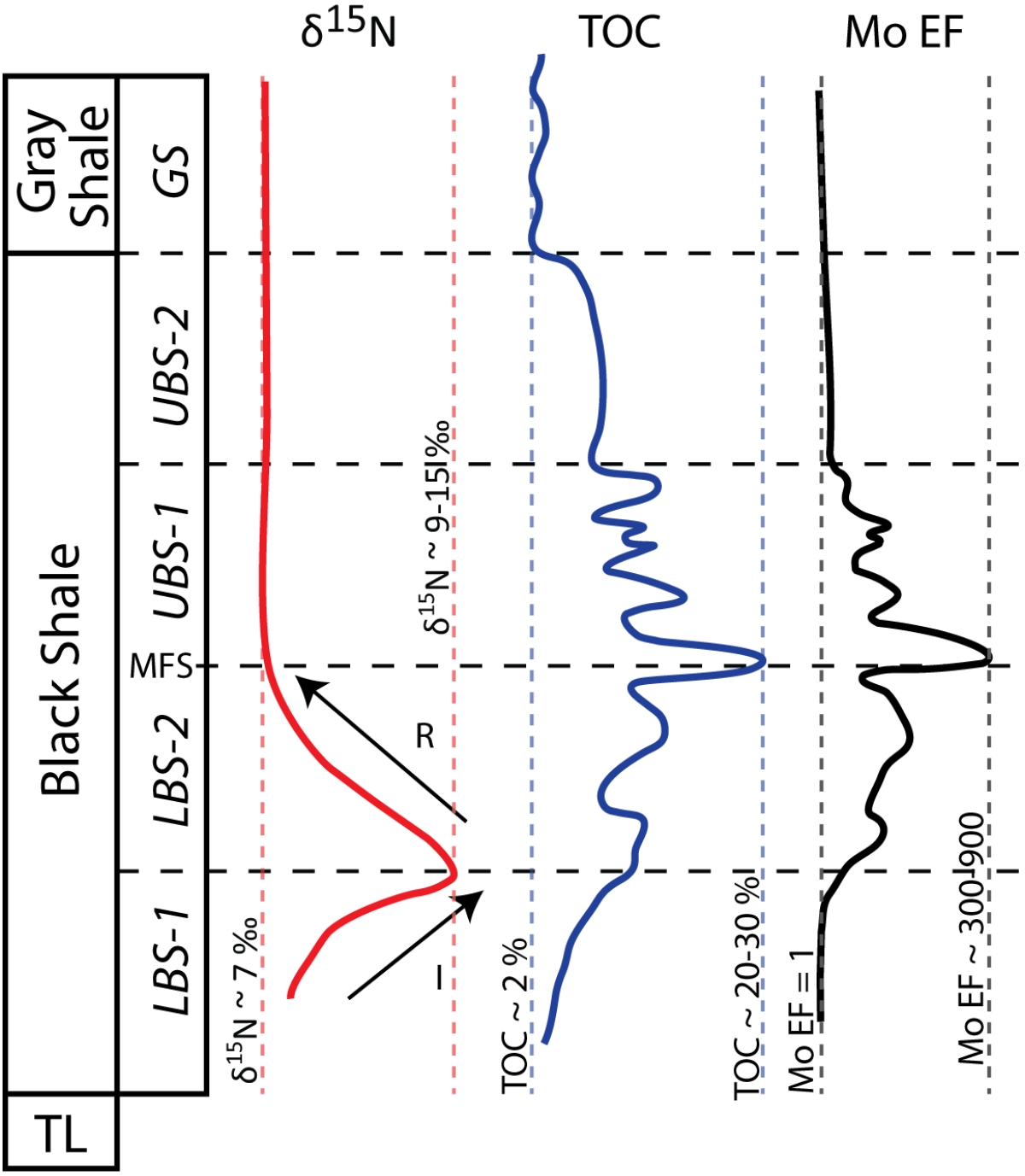

Figure 5.2 Generalized geochemical signatures used to identify depositional units of the Heebner Shale. TL = transgressive limestone, LBS = lower black shale, UBS = upper black shale, GS = gray shale, and MFS is the maximum flooding surface (per Algeo et al., 2004). TOC = total organic carbon, Mo_{EF} = molybdenum enrichment factor, and I and R show the intensification and relaxation stages of $\delta^{15}N$ excursions, respectively. Note that LBS-2 is equivalent to "MBS" of Herrmann et al. (2015).

5.3.2 REE + Y

REE profiles are normalized to Post Archean Australian values (PAAS), denoted by a "SN" or shale normalized subscript (McLennan, 2001). The distributions of REE vary widely across the chemical phases, showing partitioning. The exchangeable phase had concentrations of REE that were at or near the limit of quantification of the ICP-MS and thus, are not included in the results. In the carbonate phase, normalized REE values are near 0.1 and flat, to slightly heavy REE enriched (Fig. 5.3). The apatite phase is distinctly bell shaped, with values from 0.01 – 10. The Oxide phase expresses two patterns, one bell shaped and one flat with heavy REE enrichment, and values from ~0.01 – 1. The organic phase is heavy REE depleted, with values ~0.1, with the exception of a sample from the LBS-2 of the IRH core, which is bell shaped with values ~0.5. The residual phase has a distinctive jagged pattern, with values that range from 0.01 – 1.

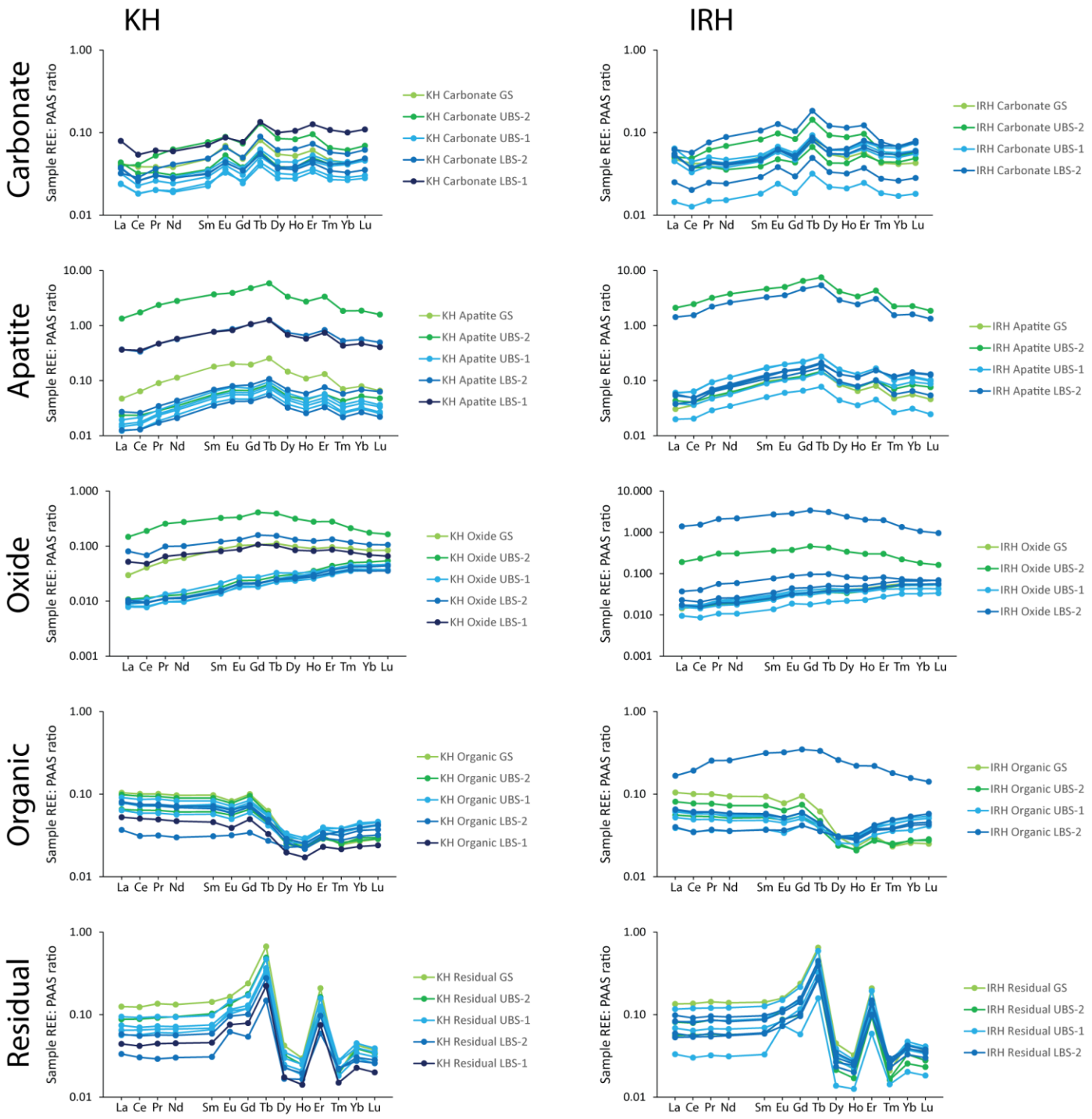

Figure 5.3 REE profiles of the two cores in each chemical phase.

Several parameters that describe the shape and enrichemnet of REE distribution quantitatively can be calculated. Heavy REE enrichment is described by Nd/Yb ratios (greater than 1 is heavy REE

depleted, less than 1 is depleted). Ce and La anomalies can be described in terms of $(Ce/Ce^*)_{SN}$ and $(Pr/Pr^*)_{SN}$ as calculated by:

$$(Ce/Ce^*)_{SN} = \frac{2 * Ce_{SN}}{La_{SN} + Pr_{SN}}$$

and

$$(Pr/Pr^*)_{SN} = \frac{2 * Pr_{SN}}{Nd_{SN} + Ce_{SN}}$$

The degree of middle REE enrichment, or bell shaped distribution can be calculated by the bell shaped index (BSI or $(MREE/MREE^*)_{SN}$) as:

$$BSI = \frac{2 * (Sm_{SN} + Gd_{SN} + Dy_{SN})/3}{\frac{La_{SN} + Pr_{SN} + Nd_{SN}}{3} + \frac{Ho_{SN} + Er_{SN} + Tm_{SN} + Yb_{SN} + Lu_{SN}}{5}}$$

The exchangeable phase has a slight negative Ce anomaly (Fig. 5.4) (KH average:0.82, stdev. 0.06, and IRH average 0.81, stdev. 0.5). The Nd/Yb in the exchangeable phase shows slight heavy REE enrichment (KH average 0.74, stdev 0.13, IRH average 0.89, stdev 0.22) and decreases with depth (Fig. 5.5). Y/Ho mass ratios are used to determine if samples are free from terrestrial influence, with samples having Y/Ho generally considered having "marine characteristics" (Tostevin et al., 2016). The exchangeable phase has Y/Ho of ~37 for KH and ~38 for IRH (stdev. of 2), and increasing with depth (Fig. 5.5). Apatite phase samples have high BSI values (KH average 1.7, stdev. 0.1, IRH average 1.6, stdev. 0.2), reflecting their bell shape.

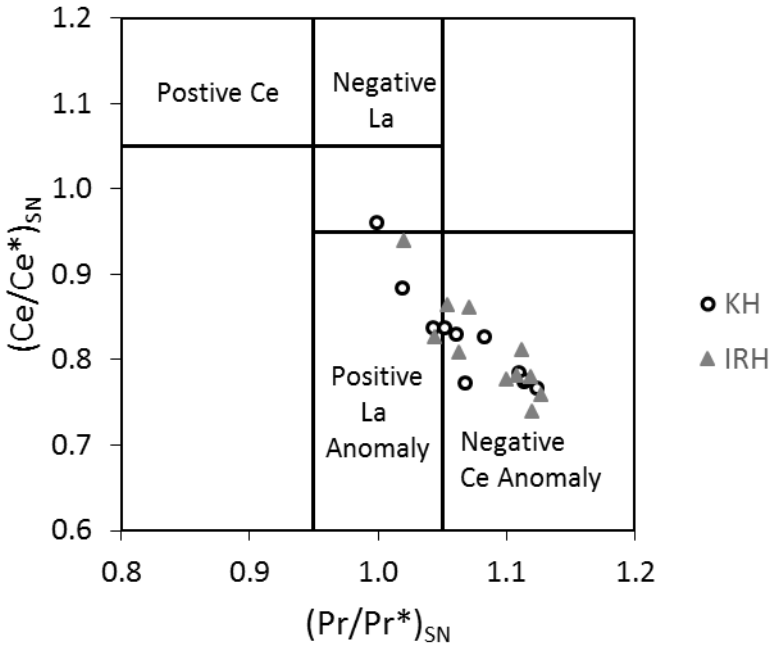

Figure 5.4 Cross plot of describing Ce and La anomalies in the carbonate phase. After Bau and Dulski (1996).

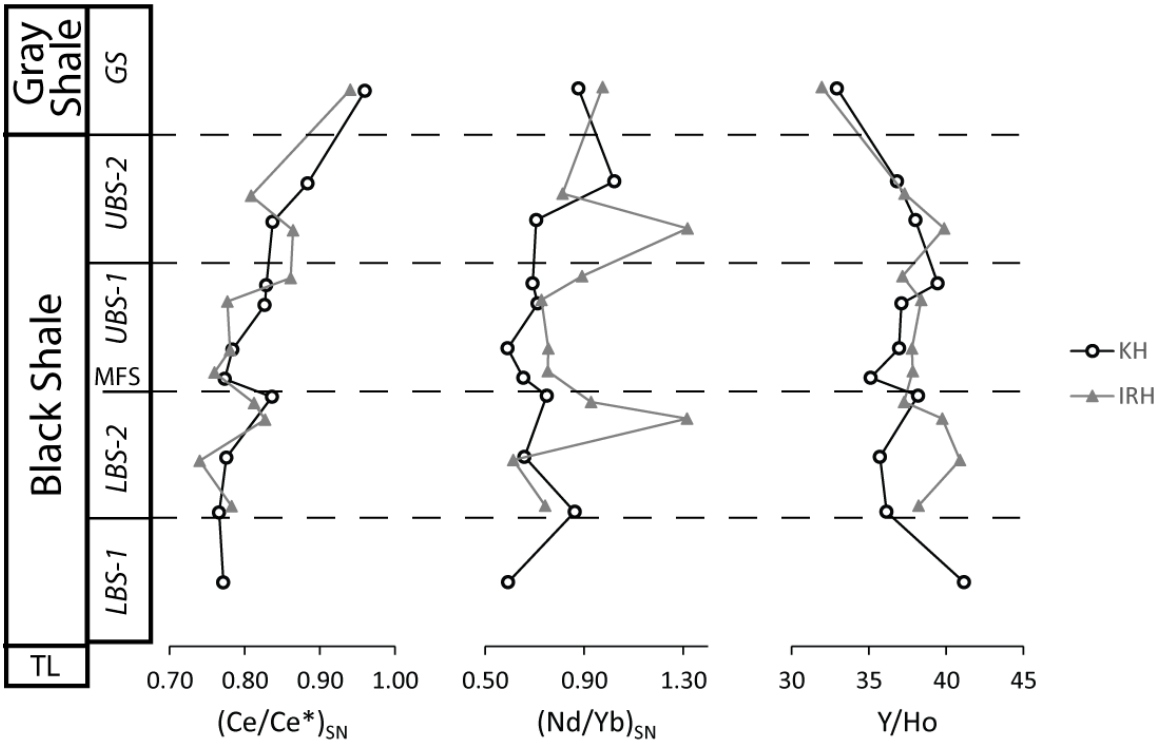

Figure 5.5 Depth plots of carbonate phase Ce anomalies $(Ce/Ce^*)_{SN}$, light REE enrichment $(Nd/Yb)_{SN}$, and Y/Ho ratio, a proxy for terrestrial influence.

5.3.4 Bulk Sediment Analysis

Geochemical analysis of the bulk sediment is detailed in chapter 2, however TOC (%) and Al normalized Fe are used presently to aid in the interpretation of the sequential extractions (Fig. 5.6). TOC ranges from ~5 – 25%, with the highest concentrations in LBS-2 and UBS-1. Both cores exhibit similar values and distributions of TOC. Al normalized Fe (Fe_T/Al) ranges from ~0.4 – 0.8, with the highest values in the UBS-1. Both study sections exhibit similar patterns and distributions of Fe_T/Al.

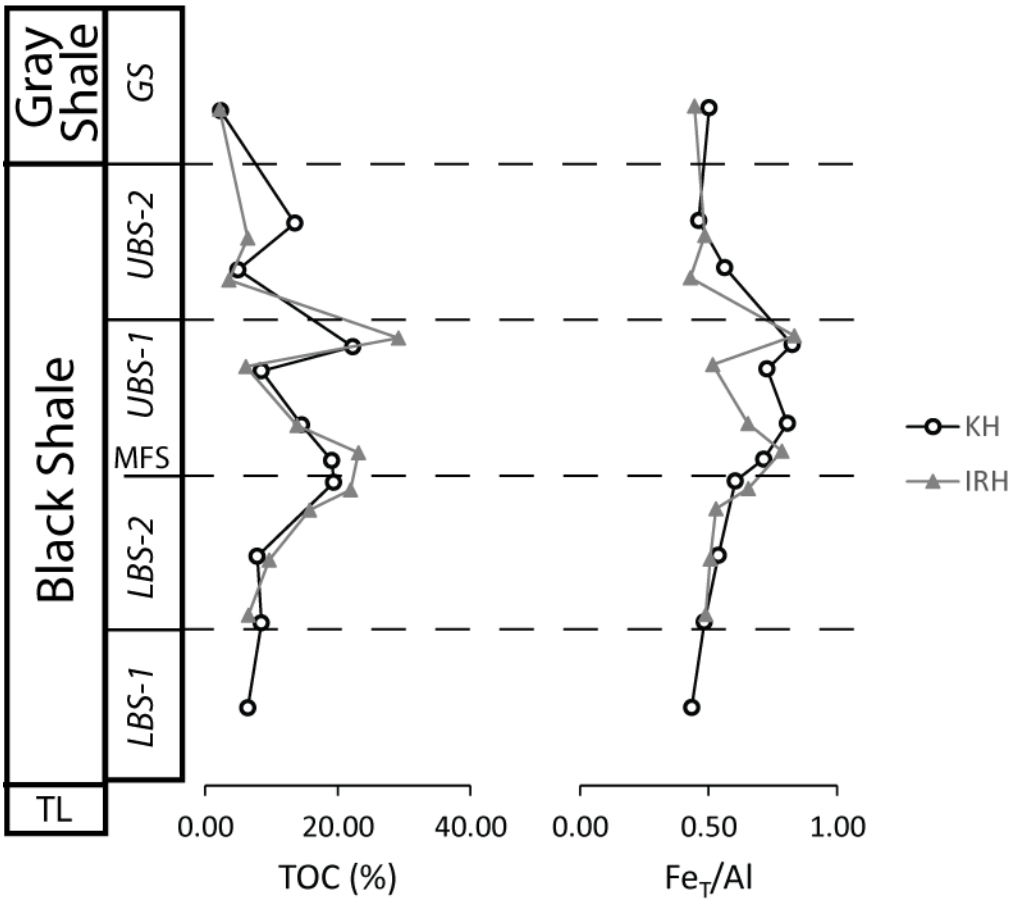

Figure 5.6 Depth plots of bulk sample TOC (%) and Al normalized Fe for both study sections.

5.3.3 Redox Sensitive Trace Metals (V, Mo, and U)

Trace metal proxies exhibit pronounced gradients between the two sites, with increasing enrichment factors at IRH relative to KH (Fig. 5.7–9). Samples are most enriched with trace elements in the LBS-2 and UBS-1, less so in LBS-1, UBS-2, and GS. V enrichment factors range from ~ 1 – 4 in the

exchangeable phase, ~0.1 in the carbonate phase, ~0.5 – 2 in the apatite phase, ~1 – 8 in the oxide phase, ~5 – 50 in the organic phase, and 0.5 – 2 in the residual phase (Fig. 5.7). Mo enrichment factors range from ~1 – 500 in the exchangeable phase, ~1 – 30 in the carbonate phase, ~5 – 80 in the apatite phase, 5 – 200 in the oxide phase, 1 – 400 in the organic phase, and 1 – 10 in the residual phase. U enrichment factors range from ~1-18 in the exchangeable phase, ~1 – 6 in the carbonate phase, ~1 – 90 in the apatite phase, ~1 – 50 in the oxide and organic phases, and ~1 – 3 in the residual phase.

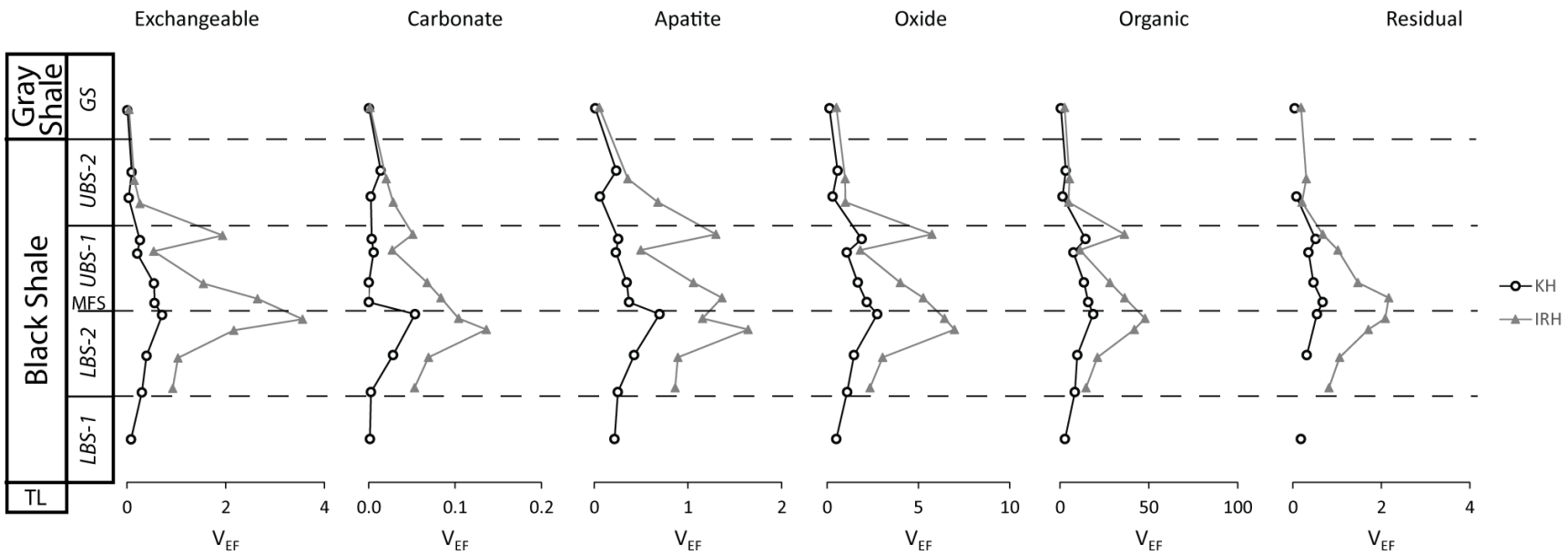

Figure 5.7 Depth-adjusted vanadium enrichment factor profiles for study locales.

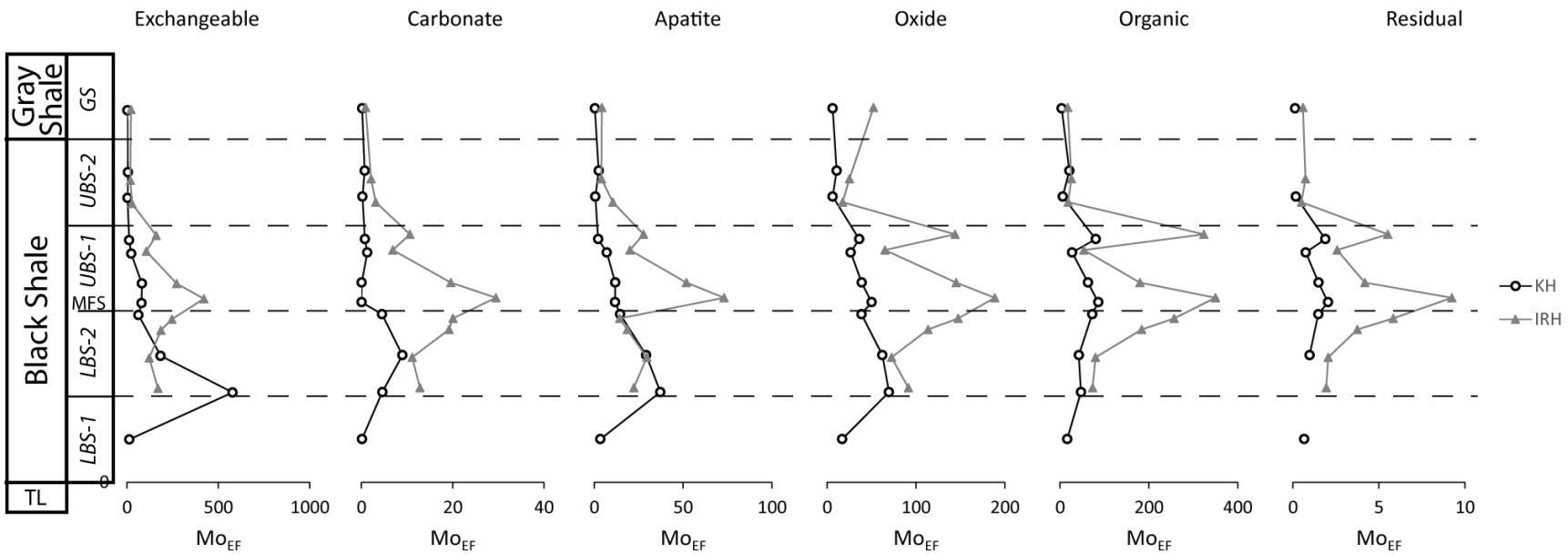

Figure 5.8 Depth-adjusted molybdenum enrichment factor profiles for study locales.

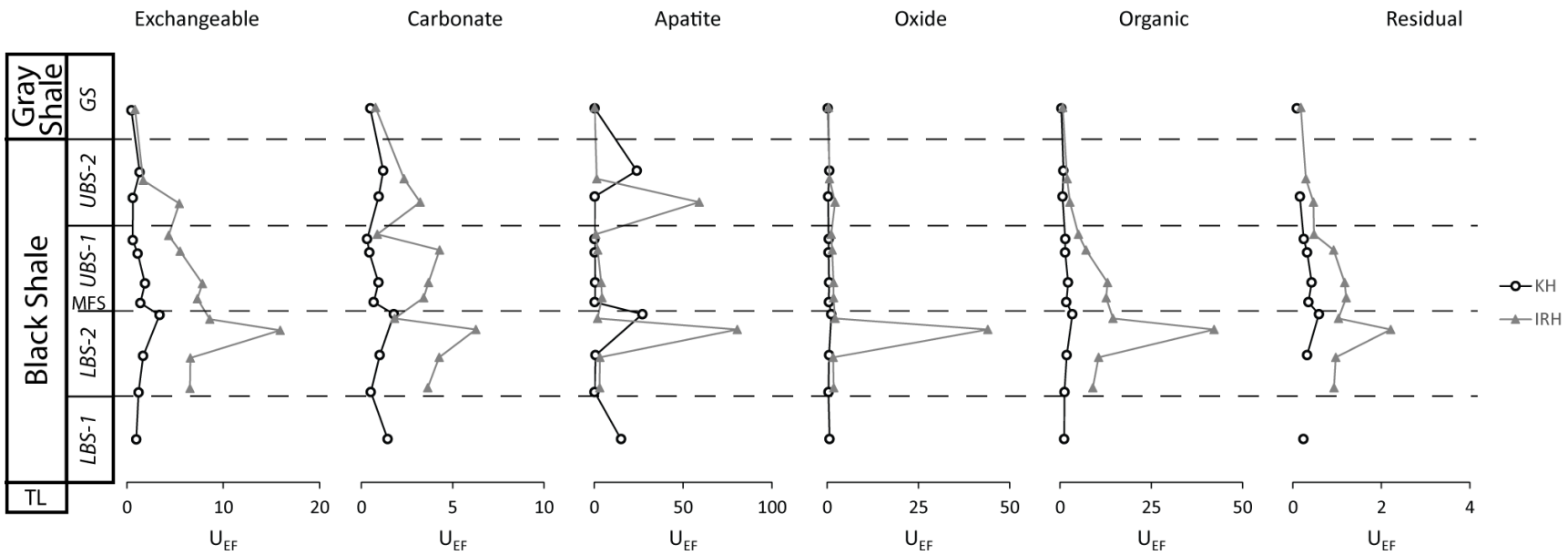

Figure 5.9 Depth-adjusted uranium enrichment factor profiles for study locales.

5.4. Discussion

5.4.1 REE + Y distribution and partitions

The carbonate phase has the potential to incorporate sea water REE values, and in this study reflects sea water characteristics more than other phases (negative Ce anomaly, high Y/Ho ratios, and enriched heavy REE) (Bau and Dulski, 1996; Piper and Bau, 2013). Ce is commonly oxidized from the 3+ to 4+ valence in seawater and preferentially removed from the water column, leaving behind oxic sweaters depleted in Ce, resulting in the negative Ce anomaly (Elderfield et al., 1990). This suggests that the carbonate precipitated in the oxic (negative Ce anomaly), brackish portion of the water column. Y/Ho ratios are used to determine terrestrial influence, as Ho is preferentially removed in oxic marine settings, leaving behind enriched Y signals (Bau et al., 1997). In general, Y/Ho ratios in carbonates greater than 36 are considered free of terrestrial influence (Tostevin et al., 2016). The carbonate phase of IRH has generally great Y/Ho values than KH, reflecting it's more central location in the NAMS. Ce anomalies and Y/Ho values decrease upcore, indicating a greater proportion of terrestrial influence during the UBS-2 and GS than in the LBS-1, LBS-2, and UBS-1 (Fig. 5.5). This occurs as sea levels are falling, and entrained bottom waters are becoming less reducing (Algeo et al., 2004).

In the NAMS, abundant phosphate nodules occur in the sediment (Heckel, 1977). The authigenic enrichment of phosphate reflects pore water REE profiles indicative of Fe-reducing conditions, with a high BSI (Haley et al., 2004). This is consistent with predicted Fe redox cycling and reducing bottom waters (Herrmann et al., 2012). Samples with more abundant phosphate nodules have a greater concentration of REE, as seen in the covariation between ΣREE and U (also preferentially enriched in phosphate nodules) (Fig. 5.10). Samples with highest concentration of REE in the apatite phase, have a similar bell shape distribution in the oxide phase (and in one case in the organic phase), in contrast to other samples which have a heavy REE enriched pattern. REE readily complex with oxides, generally forming a bell shaped distribution, however when reduced, the REE and oxides tend to reductively dissolve (Haley et al., 2004). This suggests that phosphate nodules preferentially formed under bottom

water conditions that may have been slightly less reducing than surrounding depth intervals, allowing oxide-REE complexes to become incorporated in the sediment.

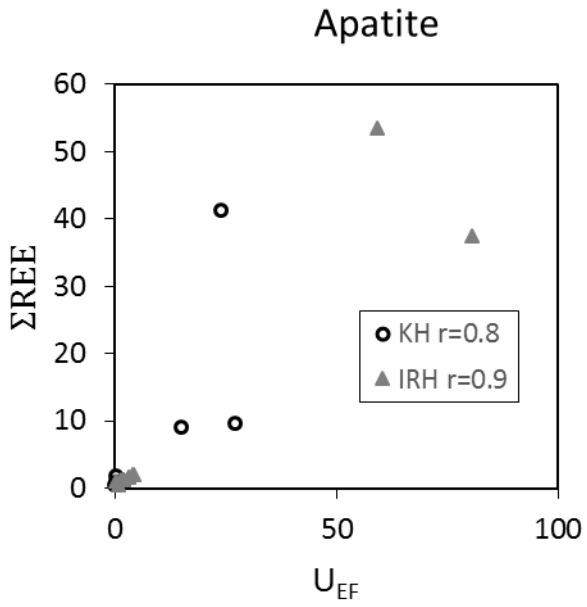

Figure 5.10 Cross plot of U and the sum of REEs from the apatite phase.

Organic phase REEs have three distinct distribution patters (Fig. 5.3). One sample from the IRH core expresses a bell shaped distribution, indicating REE complexation with the organics in the water column (Bau et al., 1997). Organics from the LBS-1, LBS-2, and UBS-1 have more enriched heavy REE than samples from the UBS-2 and GS (average Nd/Yb of 1.44 and 2.84 respectively). This corresponds to a shift in bottom waters from euxinic to anoxic conditions (see chapter 2), suggesting a change in vital effects (preferential incorporation of REE by organics) between sulfide-oxidizing bacteria and non-sulfide-oxidizing bacteria. The residual phase has a unique, jagged REE distribution (Fig. 5.3), which is generally invariant with depth or core location, suggesting it is a terrestrial signal from weathered surroundings.

5.4.2 Trace metal distributions

Vertical and lateral gradients exist between the two study sections in redox-sensitive trace elements. In all phases, trace metals are generally more enriched at IRH with respect to KH (up to ~4x

for V_{EF}, ~20x for Mo_{EF}, and ~30x for U_{EF}; Fig. 5.7-9). Previous studies have attributed this to change in primary productivity, increasingly reducing conditions, or more recently to an estuarine nutrient trap concentrating organic-reactive elements (Algeo and Herrmann, 2017; Algeo and Maynard, 2004). While trace metal gradients exist between the two study sections, TOC and Fe_T/Al suggest that a nutrient trap set up by a salt water wedge is the likely driving factor for the increase in trace metal enrichment in the Heebner core shale. This can be further investigated using a sequential extraction to chemically separate the trace metals.

In the NAMS, there are abundant phosphate nodules, which can preferentially accumulate U (Kidder, 1985). This can be seen in the sequential extraction where U is highly enriched in the apatite phase (Fig. 5.9). The apatite enrichment of U also leads to poor covariation between U and Mo or V in the apatite phase (Fig. 5.11–13). Mo and V exhibit enrichment in all phases, and covary well, suggesting similar mechanisms are affecting them (Figs. 5.7, 5.8, 5.12). The enrichment across all phases indicate that variety of mechanisms are driving enrichment. Loosely bound sulfates, identified in the exchangeable phase in previous chapters, appear to play a less important role in the strongly reducing, restricted NAMS. Enrichment of Mo and V are more closely tied to the organic and oxide phase, indicating that a permanent euxinic water column allowed for incorporation into phases that were reductively dissolved in Bahamian pore waters, scavenged from the water column by forming bonds with metal-rich particles, organic particles, and iron sulfides (Tribovillard et al., 2006). The strong gradient towards enrichment in the IRH study section across phases is consistent with a nutrient trap model, in which concentrations of organically active trace metals are controlled through an estuarine wedge, rather than variations in bottom water chemistry (Algeo and Herrmann, 2017).

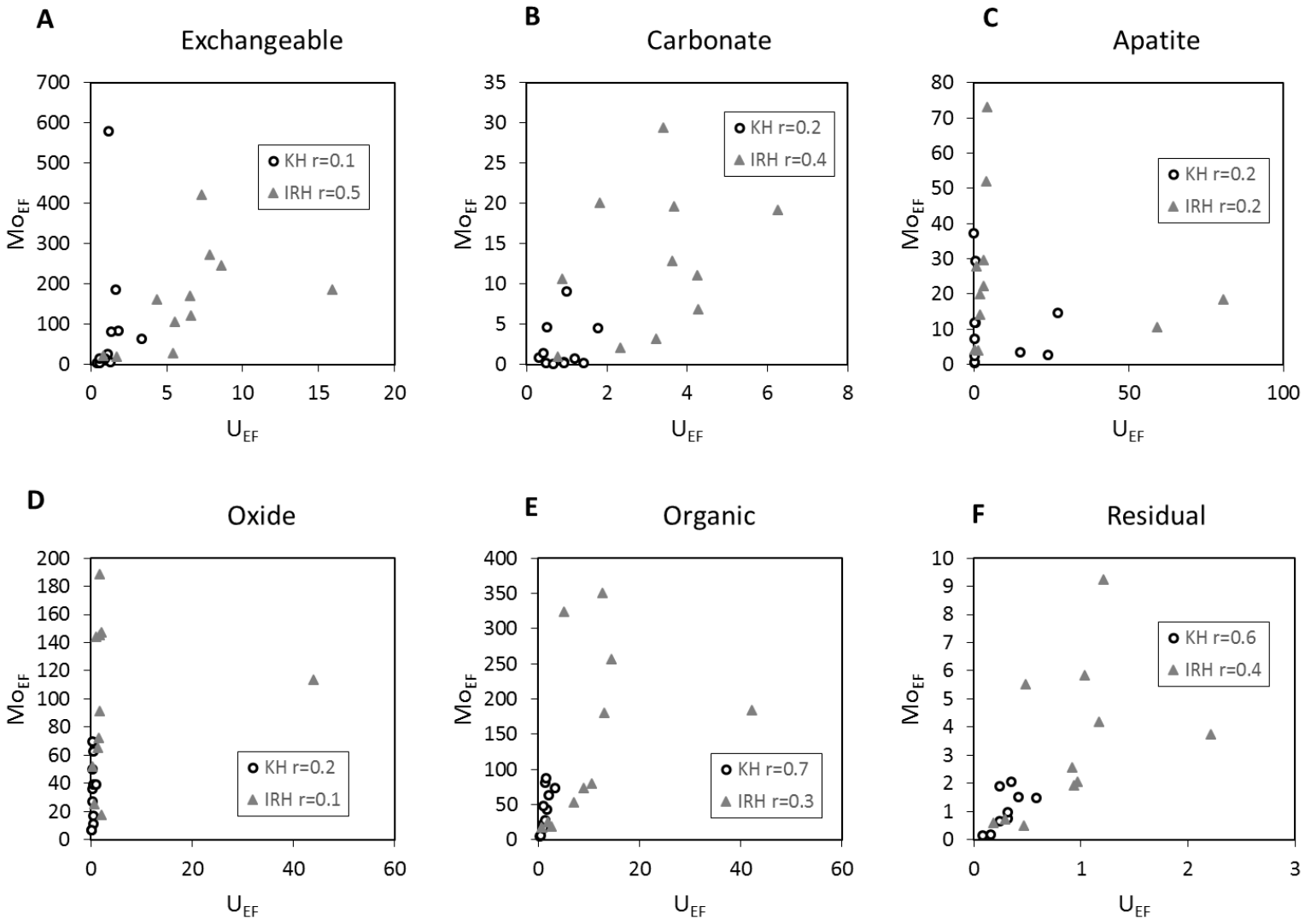

Figure 5.11 Cross plots of molybdenum enrichment factor with uranium enrichment factor for each study section in each phase.

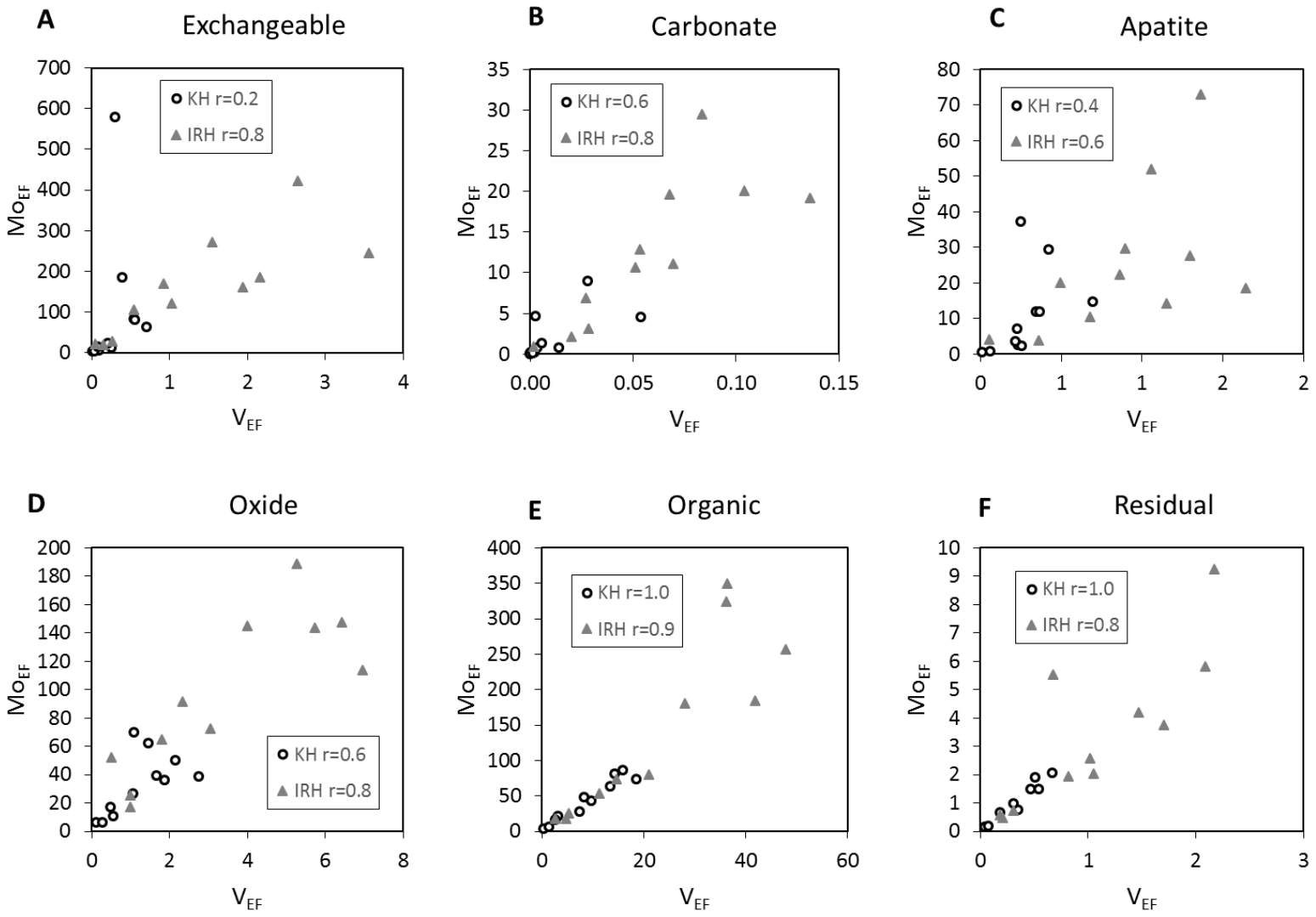

Figure 5.12 Cross plots of molybdenum enrichment factor with vanadium enrichment factor for each study section in each phase.

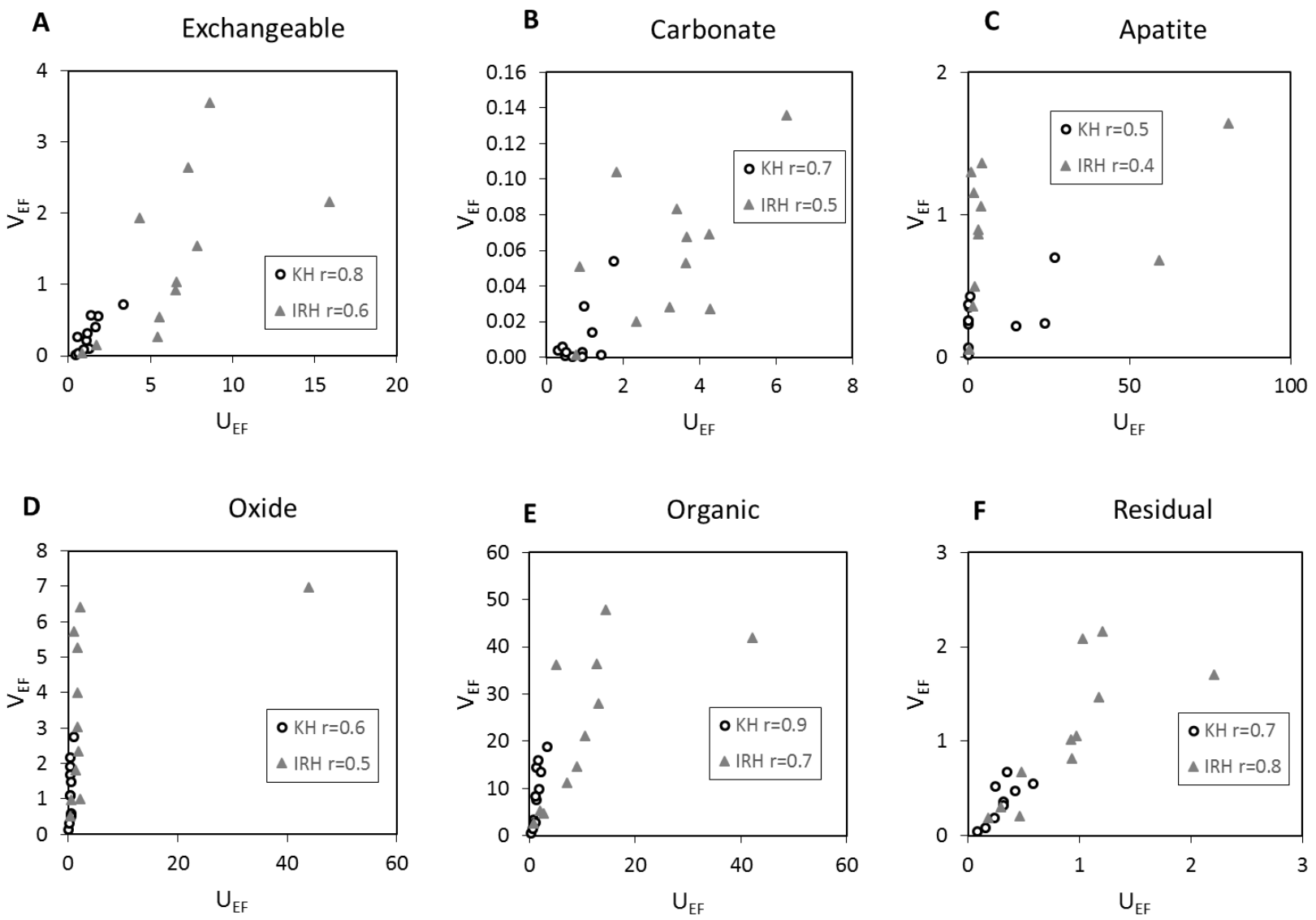

Figure 5.13 Cross plots of vanadium enrichment factor with uranium enrichment factor for each study section in each phase.

The increase in enrichment in KH with respect to IRH in Mo_{EF} requires an additional mechanism to explain, since there was likely no estuarine wedge active at KH. The enrichment is likely due a Mn particulate shuttle, previously theorized by Herrmann et al., 2012. This shuttle would be active in a permanently stratified water was, such as the NAMS, and would preferentially remove Mo with respect to U, as seen in the exchangeable phase of the sequential extraction. Unlike Fe shuttles, Mn shuttles do not require the rapid fluctuation of pycnoclines. The permanent nature of the stratification marks a significant difference from environments such as the Gulf of Mexico, where seasonal stratification occur, allowing for shift in redox state on an annual scale.

5.5. Summaries

The enrichment of trace metal in all of the chemical phases highlight the complexities of trace metal sequestration. The gradients observed between the study sections KH and IRH do not correspond to similar gradients in either TOC or Fe_T, suggesting that uptake is not controlled by scavenging from the water column by forming bonds with metal-rich particles, organic particles, or iron sulfides, but rather by the availability of trace metals in the water column. This is consistent with a nutrient trap scenario in which organically active trace metals (such as V, Mo, and U) are concentrated in an estuarine wedge as the nutrient rich bottom shallows against a bathymetric high (Algeo and Herrmann, 2017).

REY of the carbonate phase show seawater like patterns (Ce anomaly, high Y/Ho ratio), indicating the possibility of seawater values being preserved in carbonates in siliciclastic dominated environments such as the NAMS. Previous studies and chapter 3 of this study has shown the potential for carbonates to preserve REY signatures of seawater in carbonate dominated environments (such as The Bahamas). The potential to use sequential extraction to isolate carbonate in siliciclastic environments to investigate seawater Ce anomalies could provide a useful tool for future work in examining global paleoredox conditions.

5.6. References

Algeo, T.J., Heckel, P.H., 2008. The Late Pennsylvanian Midcontinent Sea of North America: A review. Palaeogeography, Palaeoclimatology, Palaeoecology 268, 205-221.

Algeo, T.J., Heckel, P.H., Maynard, J.B., Blakey, R., Rowe, H., 2008a. Modern and ancient epeiric seas and the super-estuarine circulation model of marine anoxia. Dynamics of Epeiric seas: sedimentological, paleontological and geochemical perspectives. Geological Association Canada Special Publication, 7-38.

Algeo, T.J., Herrmann, A.D., 2017. An ancient estuarine-circulation nutrient trap: The Late Pennsylvanian Midcontinent Sea of North America. Geology.

Algeo, T.J., Maynard, J.B., 2004. Trace-element behavior and redox facies in core shales of Upper Pennsylvanian Kansas-type cyclothems. Chemical geology 206, 289-318.

Algeo, T.J., Rowe, H., Hower, J.C., Schwark, L., Herrmann, A., Heckel, P., 2008b. Changes in ocean denitrification during Late Carboniferous glacial–interglacial cycles. Nature Geoscience 1, 709-714.

Algeo, T.J., Schwark, L., Hower, J.C., 2004. High-resolution geochemistry and sequence stratigraphy of the Hushpuckney Shale (Swope Formation, eastern Kansas): implications for climato-environmental dynamics of the Late Pennsylvanian Midcontinent Seaway. Chemical Geology 206, 259-288.

Bau, M., Dulski, P., 1996. Distribution of yttrium and rare-earth elements in the Penge and Kuruman iron-formations, Transvaal Supergroup, South Africa. Precambrian Research 79, 37-55.

Bau, M., Möller, P., Dulski, P., 1997. Yttrium and lanthanides in eastern Mediterranean seawater and their fractionation during redox-cycling. Marine Chemistry 56, 123-131.

Elderfield, H., Upstill-Goddard, R., Sholkovitz, E., 1990. The rare earth elements in rivers, estuaries, and coastal seas and their significance to the composition of ocean waters. Geochimica et Cosmochimica Acta 54, 971-991.

Haley, B.A., Klinkhammer, G.P., McManus, J., 2004. Rare earth elements in pore waters of marine sediments. Geochimica et Cosmochimica Acta 68, 1265-1279.

Heckel, P.H., 1977. Origin of phosphatic black shale facies in Pennsylvanian cyclothems of mid-continent North America. AAPG Bulletin 61, 1045-1068.

Herrmann, A.D., Barrick, J.E., Algeo, T.J., 2015. The relationship of conodont biofacies to spatially variable water mass properties in the Late Pennsylvanian Midcontinent Sea. Paleoceanography 30, 269-283.

Herrmann, A.D., Kendall, B., Algeo, T.J., Gordon, G.W., Wasylenki, L.E., Anbar, A.D., 2012. Anomalous molybdenum isotope trends in Upper Pennsylvanian euxinic facies: Significance for use of δ98Mo as a global marine redox proxy. Chemical Geology 324-325, 87-98.

Kidder, D.L., 1985. Petrology and origin of phosphate nodules from the Midcontinent Pennsylvanian epicontinental sea. Journal of Sedimentary Research, 55(6).

McLennan, S.M., 2001. Relationships between the trace element composition of sedimentary rocks and upper continental crust. Geochemistry, Geophysics, Geosystems 2.

Morin, G., Mangeret, A., Othmane, G., Stetten, L., Seder-Colomina, M., Brest, J., Ona-Nguema, G., Bassot, S., Courbet, C., Guillevic, J., 2016. Mononuclear U (IV) complexes and ningyoite as major uranium species in lake sediments. Geochemical Perspectives Letter 2, 95-105.

Piper, D.Z., Bau, M., 2013. Normalized rare earth elements in water, sediments, and wine: identifying sources and environmental redox conditions. American Journal of Analytical Chemistry 4, 69.

Šurija, B., Branica, M., 1995. Distribution of Cd, Pb, Cu and Zn in carbonate sediments from the Krka river estuary obtained by sequential extraction. Science of the total environment 170, 101-118.

Tessier, A., Campbell, P.G., Bisson, M., 1979. Sequential extraction procedure for the speciation of particulate trace metals. Analytical chemistry 51, 844-851.

Tostevin, R., Shields, G.A., Tarbuck, G.M., He, T., Clarkson, M.O., Wood, R.A., 2016. Effective use of cerium anomalies as a redox proxy in carbonate-dominated marine settings. Chemical Geology 438, 146-162.

CHAPTER 6 SUMMARY AND CONCLUSION

Sequential extractions have allowed for investigations into where trace metals are incorporated in a variety of reducing and organic rich sediments. The local redox conditions of Bahamian pore waters and Gulf of Mexico hypoxic zone were recorded in the trace metal content of the exchangeable phase. The mechanism responsible for this is respiration of organic matter during sulfate reduction generating pore water sulfide, that drives the authigenic uptake of Mo and V, while U can be incorporated into the reducing sediments as loosely bound mononucleur U and preserved as long as pore water conditions remain reducing. The introduction of oxic waters can remobilize U, releasing it to the water column, or forming loose bonds in different sections of the sediment.

In the NAMS, trace metal uptake is driven by the estuarine wedge effect, in which a nutrient trap may form due to the shallowing of nutrient rich marine water under an oxic, brackish, top water layer. This can be seen through the enrichment of metal in all chemical phases (forming complexations with oxides, organic material, carbonates, and authigenic sulfides and mononucleur loosely bound phases), and the gradient toward the northern edge of the NAMS, regardless of organic, Fe, or Al content. In the core shale of the NAMS, rather than informing about shifts in redox (it is reducing and euxinic at all study sections during LBS-2 and UBS-1 of the core shale), gradients in trace metal enrichment can help to investigate water mass circulation and restriction.

REYs were analyzed in all settings and can provide additional information about the environment of deposition. The Bahamas showed no change in Ce anomaly or Y/Ho ratios between diagenetic zones, suggesting the carbonate phase faithfully records seawater REY values despite syndepositional diagenesis observed in these sections. The Gulf of Mexico contained REY values in the carbonate phase indicative of riverine influence and near shore environment, which is appropriate for the section location, while other phases reflected terrestrial or pore water signals. In the NAMS, REY values of the carbonate phase reflect Ce anomalies and Y/Ho ratios appropriate to the oxic, brackish surface water, while other phases reflected pore water or terrestrial input, similar to Gulf of Mexico samples. This suggests that REY may

be an excellent tool for investigating paleoredox signals of the global ocean once isolated to the carbonate signature.

Future work should examine other locations to examine whether sequential extraction patterns remain constant. In addition, MC-ICP-MS work should be done on Mo and U from the carbonate phases of the Bahamas samples in order to determine whether or not they faithfully reflect isotopic values of seawater, making them a powerful tool in investigating global paleoredox states.

VITA

Adam Turner was born in Phoenix, Arizona, United States. He attended undergraduate college at the University of Arizona where he achieved a Bachelor of Science, majoring in physics and minoring in math, graduating in May of 2007. After a brief hiatus from university, when he worked as a professional beer brewer, he returned to academia and attended Arizona State University where he achieved a second Bachelor of Science, this time majoring in chemistry and minoring in geology. He then moved to Louisiana State University where he worked on a Ph.D. program focusing on the geochemistry of reducing, organic rich sediments.